AN INVESTIGATION INTO THE INITIATION OF LOCAL SCOURING AROUND RECTANGULAR "LONG" CONTRACTIONS

by

Simone Lyons

A Dissertation Submitted in Partial Fulfilment of the Requirements for the Degree MSc (Engineering). Promoter: Dr N. P. Armitage

Department of Civil Engineering
University of Cape Town
2003

Abstract

The introduction of man-made constrictions, for example bridge abutments or guide banks, into alluvial river channels, often results in the entrainment of sediment or the scouring of the bed in the vicinity of the constricting structure. This in turn can cause the undermining of the foundations and the consequent collapse of the structure. It is thus of interest to the hydraulic engineer to understand the influences that different constrictions will have on the river bed such that protective measures can be taken.

This thesis in particular considers the initiation of local scouring around rectangular "long" contractions under clear-water conditions. A long contraction is defined as a man-made constriction where the length of the constriction is equal to or greater than the approach width of the channel. Only the initial local scouring, in other words the lateral extent of the scoured region, was considered. If information is available on the possible extent of the expected scoured region around a structure, the affected area could be armoured with riprap thus protecting the structure from failure.

A dimensional analysis approach was undertaken to identify the parameters that have the greatest influence on the initial scouring process around a long contraction. These parameters were found to be the approach Froude number, Fr_1, the dimensionless approach depth, Y_1/L_c, and the opening ratio, α_c. The opening ratio refers to the ratio of the width of the contracted section to the width of the approach channel. The influence of the sediment size and shape of the contraction was excluded from the analysis. This was then followed by physical modelling. Experiments were conducted in a rectangular glass flume of zero bed slope. Two rectangular contraction sections of different opening ratios, $\alpha_c = ½$ and ¼, were inserted into the flume perpendicular to the approach flow. For both sections, the length of the constriction was made equal to the width of the approach channel. A thin even layer of uniform non-ripple forming quartzitic sand was placed on the bottom of the flume around the sections to set the roughness conditions for the experiment and to act as an indicator of the scoured region. The experiments involved the hourly measurements of the lateral extent of scouring at certain chosen measuring points both upstream and downstream of the contracted sections for different depth and flow combinations. The resulting temporal development of the scour extent at the various measuring points was used to determine the equilibrium scour extent values, which were then used in the analysis.

The investigation revealed that for both opening ratios, the dimensionless scour extent both upstream and downstream of the contracted section increased with increasing

values of the approach Froude number. When considering the influence of the approach depth on the initiation of scour for the smaller opening ratio, $\alpha_c = ¼$, the dimensionless scour extent in general was shown to increase with increasing values of dimensionless approach depth. A different result was however found for the scoured region around the upstream face of the contraction with the larger opening ratio, $\alpha_c = ½$, where the dimensionless scour extent appeared to be generally independent of the dimensionless approach depth. Finally, the results obtained for the influence of the opening ratio on the initial local scour revealed that for the same approach conditions, the local scour extent around the contraction was found to be larger for the smaller opening ratio. The resulting relationships between the scour extent and the various parameters were found to be dependent on the dominant coherent structures responsible for the scouring around the contraction and their interactions with each another.

Owing to the apparent lack of literature on the specific subject of local scouring around long contractions, comparisons of the findings in this investigation were made to the literature on local scour depths around abutments under clear-water scour conditions, as it was believed that long contractions could be viewed as variants of abutments. In general, the results obtained in this investigation compared favourably with those in the literature, even though the dominant coherent structures responsible for the lateral extent of the scour in this investigation were found to differ from those responsible for scour depths around abutments. In order to determine whether the scour extent values could in fact be related to the scour depth using the angle of repose of sediment in water, the probable scour depths associated with the lateral extent of scour were compared to those derived from the literature. It was found that the probable depths provided a fair approximation of the derived depths associated with abutments.

As the data sets used in the analysis were limited, only the general trends could be determined from this investigation. The information presented in this thesis on the initial local scouring around long contractions should thus be seen as a guide for further research rather than for design purposes. The method of investigation employed in this thesis did however show promise and, if larger data sets were available, could be used to provide a predictive method of determining the extent of the scoured region around the structure such that protective measures could be taken.

Declaration

I, the undersigned, hereby declare that this dissertation contains only my own original work, except where reference is made with acknowledgement to contributions from others. I also declare that this material has not been submitted for any purpose or examination to any other Department or University.

Signature ...... Signed by candidate ....

Date ....14/02/2003..............

Acknowledgements

I would like to thank the following people for their valuable assistance throughout this thesis project:

- Dr Neil Armitage for his advice and supervision. His guidance through this investigation was greatly appreciated.

- Mr Charles Nicholas in the Civil Engineering workshop for manufacturing the apparatus that was required to be built during the investigation process.

- Mr Hector Mafungwa who provided assistance in the laboratory.

- To my family for their support and understanding throughout the thesis process.

- To my friend Dominic Bright for his much needed good advice, support and patience.

Table of Contents

3. Experimental Apparatus

4. Experimental Method

5. Calculation Method

6. Development of the initial scouring around a rectangular long contraction

7. Influence of the approach Froude number, approach depth and opening ratio on the initial local scouring around a rectangular long contraction

8. Error and limitations

9. Conclusions

10. Recommendations for future research

References

Appendices

List of Illustrations

Figures **Page**

Tables

Symbols

Symbol	Description	Normal units
a	Constant	
A	Cross-sectional area of the channel	(m^2)
A_b	Cross-sectional area influenced by the bed of the channel	(m^2)
Al	Alignment of abutment relative to the flow	(Degrees)
Al_c	Alignment of a long contraction relative to the flow	(Degrees)
A_w	Cross-sectional area influenced by the walls of the channel	(m^2)
b	Constant	
b_a	Width of contracted channel for an abutment = $(B_1 - L_a)$	(m)
b_c	Width of contracted channel for a long contraction = $(B_1 - 2L_c)$	(m)
B	Width of channel	(m)
B_1	Width of channel upstream of a structure, termed the approach width	(m)
B_f	Width of flume	(m)
C_d	Coefficient of discharge	
C_D	Average drag coefficient	
d	Diameter of sediment	(m or mm)
d_c	Diameter of sediment in contracted channel	(m or mm)
d_p	Diameter of pipe	(m or mm)
$\bar{d}$	Mean diameter of sediment	(m or mm)
d_*	Dimensionless particle diameter	
$d_{\%}$	Diameter of sediment where % indicates the percentage of particles finer than the indicated value	(m or mm)
d_1	Diameter of sediment in approach channel	(m or mm)
d_{50}	Median diameter of sediment	(m or mm)
F_D	Drag force on a single particle	(N)
F_L	Lift force on a single particle	(N)
F_R	Friction force on a single particle	(N)
Fr_o	Densimetric Froude number	
Fr_1	Froude number of approach channel	
g	Gravitational acceleration	(m/s^2)
G	Cross-sectional shape of approach channel to an abutment	

G_c	Cross-sectional shape of approach channel to a long contraction	
h	Vertical height of flow above the bed	(m)
h_v	Overflow height behind V-notch weir	(m)
HL	Head loss	(m)
I	Intensity of motion	(s^{-1})
k	Coefficient	
k_r	Roughness height of bed	(m)
K	Coefficient	
$K_{p(A)}$	Channel bed correction factor for an abutment (Ahmad, 1953)	
$K_{s(A)}$	Shape correction factor for an abutment (Ahmad, 1953)	
$K_{\theta(A)}$	Alignment correction factor for an abutment (Ahmad, 1953)	
$K_{\eta(A)}$	Porosity correction factor for an abutment (Ahmad, 1953)	
$K_{\theta(L)}$	Alignment multiplication factor for an abutment (Laursen, 1962)	
$K_{s(Lim)}$	Shape factor for an abutment (Lim, 1997)	
$K_{L(Liu)}$	Shape correction factor for an abutment (Liu, 1961)	
K_d	Sediment size factor for an abutment (Melville, 1992)	
K_G	Approach channel cross-section factor for an abutment (Melville, 1992)	
K_I	Flow intensity factor for an abutment (Melville, 1992)	
K_s	Sediment size factor for an abutment (Melville, 1992)	
K_s^*	Adjusted sediment size factor for an abutment (Melville, 1992)	
K_y	Flow depth factor for an abutment (Melville, 1992)	
K_θ	Alignment factor for an abutment (Melville, 1992)	
K_θ^*	Adjusted alignment factor for an abutment (Melville, 1992)	
K_σ	Sediment gradation factor for an abutment (Melville, 1992)	
K_1	Coefficient for the abutment shape (Froehlich, 1989)	
K_2	Coefficient for the alignment of the abutment (Froehlich, 1989)	
L_a	Length of the abutment perpendicular to the approach flow	(m)
L_c	Length of face of a long contraction perpendicular to the approach flow	(m)
m	Number of particle displacements during time t	
M_a	Length of abutment parallel to the direction of flow	(m)
M_c	Length of a long contraction parallel to the direction of flow	(m)
MP	Measuring point	
n_c	Manning roughness coefficient of contracted channel	
n_1	Manning roughness coefficient of approach channel	
N	Total number of surface particles over a sample area	

p	Coefficient	
P	Wetted perimeter of channel normal to the direction of flow	(m)
P_r	Power required to keep a particle in suspension	(W/m^3)
P_t	Stream power dissipation per unit volume at any point = Applied unit stream power	(W/m^3)
q_1	Flow rate per unit width of approach channel	(m^2/s)
Q	Flow rate	(m^3/s)
Q_c	Flow rate in the contracted channel	(m^3/s)
Q_v	Flow rate that passes over V-notch weir	(m^3/s)
Q_1	Flow rate in the approach channel	(m^3/s)
r	Laursen's coefficient for an abutment	
R	Hydraulic radius = (A / P)	(m)
R_b	Effective hydraulic radius acting on the flume bed = (A_b / P)	(m)
R_w	Effective hydraulic radius acting on the flume walls = (A_w / P)	(m)
Re	Flow Reynolds Number = (UR / ν)	
Re_b	Flow Reynolds Number for the bed zone of the channel	
Re_w	Flow Reynolds Number for the wall zone of the channel	
Re_*	Particle Reynolds Number = $(u_* d / \nu)$	
S_f	Friction slope	
S_o	Bed slope	
SF	Shape factor of the sediment	
Sh	Shape of abutment	
Sh_c	Shape of a long contraction	
t	Time	(s or hrs)
t_e	Time taken for equilibrium scour conditions to be reached	(s or hrs)
$t_{1/2}$	Time required to attain half the limiting depth of scour	(s or hrs)
T	Temperature	(°C)
u	Horizontal component of velocity	(m/s)
u_*	Shear velocity	(m/s)
u_{*cr}	Critical shear velocity	(m/s)
u_{*1}	Shear velocity of the approach channel	(m/s)
U	Average velocity of the approach channel = (Q / A)	(m/s)
U_{cr}	Critical velocity of the approach channel	(m/s)
v_{ss}	Settling velocity	(m/s)

w_s	Lateral extent of scoured region	(m)
w_{save}	Averaged value of the lateral extent of the scoured region	(m)
W	Weight of a sediment particle	(g)
y	Depth of local scour hole	(m)
y_s	Equilibrium depth of local scour hole	(m)
y_{sc}	Depth eroded through constriction scour	(m)
Y	Depth of flow	(m)
Y_c	Depth of flow in the contracted channel	(m)
Y_1	Depth of flow upstream of a structure, termed the approach depth	(m)
α_a	Opening ratio of an abutment = $(B_1 - L_a / B_1)$	
α_c	Opening ratio of a long contraction = $(B_1 - 2L_c / B_1)$	
β	Length to width ratio of a long contraction = (M_c / B_1)	
γ	Specific weight of water	
γ_s	Specific weight of sediment	
Δ	Relative submerged density = $((\rho_s - \rho) / \rho)$	
Γ	Contraction ratio of an abutment = (L_a / B_1)	
θ	Alignment of an abutment relative to the direction of flow	(Degrees)
λ	Scaling factor	
λ_f	Darcy-Weisbach friction factor	
λ_{fb}	Darcy-Weisbach friction factor for the bed of the flume	
λ_{fw}	Darcy-Weisbach friction factor for the walls of the flume	
μ	Dynamatic viscosity of water	(Pa.s)
v	Kinematic viscosity of water	(Pa.s)
ρ	Density of water (≈ 1000)	(kg/m^3)
ρ_s	Particle density	(kg/m^3)
σ_g	Geometric standard deviation of sediment	
τ	Shear stress at any point within the flow	(Pa, N/m^2)
τ_c	Bed shear stress of contracted channel	(Pa, N/m^2)
τ_{cr}	Critical bed shear stress	(Pa, N/m^2)
τ_{crc}	Critical bed shear stress of the contracted channel	(Pa, N/m^2)
τ_o	Bed shear stress	(Pa, N/m^2)
τ_1	Bed shear stress of the approach channel	(Pa, N/m^2)
τ_{cr1}	Critical bed shear stress of the approach channel	(Pa, N/m^2)
φ	Coefficient	
ψ	Slope correction factor	

ϕ	Angle of notch in V-notch weir	(Degrees)
ϕ_r	Angle of repose of sediment in water	(Degrees)
ϑ	Shield's parameter	
ϑ_c	Critical Shield's parameter	

Chapter 1

Introduction

1.1 Background

As with many processes in nature, rivers will always attempt to maintain a natural balance through the continuous change in geometry due to the interaction between the flow and the erodible boundaries. As with many activities of human beings, people will attempt to interfere with this natural balance, more than often coming off second best.

A river channel is often obstructed by one means or another, for example, guide banks, bridge piers and abutments. The introduction of a man-made hydraulic structure into an alluvial river channel can lead to major changes in the flow characteristics of the river in the vicinity of the structure, thus causing a disturbance to the existing state of sediment transport along the bed. In order for the river to readjust to these changes, the area around the structure is often subject to erosion or scour which in turn can cause the undermining of the foundations of the structure. Many structures have suffered severe damage and even collapse during heavy floods as a result of these erosion phenomena. Man as a result has suffered tremendous economic loss as well as the loss of life. The issue of scour around structures in an alluvial channel is thus one of great interest and importance to the hydraulic engineer.

The aim of this thesis is to investigate the effects that a man-made constriction will have on a river bed. A constriction occurs whenever a structure causes a significant reduction in the width of the river channel. This thesis, in particular, is concerned with the investigation of scouring around a rectangular "long" contraction. A constricted reach is termed a "long" contraction when its length is equal to or greater than the length of the approach channel (Komura, 1966; Lim & Cheng, 1998(b)). A practical example of such a constriction would be when parallel guide banks are built into rivers in order to minimise the cost of constructing diversion works. One of the effects that a long contraction can have on the flow is to cause an increase in velocity in the constricted reach, which in turn can result in a general movement of the bed material and the consequent lowering of the bed through a type of scour known as constriction scour. Although this scour can eventually cause the undermining of the structure, the most detrimental type of scour to the stability of the structure has been found to be that associated with the changes in the local flow pattern as a result of the obstructing structure known as local scour. Local scour, which is associated with strong vortex action and the consequent development of scour holes in the bed in the vicinity of the structure, can occur under one of two conditions, namely clear-water and live-bed conditions. Clear-water conditions refer to when the bed material in the approach channel to the scour area is at rest. Live-bed conditions refer to when there is a general movement of the bed material from the approach channel through the scour area. For the purpose of this investigation, only the effect of local scouring around a long contraction under clear-water conditions was considered. Conditions of clear-water scour was chosen as not only are the deepest and largest scour holes known to form under this condition, but this condition was also found to be easier to model.

Local scouring around a rectangular long contraction was initially considered as a variant of local scouring around abutments. Laursen (1962) in fact stated: "A bridge crossing (abutment) is in effect a long contraction foreshortened to such an extreme that it has only a beginning and an end". Owing to the apparent lack of literature on the specific subject of local scouring around long contractions, the theoretical background for this investigation was thus based on previous research on local scouring around abutments. The common approach concerning local scour around abutments is to derive empirical equations that can be used to predict the maximum depth of the scour hole at the structure. These prediction formulae are then used to site the foundation of the structure deep enough to avoid being undermined by scouring.

This thesis, however, takes a different approach to the problem of scouring by considering the initial local scouring around a long contraction, in other words, the lateral extent of the scour as opposed to the scour depth. This provides information on the initial phase of local scouring around the structure. If information could be provided on the possible extent of the scoured region to be expected around a long contraction, the effected area could be armoured with riprap thus protecting the structure from failure. This information is especially useful when considering the protection of already existing structures in a river. It could possibly provide a less expensive alternative to the resizing or deepening of the foundations of a structure.

1.2 Process of investigation

Laboratory based research was undertaken in order to investigate the initial local scouring around a rectangular long contraction under clear-water conditions. Experiments were conducted in a horizontal glass flume rectangular in cross-section under sub-critical flow conditions. The bed of the flume comprised of a thin layer of uniform medium sized (600-850 μm) sand, the function of which was to set the roughness conditions for the experiment and to provide an indicating surface of the extent of the scouring. Two rectangular PVC contracted sections of different sized openings were placed in the flume perpendicular to the approach flow. The extent of the scoured area around the upstream and downstream region of these insert sections was measured for different flow and approach depth conditions.

It is common practice for researchers to present the results of their studies relating to scour around structures with dimensionless parameters. This provides a simple approach to an otherwise complex problem of flow around a structure. For the analysis of the experimental results in this investigation, a dimensional analysis approach was thus adopted. This also permits the limited experimental results to be applied to other situations involving different physical dimensions and flow properties. Using Dimensional Analysis, the parameters that had a significant influence on the initial local scouring around a long contraction were determined and investigated. These parameters were found to be the approach Froude number, the dimensionless approach depth and the opening ratio. Throughout this investigation the importance of distinguishing between clear-water and live-bed conditions was stressed and thus consideration was also given to the definition of the boundary between these two conditions of scour.

Although the long contraction simply consisted of two rectangular sections on either side of a centre line and the experiments were run under idealised flow conditions, which are not representative of natural rivers, it was decided to take a simple approach as at least the characteristics of the flow and the capacity of the flow to move the sediment could be described with some confidence. This of course limits the application of the findings of the investigation to natural river situations. Also experimental work is prone to a degree of error. The findings in this investigation should thus be considered as an aid to understanding the process of scour formation around a long contraction rather than providing a definite solution.

1.3 Thesis development

The thesis is laid out as follows:

Chapter 2 provides a detailed review of the research literature. The subjects reviewed are that of incipient motion of sediment, types of scour around alluvial structures, and the scouring mechanisms that occur around long constrictions (constriction scour) and abutments (local scour). Particular attention is given to local scouring around abutments.

Chapter 3 describes the apparatus used to conduct the experiments. A description of the flume is given as well as the devices that were installed into the flume for the removal of turbulence and contaminants. A description of the long contraction insert sections is given in detail as well as the new apparatus that was developed for the purpose of the investigation.

Chapter 4 explains the experimental method adopted for the investigation of the initial local scouring around a long contraction. The necessary experimental preparation and the actual experimental procedure are described and discussed. The criteria for the selection of the conditions of the experiments are also considered.

Chapter 5 provides a detailed description of the various calculation procedures that were used in the investigation. Attention is first given to the definition of the boundary between clear-water and live-bed scour conditions which is followed by the calculation method for the selection of the various flow rates and depths of flow that were acceptable for use in the investigation (clear-water conditions). The method of conversion from the measured scour extent value to the equilibrium scour extent value is shown and finally the dimensionless approach adopted for the determination of the influence of the various parameters on the local scour extent is presented.

Chapter 6 considers the development of the initial local scouring around a long contraction. In the first part of this chapter, a detailed description is given of the spatial and temporal development of the scoured regions both upstream and downstream of the contracted section. This development is explained in terms of the coherent structures responsible for the scouring of the bed. The second part of this chapter considers the behaviour of the lateral extent of the scour under conditions of clear-water/live-bed scour. Also, a review of the method chosen for the distinction between clear-water and live-bed conditions is presented and the experiments that were chosen for use in the analysis are shown.

Chapter 7 presents the results of the dimensional analysis in which the influence of the approach Froude number, approach depth and opening ratio of the long contraction on the initial local scouring is investigated. A brief description is given of the process leading up to the results, which is then followed by a detailed discussion on the findings of the results. Throughout the discussion, comparisons are made to the findings in the literature that consider the local scour depths around abutments. Finally, a comparison of the scour depths that are derived from the lateral extent of scour (using the angle of repose of sediment in water) around a long contraction is made to the scour depths as found in the literature.

Chapter 8 presents the error percentages associated with the measured and calculated values used in the investigation. Other possible errors not pertaining to measurements are also considered as well as the limits and constraints associated with laboratory based research.

Chapter 9 draws conclusions based on the results.

Chapter 10 considers recommendations for future work.

Chapter 2
Literature Review

2.1 Introduction

This chapter provides a detailed review of the literature relevant to this investigation. The subject of incipient motion and the various methods that have been adopted for the definition of incipient motion are discussed. These considerations are important when defining the boundary between clear-water and live-bed conditions. The topic of scour is then considered, paying particular attention to constriction and local scour. The behaviour of these types of scour under clear-water and live-bed conditions is discussed in depth. More detailed information is presented for local scouring around abutments as this information is more relevant to the subject of this thesis. When considering local scouring around abutments, various predictive methods of the scour depth around the abutment are presented, namely regime, analytical semi-empirical and dimensional analysis approach. More attention is given to the dimensional analysis approach as this was the method of analysis adopted in this investigation. The methods of determining total scour around structures are reviewed, followed by a description of the various protection measures that can be taken in order to prevent the detrimental influence of scouring.

2.2 Incipient motion

Incipient motion, otherwise known as the threshold of movement of a particle, is defined as the instant when the forces applied to a particle that cause the particle to move, in other words, the lift (F_L) and drag forces (F_D), exceed the stabilising forces due to the particle weight (W) and friction (F_R) (Raudkivi, 1998) (Figure 2.1). Incipient motion therefore describes the point at which particles will begin to be transported along the bed.

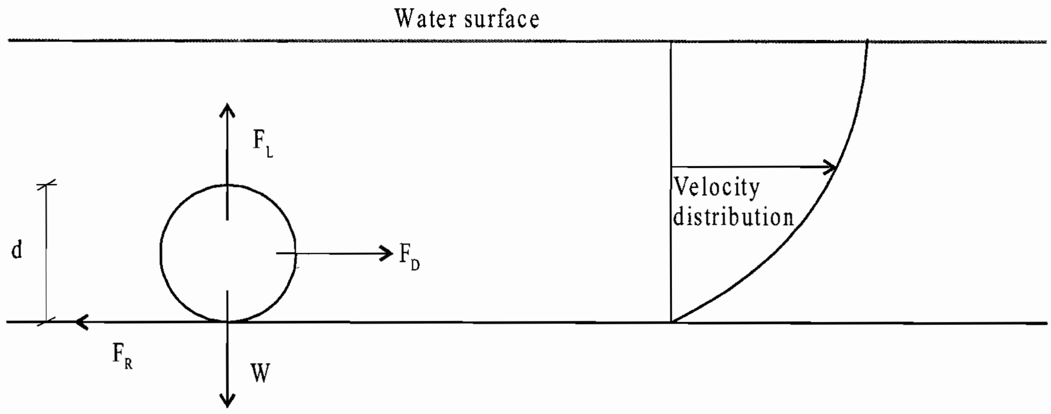

Figure 2.1: Diagram showing the applied and stabilising forces that can act on a particle

It is the usual practice to define incipient motion conditions in terms of a single well-defined physical concept, for example, in terms of the average velocity or the bed shear stress. Sediment transport along a bed, especially near incipient conditions, can however be seen to be stochastic in nature, as a typical bed surface is composed of sediment particles of varying sizes, shapes and orientations. There are also variations in the fluid forces that are applied to individual particles. The particles will therefore not all start to move and come to rest at the same time and at the same locations across the bed. This has therefore led some researchers to rather express incipient motion conditions in terms of a probability of movement or as a certain intensity of motion, *I*.

2.2.1 Probablistic approach

The difficulty involved in defining a condition below which there is definitely no movement of particles along the bed has led many researches, for example, Einstein, 1950; Grass, 1970; Engelund and Fredsoe, 1976; Cheng and Chiew, 1998 & 1999, to define incipient motion in terms of a "pick-up probability". This method assumes that the forces applied to a particular particle along the bed, as well as the forces that are required to move the particles can be described in terms of a probability density function.

If the probability density function of the forces required to move the particle totally exceeds the probability density function for the fluid forces, no movement will occur along the bed (Figure 2.2(a)). Alternatively, if the latter totally exceeds the former, a general movement of the surface will occur across the whole bed (Figure 2.2(c)). If, however, the probability density function for the fluid forces slightly overlaps the probability density function of the forces required to move the particle, only some particles will move (Figure 2.2(b)). The scale of the movement of the particles depends on the degree of overlap. The decision as to what scale of movement or which intensity of motion is sufficient to describe incipient motion is somewhat subjective in nature (Armitage, 2002).

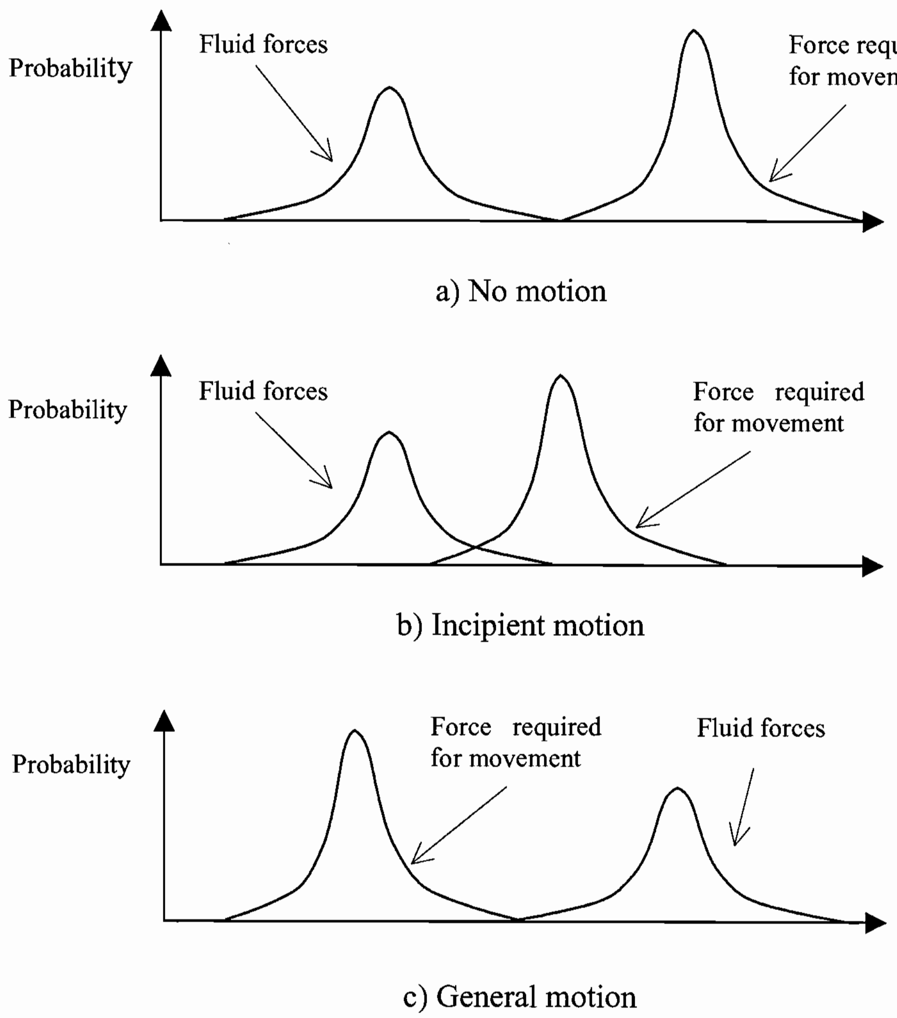

Figure 2.2: The stochastic approach to incipient motion (Van Rijn, 1993)

2.2.2 Intensity of motion

The definition of incipient motion has come to depend on the investigator. Kramer (1935), Parker et al. (1980), Schidchenko & Pender (2000) and Armitage (2002) defined these criteria using the concept of intensity of motion, *I*, which is defined as the simultaneous movement of a given number of particles over a given area of bed.

Kramer (1935), based on visual description, identified three intensities of motion that could be used to define incipient motion conditions (Vanoni, 1975):

i) "Weak movement" refers to the condition where a few or several of the smallest particles are in motion at various isolated areas on the bed in small enough quantities such that one would be able to count those moving on 1 cm^2.

ii) "Medium movement" refers to the condition at which the motion of the particles of mean diameter is too large for the particles to be counted. Such movement is no longer local in nature, but is not yet strong enough to result in appreciable sediment discharge.

iii) "General movement" refers to the condition at which particles up to and including the largest size particles are in motion at all locations along the bed and at all times.

Shvidchenko & Pender (2000) described the intensity of motion, *I*, numerically using the following expression

$$I = \frac{m}{Nt} \tag{2.1}$$

where m is the number of particle displacements during time interval t, and N refers to the total number of particles over the surface area.

Using this expression, Shvidchenko & Pender (2000) recognised "weak sediment transport" as corresponding to $I = 10^{-4}\,\mathrm{s}^{-1}$, which can be visually identified as "occasional particle movement at some locations"; and "general sediment transport" corresponding to $I = 10^{-2}\,\mathrm{s}^{-1}$, which can be visually identified as "frequent particle movement at many locations".

Parker et al. (1982) defined threshold conditions in a manner that corresponds to $I = 3\times10^{-5}\,\mathrm{s}^{-1}$. Armitage (2002) defined incipient conditions as corresponding to a "weak movement" along the bed described by $I = 2\times10^{-5}\,\mathrm{s}^{-1}$, in which "weak movement" of the bed was defined as the visual commencement of natural quartzitic sand on a flat bed with a low relative roughness. It was also reported that there appeared to be a fine line between very weak movement and general movement of sediment along the bed.

2.3 Models of incipient motion

The intensity of motion as defined by Kramer (1935), Shvidchenko & Pender (2000), Parker et al. (1982) and Armitage (2002) is directly linked to the probability of movement of any single particle (Armitage, 2002). Although this is an appropriate approach to describe the stochastic nature of sediment transport, it is often not used in practice due to the practical difficulty incurred in the prediction of the defined intensities of movement. For this reason, numerous simplified models describing the "threshold" conditions of movement have been developed. Most of these models consider a single flow-related parameter as playing the dominant role in determining whether or not there is movement (Armitage, 2002). The three flow-related parameters on which most of the incipient motion criteria are derived are flow velocity, bed shear stress and stream power.

2.3.1 Incipient motion in terms of flow velocity

The velocity of the flow has often been used to provide some correlation between the flow and incipient motion as velocity, in particular average velocity, is easy to measure and therefore convenient to use. Most of the early approaches (for example, Fortier and Scobie, 1926; Hjulström, 1935; Shamov, 1952 and Levy, 1956) involved the use of the average velocity of the flow, which did not provide an accurate assessment of incipient motion. This is because the drag and lift forces exerted by the flow on the sediment particles are dependent on the velocity distribution in the vicinity of the particle, and not on the average velocity. In addition, although the average velocities in two different channels may be identical, the velocity gradients may differ in the two channels, and thus the incipient motion conditions. Although measuring the local velocity at the specific points of interest would provide a more accurate assessment, it has been observed that determining these local velocities is problematic as the particles under inspection usually occur in regions of high velocity gradients.

Work carried out by Liu (1957) and Yang (1973) regarded the lift and drag forces on a particle that were caused by the local velocity, and demonstrated that the particle Reynolds Number, Re_*, could be related to the drag coefficient, where

$$Re_* = \frac{u_* d}{v_{ss}} \tag{2.2}$$

where u_* = shear velocity
d = sediment diameter
v_{ss} = settling velocity

It was established that there is a unique relationship between the ratio of shear velocity to particle settling velocity (called the Movability Number by Liu (1957)), and the particle Reynolds Number, and thus a correlation could be established without the inclusion of the average velocity or the local velocity. Furthermore, in tests conducted in a laboratory flume, Yang showed that the particle Reynolds Number is the most significant independent variable in determining incipient motion, although its application to natural rivers was disputed by Chien and Wan (1999).

2.3.2 Bed Shear Stress

Shields (1936) examined incipient motion by considering only the effect of the drag force on the particle, and not the lift force. Using Dimensional Analysis, Shields found the drag force to be a function of the particle diameter, the grain-shape factor, the bed form, the particle Reynolds Number, Re_*, and the bed shear, τ_o.

Shields produced a diagram of a dimensionless mobility factor (also known as the Shield's parameter), ϑ, versus the particle Reynolds Number, from which the initiation of motion of the particle in the flow could be deduced. The mobility factor is defined by the following identity

$$\vartheta = \frac{\tau_o}{(\rho_s - \rho) g d_{50}} \tag{2.3}$$

where ρ_s = density of sediment
ρ = density of water
g = gravitational acceleration
d_{50} = the median diameter of the bed particles
$= \dfrac{d_{15.9} + d_{84.1}}{2}$
where $d_{84.1}$ is the particle size of the bed material for which 84.1%, by weight, is finer; and $d_{15.9}$ is the particle size of the bed material for which 15.9%, by weight, is finer.

Although this method is one of the most commonly used, it produces results exhibiting wide scatter, and employs a trial-and-error solution as the same unknown, shear velocity, is present on both the axes. In addition, contrary to Shield's assumptions regarding the forces acting on the particle, the lift force cannot be neglected, especially at high shear velocity Reynolds Numbers (Yang, 1996).

2.3.3 Stream Power

The stream power approach relies on the fact that the expenditure of energy is required for the movement of water and sediment. Under conditions of steady uniform flow, the kinetic energy remains constant, and therefore the only energy the water can use is its potential energy above a specific datum. If there is neither scour nor deposition, and if the bed configuration is fully developed, some of the energy in the flow is spent in transporting sediment and some is dissipated as heat through frictional dissipation of turbulence. However, as the sediment is transported, its motion also releases potential energy that facilitates further movement of the sediment. The amount of sediment transported is related to the balance between the rate at which energy is expended overcoming fluid forces, and transporting sediment, which is defined as the "stream power".

Bagnold (1966) introduced the concept of stream power to sediment transport from general physics. He defined stream power as the product of the shear stress along the bed and the average flow velocity, and gave stream power the dimension of power per unit bed area. Bagnold's stream power concept was later used by Ackers & White

(1973), and Engelund and Hanson (1972) in their well known transport functions (Yang, 1996). Yang (1972) however considered that sediment transport should be related to unit stream power rather than stream power. Unit stream power is defined as the rate of energy per unit weight of water available for transporting water and sediment in an open channel.

Bagnold, Ackers & White, Engelund & Hanson and Yang based their definitions of stream power on the average velocity in the water column and hence only considered the average value of the stream power through the column. This is not a reliable approach as stream power can be shown to vary greatly through the water column from zero at the water surface to a maximum at the bed. It was thus recognised by Rooseboom (1975, 1992) that in order to describe the condition for incipient motion more accurately in terms of stream power, the conditions on the bed need to be examined.

Rooseboom (1992) developed a model to describe incipient motion in terms of the unit stream power. He described the power that is dissipated at any point in the water column, P_t, as

$$P_t = \tau \frac{du}{dh} \tag{2.4}$$

where τ = shear stress at any point within the flow

$\frac{du}{dh}$ = velocity gradient of the flow

where u is the horizontal component of the velocity at a height h above the bed

and stated that when P_t is equal to or greater than a fixed proportion of the power required to lift a particle from the bed, P_r, which can be defined as

$$P_r \approx (\rho_s - \rho) g v_{ss} \tag{2.5}$$

the particle will begin to move along the bed.

Based on this concept, Rooseboom derived a graph describing incipient motion conditions in terms of the Movability Number and the particle Reynolds Number

(Figure 2.3). He found that for laminar boundary conditions, the threshold point of motion could be described by

$$\frac{u_*}{v_{ss}} = \frac{1.6}{Re_*} \tag{2.6}$$

and for turbulent boundary conditions, the threshold point of motion could be described by

$$\frac{u_*}{v_{ss}} = 0.12 \tag{2.7}$$

Rooseboom made no attempt to describe incipient motion for a transitional boundary, instead he extrapolated equations 2.6 and 2.7 to a common meeting point that was found to be $Re_* = 13$.

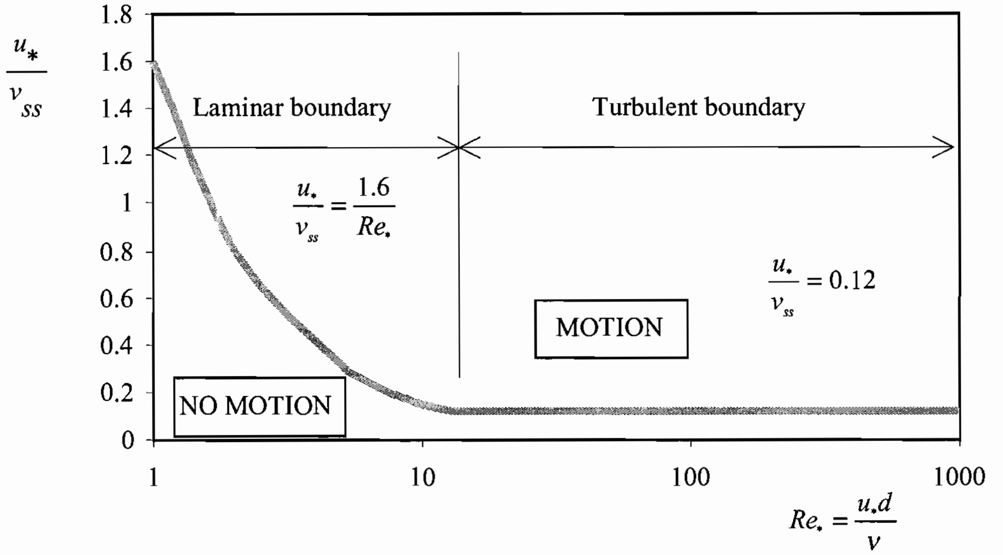

Figure 2.3: The Rooseboom diagram for incipient motion (Rooseboom, 1992)

Armitage (2002) adopted a similar approach to that of Rooseboom (1992) by considering incipient motion along the bed in terms of unit stream power. Armitage, however, recognised that due to the stochastic nature of sediment transportation along a bed, particle motion can theoretically take place under any flow condition, and thus it would be necessary to relate incipient motion conditions to an intensity of motion, *I*.

By recognising the importance of the intensity of motion, Armitage derived the following equation relating the intensity of motion to the Movability Number:

$$\frac{u_*}{v_{ss}} = \psi(0.2405 + 0.0066\ln(I) + 0.204\frac{d}{Y}) \tag{2.8}$$

where ψ is the slope correction factor and Y is the depth of flow in the channel.

Armitage calculated the Movability Number and the particle Reynolds Number from a large selection of data (taken from literature) under both turbulent and laminar boundary conditions. Data was selected that fitted the criteria of weak movement along flat beds of natural quartzitic sand with a low relative roughness. The I values for this were found to be in the range of $3\times10^{-6}\,s^{-1} < I < 3\times10^{-4}\,s^{-1}$. Using the data, Armitage then derived a Liu-type diagram of the Movability number versus the particle Reynolds Number (Figure 2.4) and found that the condition of incipient motion for laminar and turbulent boundaries could best be described by the following equations:

$$\frac{u_*}{v_{ss}} = \frac{2.2}{Re_*^{1.4}} \quad \text{(laminar boundary)} \tag{2.9}$$

and

$$\frac{u_*}{v_{ss}} = 0.17 \quad \text{(turbulent boundary)} \tag{2.10}$$

Armitage noted that the equations 2.9 and 2.10 could be linked by a curve through the transitional region. For the purpose of numerical modelling, this curve was however approximated by the extrapolation of the curves described by equations 2.9 and 2.10 until they met at the point corresponding to $Re_* = 6.23$.

Armitage found that for turbulent boundaries, incipient motion conditions could be conveniently described by $I = 2\times10^{-5}\,s^{-1}$ which indicates a "very weak" movement of particles along the bed. Armitage also included plots representing other intensities of motion to allow for the defining of other types of motion.

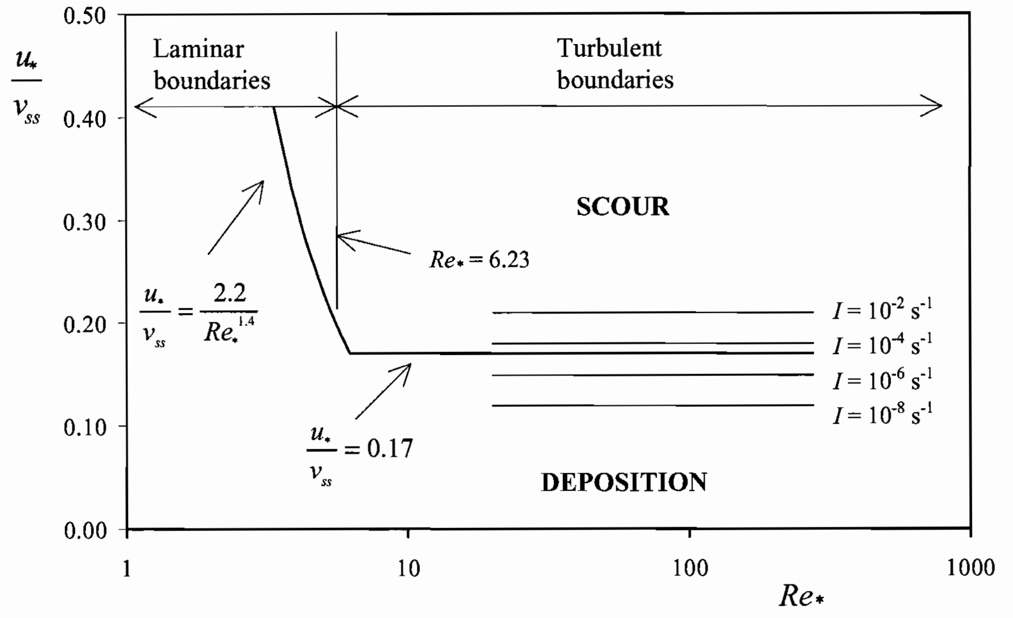

Figure 2.4: The Armitage diagram for incipient motion (Armitage, 2002)

2.4 Scour

This section considers the definition of the various types of scour that can occur along a river bed. Particular attention is given to constriction and local scour. These types of scour are also further defined in terms of clear-water or live-bed conditions. Various theories for the prediction of scouring around structures in alluvial rivers are also described in terms of constriction scour through a long contraction and particularly local scour depths around abutments. The vortex systems associated with local scour around abutments as well as the temporal and spatial development are also reviewed. Total scouring is considered as well as the various measures that can be taken to protect the bed from scour.

2.4.1 Types of scour

Scour can be categorised into three components (Hamill, 1999; HEC-18, 2001):

i) Long-term aggradation and degradation of the river bed

ii) General scour

iii) Local scour

Where general scour can be further broken down into the following three further categories:

i) Constriction scour

ii) Bend scour

iii) Confluence scour

It is usual practice in the literature to class long-term degradation under the heading of general scour and to include constriction scour as a category on its own (Breusers & Raudkivi, 1991; Raudkivi, 1998). General scour, however, can be viewed as being different from long-term degradation in that general scour may be cyclic and/or related to the passing of a flood (HEC-18, 2001). Seeing that this can apply to constriction scour as well, it can be classed as a component under general scour.

Only constriction scour and local scour were considered in this investigation and will thus provide the main focus of this chapter. Constriction scour and local scour can be further categorised under two conditions: clear-water or live-bed scour. These conditions are important to consider as they determine the temporal and spatial development of the scouring process.

2.4.2 Long-term aggradation and degradation of the river bed

Long-term aggradation and degradation of the riverbed involves the long-term adjustment of the river bed elevation over a large area in response to natural or man-induced changes in the water or sediment flow. Examples of such changes include:

a) The construction of dams.

b) Changes in the watershed land-use, for example, urbanisation or deforestation.

c) Channelisation.

d) Meander cut-offs.

e) Dredging.

f) Mining of the streambed.

g) Inter-basin water transfer schemes, which involves the divergence of water into and out of the stream.

h) Natural lowering of the fluvial system.

This investigation will not look at long-term aggradation and degradation on the river bed any further.

2.4.3 General scour

General scour involves the general lowering of the bed elevation and does not include long-term changes or local scouring effects around structures. Unlike long-term aggradation and degradation of a riverbed, general scour may not have a uniform depth across the river channel and can be cyclic, in other words, there could be an increase and decrease in the bed elevation during the passage of a flood. Examples of general scour include constriction scour, bend scour and confluence scour. As only constriction scour will be considered in this investigation, further attention will only be given to this type of general scour.

Constriction scour occurs due to the narrowing of the channel by any constriction whether man-made or natural. Following the law of continuity, the velocities in the constricted channel increase to compensate for the reduction in the flow area. This increase in flow velocity within the contracted region increases the sediment transport capacity of the flow, thus resulting in a general lowering of the bed within the reach. As the bed level decreases, the flow area increases and the velocity decreases until eventually equilibrium is reached.

Constriction scour can be further categorised under clear-water and live-bed scour. Clear-water scour refers to when the bed material upstream of the scour area is at rest, in other words, the flow conditions are equal to or below the critical condition for incipient motion. The critical condition for incipient motion can be defined as the condition beyond which sediment will begin to move. This means that the sediment that is removed from the scoured area is not being replaced by sediment that is being transported by the approach flow.

Thus for constriction scour under clear-water conditions, as the scouring in the contracted reach develops, the area of the contracted region will increase and the velocity decrease (continuity) until the flow conditions in the contracted region fall just below the critical condition for incipient motion, in other words, a static equilibrium comes into existence. At this equilibrium point, the constriction scour is at a maximum for clear-water scour conditions

Live-bed scour occurs when there is a general movement of bed material upstream of the scour area, in other words, the flow conditions exceed the critical condition for incipient motion. The sediment that is removed from the scoured region is thus continuously being replaced by sediment that is being carried by the approach flow.

Thus for constriction scour under live-bed conditions, initially more sediment will be transported out of the contracted region than being transported in from the upstream approach flow. However, as the scour develops, the area of the contracted region will increase. This results in the decrease of the flow velocity until the velocity is reduced to a point that the sediment transported into the contracted section equals the sediment transported out. The maximum scour depth under live-bed conditions is reached at this point of dynamic equilibrium.

In general, the maximum constriction scour depth occurs at equilibrium conditions for clear-water scour at the point just prior to the onset of live-bed scour. This maximum scour depth is reached over a longer period of time compared with live-bed scour.

2.4.4 Local scour

Local scour arises from changes in the local flow patterns around an obstructing structure built into the river channel. The introduction of a structure into a river channel results in increased velocities and associated vortex systems as the flow accelerates around it, thus resulting in scouring in the immediate vicinity of the structure. Local scouring has been known to cause the undermining of foundations of structures during flooding events, thus resulting in damage to the structure or even collapse. The time scale for local scour is generally shorter that the time scales for long-term lowering of the bed and for general scour (Hoffmans & Verheij, 1997).

As with constriction scour, local scour can be further categorised into clear-water and live-bed scour. Under clear-water conditions, as the size of the scour hole increases, the flow velocity in the hole decreases until the flow can no longer remove the material from the scoured area, in other words, the flow condition drops to the critical condition for incipient motion. At this point of static equilibrium, the maximum clear-water scour depth is reached. Under live-bed conditions, the maximum scour depth is reached when the material from the approach flow is transported into the scour hole at the same rate as material is being transported out (dynamic equilibrium). The development of local scour under clear-water and live-bed conditions can best be described by Figure 2.5(a) and (b).

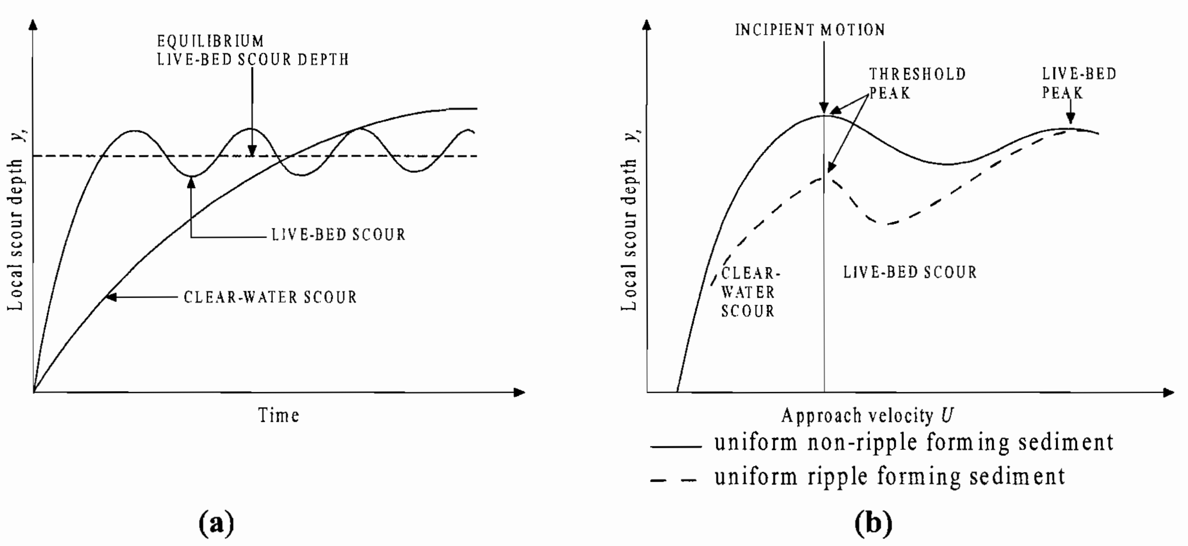

Figure 2.5: Figure showing clear-water and live-bed scour conditions for local scour

Figure 2.5 (a) shows the typical temporal behaviour of the local scour depth around an abutment under conditions of clear-water and live-bed scour. Under live-bed conditions, scouring is more intensive and the maximum live-bed scour value is reached within a shorter period of time in comparison with clear-water conditions, where the scour depth approaches its maximum value asymptotically. Also, under live-bed conditions, the scour depth fluctuates about an average equilibrium value due to the passage of bed forms past the scour hole.

Whether the maximum local scour depth at an abutment occurs under clear-water or live-bed conditions is dependent on whether the sediment is ripple or non-ripple forming, uniform or non-uniform (Breusers and Raudkivi, 1991).

According to Raudkivi & Ettema (1983), Melville (1997) and Hamill (1999), sediment is ripple-forming when $d_{50} <$ 0.7 mm and non-ripple forming when $d_{50} > 0.7$ mm.

The uniformity of the sediment can be determined by considering the standard geometric deviation of the sediment (σ_g), which is defined as:

$$\sigma_g = \sqrt{\frac{d_{84.1}}{d_{15.9}}} \tag{2.11}$$

If $\sigma_g < 1.3$, the sediment is considered to be uniform. If $\sigma_g > 1.3$, the sediment is considered to be non-uniform (Melville, 1997).

For uniform non-ripple forming sediment, the maximum local scour depth occurs at the critical conditions for incipient motion of the channel under clear-water conditions (Figure 2.5(b)). This maximum is termed the threshold peak (Melville, 1997). At flow conditions beyond the critical conditions, in other words, under live-bed conditions, the scour depth decreases to a minimum value after which it increases again towards a second maximum, which is termed the live-bed peak (Melville, 1997). The live-bed peak occurs at the transition flat bed stage of sediment transport where the bed forms are very long and of negligible height. The live-bed peak does not exceed the threshold peak (Breusers and Raudkivi, 1991; Melville, 1997).

For uniform ripple forming sediment, the local scour depth near incipient conditions (threshold peak) is reduced in comparison to non-ripple forming sediment (Figure 2.5(b)). The reason for this is that near threshold conditions, ripples develop in the bed and a small amount of sediment transport takes place, which replenishes some of the sand previously removed from the scour hole by the flow. As for non-ripple forming sediment, beyond threshold conditions (live-bed conditions) the scour depth decreases to a minimum value before increasing to a second maximum at the live-bed peak. Unlike for non-ripple forming sediment however, the live-bed peak exceeds the threshold peak (Breusers & Raudkivi, 1991; Melville, 1997).

Non-uniformity of the sediment is known to reduce both the rate of scour development and the equilibrium scour depth for both ripple forming and non-ripple forming sediment (Raudkivi and Ettema, 1977). This is attributable to the fact that for non-uniform sediment an armour layer forms at the base of the scour hole, thus protecting it from further scouring. This armouring effect however diminishes for increasing flow velocities until all the particles are moved away from the scour hole at high flow intensities.

2.5 Constriction scouring associated with a long contraction

A contraction refers to a reduction in the width of the river channel such that the width within the contraction remains constant (Gill, 1981). The contraction is termed as "long" when its length is equal to or greater than the approach width of the channel (Komura, 1966; Lim & Cheng, 1998(b)). A river within guide banks is a typical example of such contractions. Guide banks are built into rivers to deflect flow away from structures, for example road embankments, to protect them from erosion (Breusers & Raudkivi, 1991).

The reduction of the channel width results in the increase of flow velocity within the constricted reach and can therefore cause a general lowering of the bed within the contraction through constriction scour. Besides constriction scour, the long contraction also promotes 3-D flow patterns in the vicinity of the structure, thus resulting in local scouring. The local scouring processes around a long contraction are comparable to that around abutments (Section 2.6). It was Laursen (1962) who, in fact, stated that a "bridge crossing is in effect a long contraction foreshortened to such an extent that it has only a beginning and an end."

Although this investigation is more concerned with the local scouring effects in the vicinity of the entrance and exit area of a long contraction, some attention will also be given to the effect of constriction scour. The remainder of this section thus considers the various equations that have been derived for the prediction of the constriction scour depth within a long contraction.

Straub (1934) appears to be the first to analyse the equilibrium constriction scour depth in a long contraction. He based this analysis, which was performed under live-bed conditions, on the Du Boys transport equation and the Manning equation that he applied to both the uncontracted and contracted reach. He obtained the following formula:

$$\frac{y_{sc}}{Y_1} = \left(\frac{B_1}{b_c}\right)^{6/7} \left[\frac{\tau_{cr}}{2\tau_1} + \sqrt{\frac{\tau_{cr}}{2\tau_1} + \left(1 - \frac{\tau_{cr}}{\tau_1}\right)\frac{B_1}{b_c}}\right]^{-3/7} - 1 \tag{2.12}$$

where y_{sc} = constriction scour depth in contracted channel
Y_1 = approach depth
B_1 = approach width
b_c = width of the contracted channel
τ_{cr} = critical bed shear stress
τ_1 = bed shear stress of the uncontracted approach channel

Lim & Cheng (1998(b)) found the application of Straub's formula to be limited because the term beneath the square-root sign must always be positive in order to give a meaningful prediction of the scour depth.

Arguably one of the most well-known equations used for the prediction of the maximum equilibrium scour depth in a long contraction are those of Laursen (1962 & 1963). Laursen performed his analysis for both clear-water (Laursen, 1963) and live-bed scour conditions (Laursen, 1962). He assumed the sediment to be non-ripple forming and of the same size in both the uncontracted and contracted reach. He also assumed there to be no difference in slope between the reaches and that the head loss (*HL*) was negligible.

Based on his total sediment transport formula, Laursen (1962) proposed the following equation to describe the maximum equilibrium scour depth for live-bed conditions:

$$\frac{Y_c}{Y_1} = \left(\frac{Q_c}{Q_1}\right)^{\frac{6}{7}} \left(\frac{B_1}{b_c}\right)^{\frac{6}{7}\left(\frac{2+a}{3+a}\right)} \left(\frac{n_c}{n_1}\right)^{\frac{6}{7}\left(\frac{a}{3+a}\right)} \tag{2.13}$$

where Y_c = depth of flow in the contracted channel
Q_c = rate of flow in the contracted channel
Q_1 = rate of flow in the approach channel
n_c = Manning roughness coefficient in the contracted region
n_1 = Manning roughness coefficient in the approach channel

$$a = \frac{1}{4}, \text{ if } \frac{u_*}{v_{ss}} < \frac{1}{2}$$

$$a = 1, \text{ if } \frac{u_*}{v_{ss}} = 1$$

$$a = \frac{9}{4}, \text{ if } \frac{u_*}{v_{ss}} > 2$$

For a compound channel, Laursen ignored the effect of the flow rate over the flood plains on the sediment transport and thus assumed the flow in the main channel to be Q_1, in other words, $Q_1 \approx Q_c$. He also recommended that the Manning *n*-value ratio be neglected from the equation seeing that $n_1 \approx n_c$. Assuming that $y_{sc} = Y_c - Y_1$, Equation 2.13 can thus be written as:

$$\frac{y_{sc}}{Y_1} = \left(\frac{B_1}{b_c}\right)^{\frac{6}{7}\left(\frac{2+a}{3+a}\right)} - 1 \tag{2.14}$$

It can be seen from the above equation that under conditions of live-bed scour, the constriction scour depth only depends on the approach depth and the width ratio between the uncontracted and contracted reach.

Laursen followed a similar approach as described above when deriving an equation to predict the maximum equilibrium scour under clear-water conditions (Laursen, 1963).

He assumed the bed shear stress in the contracted reach to be critical, thus allowing the maximum equilibrium clear-water scour depth to be predicted by the following equation:

$$\frac{y_{sc}}{Y_1} = \left(\frac{\tau_o}{\tau_{cr}}\right)^{3/7} \left(\frac{B_1}{b_c}\right)^{6/7} - 1 \tag{2.15}$$

From the above equation it is apparent that the maximum clear-water scour depth is dependent on the approach depth, width ratio between the uncontracted and contracted reach, approach velocity and the sediment size (the bed shear stress is a function of the approach velocity and sediment size).

Based on experimental data and dimensional analysis, Komura (1966) developed equations to predict the maximum constriction scour depth in a long contraction for both live-bed and clear-water conditions:

$$\frac{y_{sc}}{Y_1} = \left(\frac{\tau_1}{\tau_c}\right)^{2/7} \left(\frac{B_1}{b_c}\right)^{6/7} - 1 \text{ (live-bed conditions)} \tag{2.16}$$

and

$$\frac{y_{sc}}{Y_1} = \left(\frac{\tau_{cr1}}{\tau_{crc}}\right)^{2/7} \left(\frac{B_1}{b_c}\right)^{6/7} - 1 \text{ (clear-water conditions)} \tag{2.17}$$

where τ_c = bed shear stress in contracted channel
τ_{cr1} = critical bed shear stress in the approach channel
τ_{crc} = critical bed shear stress in the contracted channel

In the derivation of the above two equations, it was assumed that the sediment sizes in the two reaches were the same. If it is necessary to calculate the equilibrium scour depth for a variation of sediment sizes in the contracted channel, d_c, and the approach channel, d_1, the first term on the right hand side of equations 2.16 and 2.17 can be multiplied by the term $(d_c / d_1)^{1/7}$.

Komura investigated the effect that sediment size has on the equilibrium scour under both conditions of clear-water and live-bed scour by producing plots of Y_c / Y_1 against d_c / d_1 for varying contraction ratios. He found that under live-bed conditions, the equilibrium scour depth is independent of the sediment size and is only dependent on the approach depth and contraction ratio. Under clear-water conditions, however, he found that the equilibrium scour depth was both dependent on the sediment size as well as the approach depth and contraction ratio.

For conditions of live-bed scour, Gill (1981) presented a similar equation for the prediction of the equilibrium scour depth to that of Straub (1934):

$$\frac{y_{sc}}{Y_1} = \left(\frac{B_1}{b_c}\right)^{6/7} \left[\left(\frac{B_1}{b_c}\right)^{1/k} \left(1 - \frac{\tau_{cr}}{\tau_1}\right) + \frac{\tau_{cr}}{\tau_1}\right]^{-3/7} - 1 \tag{2.18}$$

The value of the coefficient k ranges from 1.5 to 3.0. For design purposes it is advisable to adopt a value of k that will give the highest equilibrium scour depths.

When Equation 2.18 was validated against experimental data (using $k = 3$), it was found that for design purposes, the calculated equilibrium scour depth should be scaled up by about 58% to get a maximum design value. Areas of severe local scouring were observed around the entrance of the contraction near the walls. It was concluded that in order to find the maximum local scour depth in these regions, the equilibrium constriction scour depth as determined from Equation 2.18 should be multiplied by 2.65.

Finally, Lim & Cheng (1998(b)) derived a simple formula for the prediction of the equilibrium scour within a contraction based on continuity of flow and sediment:

$$\frac{y_{sc}}{Y_1} = \left(\frac{B_1}{b_c}\right)^{0.75} \tag{2.19}$$

Although the formula was derived for live-bed scour conditions, Lim & Cheng showed the formula to be valid for clear-water conditions as well. From the above formula it can be seen that the equilibrium constriction scour depth is only a function of the approach depth and the ratio between the contracted and uncontracted reach.

2.6 Local scouring around abutments

The need to keep bridge crossings as short as possible, for economic reasons, subsequently results in the encroachment of the approach embankments or abutments of the bridge into the main channel. This encroachment results in the increase of local velocities in the vicinity of the abutment and can thus cause local scouring. Local scouring is associated with the formation of complex 3-D flow patterns in the vicinity of the structure and the consequent development of scour holes. During flooding events, scour holes may get deep enough to undermine the foundations of the abutments and thus cause severe damage or even collapse of the bridge. The understanding of the local flow patterns around an abutment as well as the prediction of the extent of local scouring is thus of vital importance to the hydraulic engineer.

It must be stated here that research done on scouring around spur-dikes is also considered as relevant to that around abutments, as the scour phenomena around spur-dikes and abutments is regarded as practically the same (Melville, 1992). Thus any reference made to scour around spur-dikes from here forth holds good for scour around abutments.

2.6.1 Types of abutments

Bridge abutments are designed in a wide variety of shapes; the most common of which are the vertical-wall, spill-through and wing-wall abutments (Figure 2.6). Different shapes divert flows in different manners; for example, streamlined shapes create less of a disturbance on the flow than blunt shapes, consequently resulting in less scouring (Melville, 1992). It has been shown that the scour depth around vertical-wall (blunt) abutments is approximately double that around spill-through (streamlined) abutments (Hamill, 1999; HEC-18, 2001).

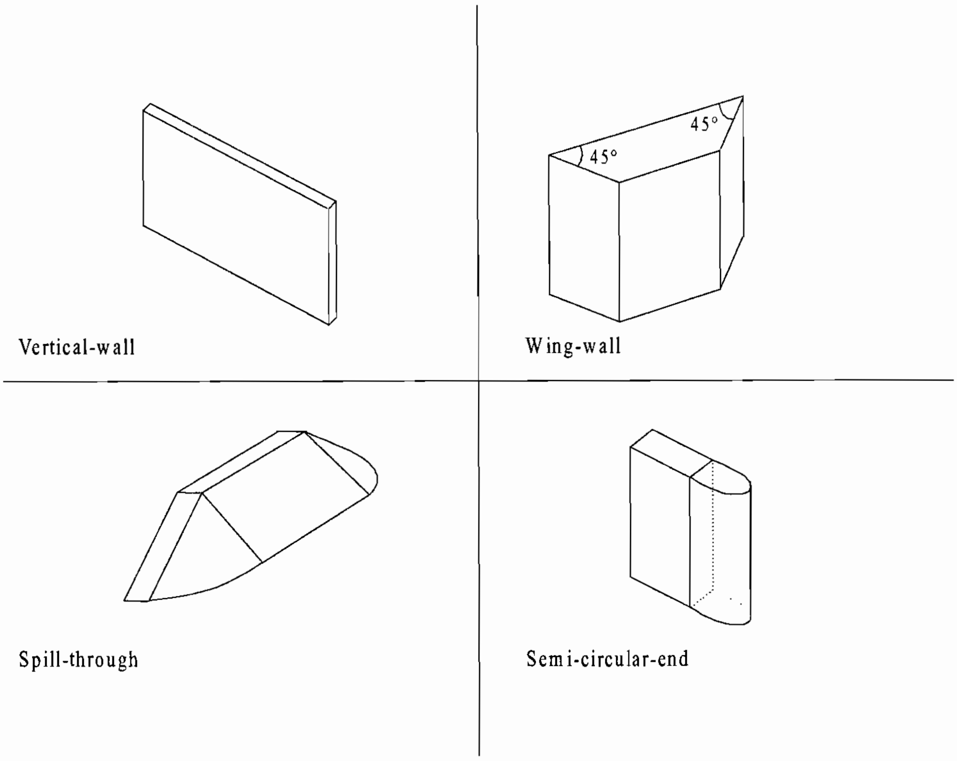

Figure 2.6: Figure showing different types of abutments

The alignment of the abutment relative to the approach flow, defined by the angle θ, can also have an effect on the local scour depth. It has been found that the scour depth is reduced for abutments angled downstream ($\theta < 90^\circ$) and increased for abutments angled upstream ($\theta > 90^\circ$) (Melville, 1992; HEC-18, 2001). For example, Ahmad (1953) stated in his investigation into the local scour depth at abutments that the maximum depth at abutments angled 45° downstream is reduced by 20% relative to an abutment perpendicular to the flow, whereas the maximum depth of scour that occurs at abutments angled 45° upstream is increased by 10%.

Although there are abutments of many different shapes and alignments, it is usual practice to describe the scour around the various types of abutments by using the vertical-plate abutment perpendicular to the flow direction ($\theta = 90^\circ$) as a reference (Breusers & Raudkivi, 1991; Melville & Kwan, 1994; Hoffmans and Verheij, 1997; Raudkivi, 1998). A vertical-wall abutment can be regarded as being the equivalent to the vertical plate abutment if the length of the abutment perpendicular to the approach flow is at least five times the width of the abutment (Hoffmans and Verheij, 1997).

2.6.2 Flow patterns around abutments

Figure 2.7 shows a diagram of the complex flow components responsible for local scouring around an abutment. These are the downflow, the principal vortex, the bow wave (not depicted), the wake vortices shed from the abutment corners, and the eddying action induced in the "dead" water regions. A description of each of these flow components is given below.

i) The downflow

As the flow approaches the abutment it decelerates and comes to a rest along the boundary between the fast-moving upstream flow section and the "dead" water trapped in the corner between the abutment and the banks of the channel. This leads to a rise in pressure known as the stagnation pressure. The stagnation pressure is proportional to the square of the velocity of the oncoming flow; therefore, since the approach velocity decreases from the surface to zero at the bed, the stagnation pressure also decreases in the same direction. This vertical pressure gradient provides the driving mechanism for a vertical "downflow".

A scour hole will develop if the velocity associated with the downflow is strong enough to overcome the critical conditions for incipient motion at the bed. It should be noted that it is also this increased pressure upstream of the abutment face that provides the necessary force for the acceleration of the flow around the sides of the abutment and into the main channel (Armitage, 2002).

ii) The principal vortex

As the scour hole develops, the downflow is deflected outwards and away from the abutment on reaching the bed surface. The upper layers of the approach flow are thus moving towards the abutment face while the bottom layers near the bed are being directed away. This results in the generation of a large rotational flow known as the "principal vortex" (Melville & Kwan, 1994). The combination of the downflow and the principal vortex is the dominant scour mechanism around an abutment (Breusers & Raudkivi, 1991).

The principal vortex usually commences from a point upstream of the abutment and lies along the boundary between the upstream flow section and the dead water

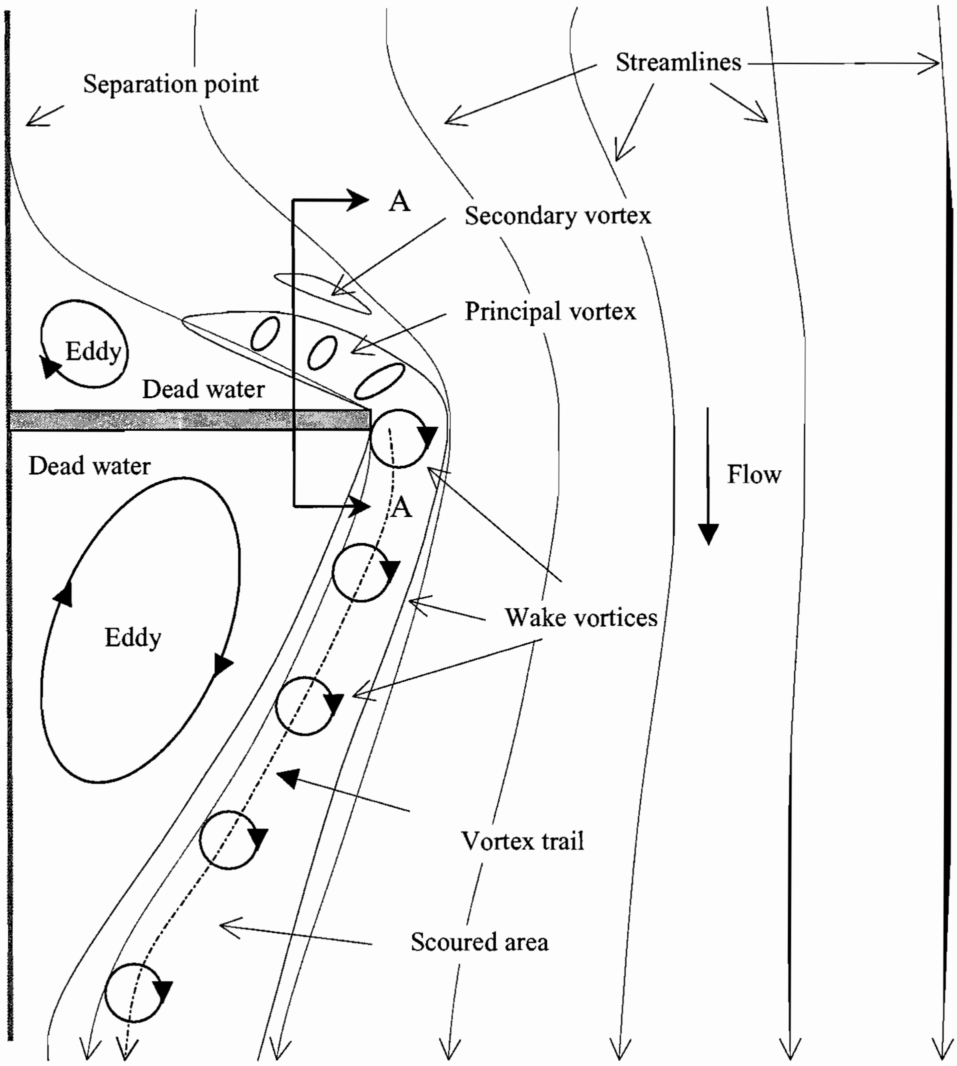

a) Plan

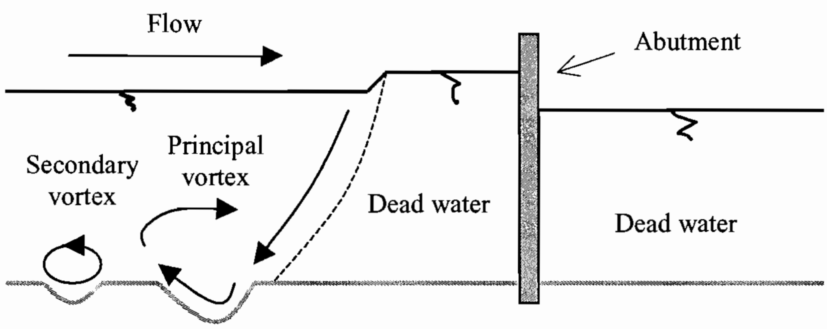

b) Section A-A

Figure 2.7: The top and side views of the vortex structures around an abutment (After Breusers & Raudkivi, 1991; Hoffmans & Verheij, 1997; Raudkivi, 1998; Armitage, 2002)

region upstream of the abutment. As it travels towards the abutment, it increases in size until it is deflected around the abutment and into the main channel where it eventually dissipates in the general turbulence. The principal vortex also induces a secondary counter-rotating vortex immediately upstream of it.

Melville & Kwan (1994) found that the principal vortex resembles the Rankine vortex, in other words, the core region approximates that of a forced vortex and the outer region approximates that of a free vortex. They also found the principal vortex to be elliptical in shape with its main axis being parallel to the bed surface.

iii) The bow wave or roller

Not only does the sudden deceleration of the flow upstream of the abutment result in the formation of the downflow, but the increase in pressure also results in a rise in height of the water surface. This rise in height corresponds with the velocity head of the oncoming flow that is a maximum at the surface. The flow is forced upwards and back onto itself to form a "bow wave" or a "roller" that has a counter rotation to that of the principal vortex. As for the principal vortex, the bow wave forms along the boundary between the fast-flowing water in the main channel and the upstream "dead" water region. The strength of the bow wave also increases as it approaches the abutment face. The bow wave only really has a significant affect on the scouring process at an abutment when the flow depth is shallow enough that it interferes with the counter rotating principal vortex.

iv) The wake vortices

Flow separation at the corner of the abutment results in the shedding of small vertical "wake vortices" that travel downstream along the boundary between the main flow and the second "dead" water region. The intensity of the wake vortices diminishes rapidly as the distance downstream of the abutment increases until eventually dying out in the general turbulence. Further downstream of the abutment, the flow will reattach itself to the channel sides.

v) Eddies induced in "dead" water regions

Although the "dead" water regions are separated from the main channel by the principal vortex upstream and the vortex trail downstream of the abutment, strong eddies can be induced in them as a result of the shearing action that occurs between them and the fast moving flow in the main channel. These eddies can also lead to the formation of scour holes along the bed.

2.6.3 Spatial development of the scour hole

The erosion process typically begins at the upstream corner of the abutment near the main channel where the velocity, associated with the downflow, is the largest. At this position the velocity is almost constant throughout the depth (Melville & Kwan, 1994). The erosion capacity of the flow is the most severe at this stage of the scouring process and has been described by Zanke (1978) as forming the "initial phase" in the evolution of scour.

As the scour hole develops, the side material of the hole as well as the material reaching the upstream edge of the hole (if live-bed conditions exist) slides towards the bottom of the hole and is forced upstream and laterally away from the hole by the principal vortex. It can thus be said that the erosive process is concentrated at the bottom of the scour hole and that lateral widening of the hole occurs as a consequence of the collapse of the hole sides.

The most rapid rate of scouring occurs at the upstream part of the scour hole (close to the abutment corner) and decreases further downstream where the capacity of the flow to pick up sediment is less. Consequently, the upstream slope forms quickly and remains approximately constant with time, while the milder downstream slope can be seen to be more varying over time (Ballio & Orsi, undated). The reason for this is that the area further downstream of the abutment corner is affected by the interactions among the main stream, the principal vortex coming from the front, and the vortex trail from the abutment corner; thus forming a complex flow field.

The limit of scour around the abutment is reached when the enlargement of the scour hole and subsequent reduction in velocity, results in the flow conditions becoming equal to or less than the critical conditions required for incipient motion. At equilibrium conditions the scour hole is deepest. At this stage of limiting scour, the upstream part of the scour hole has approximately the shape of a quarter of a cone with its vertex at the abutment corner (Ballio & Orsi, undated; Garde et al, 1961;

Laursen, 1963; Zaghloul, 1983; Breusers & Raudkivi, 1991; Melville & Kwan, 1994). The slope of the scour hole is approximately equal to the sediment angle of repose in water (Ballio & Orsi, undated; Breusers & Raudkivi, 1991; Lim, 1997).

Ballio & Orsi (undated) showed experimentally that the geometry of the front region of the scour hole approximately scales with the scour depth, so that all the geometrical properties of the scour hole, such as the width and volume, can be determined from knowing the value of the scour depth and vice-versa. This is not the case, however, for the scoured area further downstream due the complexity of the flow.

2.6.4 Temporal development of the scour hole

When dealing with local scour problems, it is common practice in the literature to only consider the maximum scour depth at equilibrium conditions. The actual temporal development of local scouring has been little investigated and is thus poorly understood. In particular, it is not yet fully understood whether a limiting scour depth is, in fact, attainable, and if so, under which condition of scour.

The rate of scour at an abutment can be seen to increase initially quite rapidly and then slow down as it approaches its limiting state; thus when using a logarithmic scale, the scour depth can be seen to be increasing linearly with time (Laursen, 1963; Lim, 1997; Zaghloul, 1983; Ballio & Orsi, undated). Ballio & Orsi observed, from an experimental investigation, that under clear-water conditions, the scour depth increased approximately the same amount in the first hour as it did in the following week.

Probably the topic under the most debate is that regarding the equilibrium scour depth under clear-water conditions. Rouse (1940), Doddiah et al. (1953), Liu et al. (1961) are among some of the researchers that believe that the scour depth cannot reach a stage of equilibrium over any period of time under clear-water scour conditions. Melville (1992) and Lim (1997), based on experimental investigation, found that an equilibrium depth could, in fact, be reached, but could take up to as much as 10 days. But even this result is questionable, as it is very difficult to be able to measure the exact time at which equilibrium conditions occur when using small-scale laboratory apparatus, and thus in most cases the researcher defines a state of scouring at which it can be considered to have reached equilibrium (Melville & Chiew, 1999).

Ballio & Orsi (undated) also considered the temporal development of scour at an abutment using an experimental approach and found that even after 38 days, the scour depth had not yet reached a steady state value. They did, however, determine an equation relating the equilibrium scour depth with time that best fitted their data. This formula was adapted from that of Franzetti et al. (1994), who considered the temporal development of scour around piers, through the appropriate modification of the coefficients. The formula is as follows

$$\frac{y}{y_s} = 1 - e^{-0.028\left(\frac{tU}{\lambda}\right)^{0.33}} \tag{2.20}$$

Where y = scour depth
y_s = equilibrium scour depth
t = time
U = average approach velocity
λ = scaling length
L_a = length of the abutment perpendicular to the approach flow

Laursen (1963) believed that an equilibrium value of scour depth could be reached at a certain time under clear-water conditions, and also derived an equation expressing such a time:

$$t_{1/2} = 0.03\frac{\left(\frac{1}{Y_1}\right)^2\left(\frac{\tau_o}{\tau_{cr}}\right)^{1.5}}{\left(\frac{\bar{d}}{Y_1}\right)^{1.5}\left(\frac{g}{Y_1}\right)^{0.5}} \tag{2.21}$$

where $t_{1/2}$ = time required to attain half of the limiting depth of scour
$\bar{d}$ = mean diameter of sediment

Although, in comparison for clear-water conditions, little research has been carried out on the temporal development of the scour depth under live-bed conditions, it has generally been found that the equilibrium scour depth is effectively attained within a few hours (Garde et al., 1961; Cunha, 1973; Melville & Chiew, 1999).

2.6.5 Previous research on local scour depths around abutments

Much research has been focussed towards developing equations for the prediction of the maximum local scour depth around abutments. From the literature it is evident that there are three main approaches that have been employed in the prediction of the local scour depth around abutments: the regime approach (Ahmad, 1953); the analytical/semi-empirical approach (Laursen, 1962 & 1963; Gill, 1972; Zaghloul, 1983; Lim, 1997; Lim & Cheng, 1998(a)); and the dimensionless approach (Garde et al., 1961; Liu et al., 1961; Froehlich, 1989; Melville, 1992; Melville & Kwan, 1994; Melville, 1997; Raudkivi, 1998).

The regime approach relates the scour depth to the flow around the abutment, the analytical/semi-empirical approach is based on the sediment transport relation for the approach flow and increased shear at the abutment site, and the dimensionless approach involves the correlation of relevant dimensionless parameters.

The published scour prediction formulae are numerous and often contradictory. This section provides insight into the different approaches undertaken, the assumptions that were made and the conclusions that were drawn. Attention has been given to the prevailing scour condition, in other words live-bed or clear-water scour, that was considered in the studies, as this was found to be an important factor in determining the parameters that affect the local scour depth. This is also an area of much debate.

Unless otherwise stated, the various equations given below apply to vertical plate abutments aligned perpendicular to the flow in a horizontal channel that consists of uniform cohensionless sediment in subcritical flow.

2.6.5.1 The regime approach

Ahmad (1953) proposed an equation describing the scour depth relationship for spur-dikes by using the flow intensity (flow per unit width) in the contracted section as the independent variable. Ahmad's equation was based on field studies of spur-dikes in alluvial rivers in Pakistan as well as on model studies. The studies were performed under live-bed conditions.

The equation is as follows:

$$y_s + Y_1 = 2K_{p(A)}K_{s(A)}K_{\theta(A)}K_{\eta(A)}\left(\frac{q_1}{1-\Gamma}\right)^{2/3} \qquad (2.22)$$

where $K_{p(A)}$ = correction factor for the influence of the channel bed
$K_{s(A)}$ = correction factor for the influence of the shape of the abutment
$K_{\theta(A)}$ = correction factor for the influence of the abutment alignment
$K_{\eta(A)}$ = correction factor for the influence of the porosity
q_1 = flow rate per unit width of the approach channel
Γ = L_a / B_1 = contraction ratio

(The tables containing the correction factors can be found in Breusers & Raudkivi (1991) pages 54 and 55.)

It is apparent from Ahmad's equation that the scour depth around an abutment for live-bed conditions is influenced by the approach depth, the geometry of the contraction, and the flow velocity (the discharge per unit width is the product of the velocity and the depth). It is also apparent from the above equation that the sediment size has negligible effect on the scour depth. Ahmad in fact tested this by comparing the influence of two different sized sands of d = 0.35 mm and d = 0.7 mm on the scour depth, and found that there was negligible difference.

2.6.5.2 Analytical semi-empirical approach

Several analytical/semi-empirical formulae to predict the local scour depth around abutments have been proposed, probably the most widely known of which are by Laursen (1962 & 1963). Laursen based his approach on treating the abutment as a limiting case of scour through a long contraction. The solution for the scour depth in the long contraction was modified for that of the abutment by assuming that the scour depth at the abutment would be a multiple (r) of the scour depth in an imaginary long contraction that had the same width as the scour hole. This width was assumed to be 2.75 times the scour depth at the abutment.

Based on the above assumption and on laboratory data, Laursen developed scour depth relations for abutments under both live-bed (Laursen, 1962) and clear-water conditions (Laursen, 1963).

For the case of live-bed conditions, Laursen developed the following equation

$$\frac{L_a}{Y_1} = 2.75\frac{y_s}{Y_1}\left[\left(\frac{y_s}{rY_1}+1\right)^{7/6}-1\right] \tag{2.23}$$

Laursen assumed the factor r to be 11.5.

From the above equation it is apparent that under live-bed conditions the scour depth depends only on the approach depth and the geometry of the contraction. The channel velocity and sediment size does not have a significant effect on the scour depth. Laursen argued that the channel velocity has no effect on the scour depth because as the velocity increases, not only does the amount of sediment that is being transported into the scour hole from upstream increase, but so too does the strength of the vortex responsible for transporting the sediment out of the hole (Laursen, 1962).

For the case of clear-water conditions, Laursen developed the following equation:

$$\frac{L_a}{Y_1} = 2.75\frac{y_s}{Y_1}\left[\frac{\left(\frac{1}{r}\frac{y_s}{Y_1}+1\right)^{7/6}}{\left(\frac{\tau_o}{\tau_{cr}}\right)^{1/2}}-1\right] \tag{2.24}$$

where

$$\frac{\tau_o}{\tau_{cr}} = \frac{U^2}{120d^{2/3}Y_1^{1/3}} \tag{2.25}$$

Laursen assumed the factor r to be 12.

As in the case for live-bed conditions, the scour depth under clear-water conditions was found to be a function of the approach depth and the geometry of the contraction; but unlike for live-bed scour conditions, the scour depth was also found to be a function of the average approach velocity and the sediment size. Laursen used the case of a long contraction to explain the fundamental difference between clear-water and live-bed scour conditions: "If one now considers a contraction of some given geometry, two widths and a depth of flow, it is possible for the velocity of flow to be so small that there is no movement of the sediment anywhere. At or below this velocity, that is dependent on the sediment size, there will be no scour, and the flow will behave as if there were a rigid bed. If the velocity is increased, but not to such an extent that there is sediment movement in the uncontracted approach, the contraction will scour. The limit of the depth of scour will be a velocity that will not move the bed sediment. For this case of clear-water flow in the long contraction, it is readily apparent that the velocity of the flow and the sediment size, as well as the geometry, will affect the depth of scour." (Laursen 1962)

Laursen recognised the importance of distinguishing between clear-water and live-bed conditions (Laursen, 1962). He found that not only did the prevailing mode of sediment transport in the approach channel influence the parameters that have an effect on the scour depth, but also recognised that at the threshold condition for clear-water scour, the scour depth produced is a maximum. At threshold conditions for clear-water scour $\tau_o / \tau_{cr} = 1$, thus Equation 2.24 can be expressed as the following:

$$y_s = 1.93(Y_1 L_a)^{1/2} \tag{2.26}$$

Laursen's equations are applicable to vertical abutments that are aligned perpendicular to the flow. A multiplication factor $K_{\theta(L)}$ can be applied to take into account the alignment of the abutment relative to the flow. This can be found in Raudkivi (1998).

Gill (1972) adopted a similar approach to that of Laursen in defining scour depth relations around a spur-dike. He modified Straub's equation for predicting scour in a long contraction and related it to the local scour around a spur-dike with the use of a coefficient. In Gill's analysis he used data for both clear-water and live-bed scour conditions and did not appear to distinguish between the two conditions. Gill found experimentally that the coefficient was a function of the approach depth and the size of the sediment. He also stated in his conclusion that it was unimportant to distinguish between clear-water and live-bed conditions for design purposes. Gill's equation for the prediction of the scour depth around spur-dikes is as follows:

$$\frac{y_s}{Y_1} = \varphi\left(\frac{B_1}{b_a}\right)^{6/7}\left[\left(\frac{B_1}{b_a}\right)^{1/3}\left(1-\frac{\tau_{cr}}{\tau_1}\right)+\frac{\tau_{cr}}{\tau_1}\right]^{-3/7} \tag{2.27}$$

where b_a is the width of the contracted channel caused by the abutment ($B_1 - L_a$), and

$$1-\frac{\tau_{cr}}{\tau_1}=0 \quad \text{for} \quad \frac{\tau_{cr}}{\tau_1}\geq 1$$

The coefficient φ was found to be dependent on the approach depth and sediment size and is expressed as the following:

$$\varphi = 8.375\left(\frac{d}{Y_1}\right)^{0.25} \tag{2.28}$$

Cunha (1973) and Zaghloul (1983) contested that Gill's approach and findings were erroneous. Cunha (1973) found an error in Gill's equations with respect to the effect that the length of the spur-dike has on the scour depth. Gill's equation, which can be used for both clear-water and live-bed conditions, shows that if all other conditions remain the same, an increase in the length of the spur-dike will always result in a decrease of the scour depth. Based on his own experimental analysis, Cunha found that under clear-water conditions, the scour depth is independent of the geometry of the contraction and is only affected when $(B_1 - b_a) / B_1 > 0.09$. He also found that under live-bed conditions, the local scour depth only becomes affected by the contraction geometry when the scour hole reaches the opposite bank.

Zaghloul criticised Gill for mixing the data of the clear-water and live-bed conditions and believed that this resulted in the sediment size being an important factor affecting the local scour depth. On closer inspection of Gill's data, Zaghloul found that for live-bed scour conditions under the same flow conditions and spur-dike geometry, the scour depth was almost identical for the two different sand sizes used in the experiments. He thus concluded that variations in the sediment size under live-bed conditions have no effect on the scour depth. This is consistent with the findings of Laursen (1962). Zaghloul also stated that he believed it to be important to distinguish between clear-water and live-bed conditions because the scour hole reaches its maximum depth under clear-water conditions.

Zaghloul (1983) developed his own empirical formula to predict the local scour depth around spur-dikes for conditions of clear-water scour. He first performed a dimensional analysis in order to determine the parameters that have a significant influence on the local scour depth and found these to be the contraction ratio, the alignment of the spur dike relative to the flow and the Froude number of the approach flow. These parameters were then verified with the use of experimental data. The sediment size was kept constant throughout the analysis and thus the effect of sediment size on the scour depth was not investigated.

Zaghloul concluded from the analysis of the experimental data with respect to the chosen parameters that the local scour depth is significantly affected by the approach Froude number and the opening ratio. Seeing that the approach Froude number is a function of the velocity and depth of the approach flow, it can also be said that the local scour depth is influenced by the channel velocity and the approach depth. These findings are consistent with those of Laursen (1963). Based on his findings, Zaghloul derived the following empirical formula:

$$y_s = 0.825\alpha_a^{-1}\theta^{0-0.043}q_1^{\frac{2}{3}} \tag{2.29}$$

where α_a = opening ratio $= (B_1 - L_a) / B_1$

The above formula appears to be close to the form of the regime equation of Ahmad, although Ahmad's equation applies to conditions of live-bed scour.

Lim adopted an analytical/semi-empirical approach for the determination of local scour depth prediction formulae around abutments under both clear-water (Lim, 1997) and live-bed conditions (Lim and Cheng, 1998(a)). Lim based his method of analysis on the fact that the projection of the abutment into the flow results in the increase of shear stress along the bed, thus subsequently resulting in local scouring around the abutment.

Under conditions of clear-water scour, Lim developed the following formula:

$$\frac{y_s}{Y_1} = 0.9\left\{(\vartheta_c)^{-0.375}(Fr_o)^{0.75}\left(\frac{d_{50}}{Y_1}\right)^{0.25}\left[0.9\left(\frac{L_a}{Y_1}\right)^{0.5}+1\right]\right\}-2 \tag{2.30}$$

In the preceding equation, ϑ_c is the critical Shield's parameter and Fr_o is the densimetric Froude number, the definitions of which are given below.

$$\vartheta_c = \frac{\tau_{cr}}{(\rho_s - \rho)gd_{50}}$$
(2.31)

$$Fr_o = \frac{U}{\sqrt{\left(\frac{\rho_s}{\rho} - 1\right)gd_{50}}}$$
(2.32)

In consideration of the above equations it is evident that the local scour depth around the abutment is a function of the approach depth, geometry of the opening, channel velocity (the densimetric Froude number is a function of the velocity), abutment alignment and the sediment size. These findings are consistent with those of Laursen (1963). When considering threshold conditions for a vertical abutment aligned perpendicular to the approach flow, Equation 2.29 can be simplified to:

$$y_s = 1.8\sqrt{Y_1 L_a}$$
(2.33)

This equation is in close agreement with Equation 2.26 (Laursen, 1962). It should be noted that a shape factor $K_{s(Lim)}$ can be incorporated into Equation 2.30 in order to take into account the influence of the abutment shape on the scour depth, the values of which are shown in Table 1 of Lim (1997).

Lim & Cheng (1998(a)) undertook a similar analysis of the scour depth under live-bed conditions, except in this case, a generalised bed-load transport relationship was included. The following equation was derived:

$$\left(1 + \frac{y_s}{2Y_1}\right)^{4/3} = \frac{1 + 1.2\sqrt{\frac{L_a}{Y_1}}}{\sqrt{\frac{u_{*cr}}{u_{*1}} + \left(\frac{L_a \tan\phi_r}{y_s} + 1\right)^{2/3}\left(1 - \frac{u_{*cr}}{u_{*1}}\right)}}$$
(2.34)

where u_{*cr} = critical shear velocity

u_{*1} = shear velocity in the approach channel

$$\tan\phi_r = 0.457\left(\frac{\sqrt{gd_{50}}\,d_{50}}{v}\right)^{0.05}\left(\frac{\gamma_s - 1}{\gamma_s}\right)^{0.106} SF^{-0.8}\sigma_g^{\;0.12} \tag{2.35}$$

where ϕ_r = angle of repose of sediment in water
γ_s = specific gravity of the sediment
SF = shape factor of the sediment particles
v = kinematic viscosity

Under live-bed conditions, Lim & Cheng thus found the scour depth around an abutment to be a function of approach depth, geometry of the opening, channel velocity (u_{*cr} / u_{*1} is a function of the velocity in the approach channel), and the sediment size. This is contrary to the belief of Laursen (1962) who concluded that the scour depth around an abutment is independent of the sediment size.

2.6.5.3 Dimensionless approach

Owing to the complexity of the flow around an abutment, many researchers have developed scour depth relations using the dimensionless approach. This approach involves the use of Dimensional Analysis in order to determine the dimensionless parameters that have a significant influence on the scour depth.

The variables that could be considered in a dimensional analysis can be grouped as the following:

i) *Variables describing the geometry of the channel and the obstruction*: width of the channel, B; bed slope of channel, S_o; upstream flow depth, Y_1; maximum scour depth, y_s; abutment length, L_a; alignment of the abutment relative to the flow, θ; and shape of the abutment, Sh.
ii) *Variables describing the flow:* mean approach velocity, U.
iii) *Variables describing the fluid*: mass density of water, ρ; specific weight of water, γ; dynamic viscosity, μ; and kinematic viscosity, v.

iv) *Variables describing the sediment*: sediment diameter, d; geometric standard deviation, σ_g; particle settling velocity, v_{ss}; shear stress, τ; and specific gravity, γ_s.

One of the earliest investigations on scour depth relations around an abutment using Dimensional Analysis was that of Liu et al. (1961). In their investigation Liu et al. combined Dimensional Analysis with laboratory data that was obtained under conditions of live-bed scour. Liu et al. recognised the approach depth, channel velocity and the abutment length and shape as the important parameters that affect the scour depth at the abutment. They expressed these relations in the following dimensionless form:

$$\frac{y_s}{Y_1} = K_{L(Liu)}\left(\frac{L_a}{Y_1}\right)^{0.4} Fr_1^{1/3} \tag{2.36}$$

where Fr_1 = approach Froude number
$K_{L(Liu)}$ = correction factor for the shape of the abutment
= 1.1 (streamlined abutments)
= 2.15 (blunt-nosed abutments)

Liu et al. recommended that in the case where dunes form on the natural river bed and thus move through the constriction, the resultant scour depth determined from Equation 2.36 should only be used to predict the equilibrium scour depth. For the determination of the maximum scour depth, however, the scour depth value as determined from the Equation 2.36 must be increased by 30%. Liu et al. also observed that for abutments with sloping faces ($1V:1.5H$), the resultant scour depths were 50-60% of those for vertical abutments.

Richardson et al. (1975) compared Liu et al.'s equation for scour depth at an abutment with field data that was obtained from dikes in the Mississippi River. He subsequently adjusted Liu et al.'s equation and expressed the maximum scour depth as:

$$\frac{y_s}{Y_1} = 4Fr_1^{1/3} \tag{2.37}$$

Also using a dimensionless approach, Garde et al. (1961) determined the following dimensionless parameters to have the most significant effect on the maximum dimensionless scour depth:

$$\left(\frac{Y_1 + y_s}{Y_1}\right) = f(\alpha_a, Fr_1, C_D) \tag{2.38}$$

where C_D is the average drag coefficient of the sediment and is defined by:

$$C_D = \frac{4}{3}\frac{(\gamma_s - \gamma)\, d}{v_{ss}{}^2 \rho} \tag{2.39}$$

Through experimental investigation, Garde et al. then found that the dimensionless scour depth can be calculated by the use of the following equation:

$$\left(\frac{Y_1 + y_s}{Y_1}\right) = K \frac{1}{\alpha_a} Fr_1{}^p \tag{2.40}$$

where K and p are a function of C_D and can be determined from Figure 12 shown in Garde et al. (1961).

Garde et al. reported that all experiments were performed under conditions of live-bed scour. They thus criticised the findings of Laursen (1962), commenting that under live-bed conditions, the sediment size and channel velocity have a significant influence on the local scour depth around an abutment, the exact opposite to the findings of Laursen. Zaghloul (1983), on the other hand, found both Garde et al.'s findings and their criticism of Laursen as erroneous.

On inspection of the experimental method adopted by Garde et al., Zaghloul commented that it appeared that the experiments, which were carried out in a non-recirculating flume, were performed under clear-water or nearly clear-water conditions. This would provide an explanation as to why the sediment size and the channel velocity were seen to be important parameters. Laursen, on the other hand, used a transport flume that would enable a much more accurate assessment of the parameters that affect the scour depth under live-bed conditions. Also when comparing the analysis and findings of that of Garde et al. (1961) and Zaghloul (1983), who analysed scour depth under clear-water scour conditions, it can be seen that they are very similar in nature. This also leads to the suspicion that Garde et al.'s analysis should be relevant for clear-water conditions as opposed to the stated live-bed conditions.

As for Liu et al. (1961), Froehlich (1989) also used Dimensional Analysis to determine the important factors that affect the scour depth around abutments under live-bed conditions. Froehlich then completed a regression analysis on 170 live-bed scour depth measurements and proposed the following dimensionless equation for the prediction of the local scour depth:

$$\frac{y_s}{Y_1} = 2.27K_1K_2\left(\frac{L_a}{Y_1}\right)^{0.43} Fr_1^{0.61} + 1 \tag{2.41}$$

Where K_1 = coefficient for the abutment shape (values can be read off table 8.8 in Hamill (1999))

K_2 = coefficient for the alignment of the abutment with respect to the flow, which is given by $(\theta / 90)^{0.13}$

Equation 2.41 is similar to that derived by Liu et al. (1961), and as for Liu et al., Froehlich recognised the approach depth, abutment length and channel velocity as the important factors that affect the scour depth under conditions of live-bed scour.

Arguably one of the most invaluable contributions to the subject of local scouring around abutments is that of Melville (1992, 1997). Melville analysed a large number of results on abutment scour from several studies completed at Auckland University and using this data, developed simple design equations that predict the maximum equilibrium scour at an abutment. Melville also contributed greatly to the understanding of the parameters that have the most pronounced influence on the scour depth around an abutment.

According the Melville (1992), the maximum equilibrium scour at an abutment can be expressed as

$$y_s = f(\rho, v, U, Y, \rho_s, d, \sigma_g, L_a, Sh, Al, G, g) \tag{2.42}$$

in which Al refers to the alignment of the abutment respective to the flow direction and G is the parameter that describes the effects of lateral distribution of flow and the cross-sectional shape of the approach channel.

Assuming a constant density of sediment and the absence of viscous effects, Equation 2.42 can be expressed in the following dimensionless forms:

$$\frac{y_s}{L_a} = f\left(\frac{U^2}{gd_{50}}, \frac{Y_1}{L_a}, \frac{d_{50}}{L_a}, \sigma_g, Sh, Al, G\right) \tag{2.43}$$

or,

$$\frac{y_s}{Y_1} = f\left(\frac{U^2}{gd_{50}}, \frac{L_a}{Y_1}, \frac{d_{50}}{Y_1}, \sigma_g, Sh, Al, G\right) \tag{2.44}$$

For the purpose of evaluation of the experimental data, Melville expressed the above equations in terms of *K*-factors that describe the influence of each parameter on the maximum scour depth:

$$\frac{y_s}{L_a} = K_I K_y K_d K_\sigma, K_s, K_\theta, K_G \tag{2.45}$$

and

$$\frac{y_s}{Y_1} = K_I K_y K_d K_\sigma, K_s, K_\theta, K_G \tag{2.46}$$

Where K_I = flow intensity factor, K_y = approach flow depth factor, K_d = sediment size factor, K_σ = sediment gradation factor, K_s = abutment shape factor, K_θ = abutment alignment factor and K_G = approach channel geometry factor.

The parameter U^2 / gd_{50} can be written as the ratio U / U_{cr} in which U_{cr} refers to the critical velocity of the approach channel. This ratio is a measure of the flow intensity and determines whether clear-water or live-bed conditions exist in the channel. Under clear-water conditions, Melville (1992) recognised that the scour depth was approximately proportional to the flow velocity and reached a maximum at the threshold condition where $U / U_{cr} = 1$. He also recognised that the maximum live-bed scour occurred at the threshold condition, beyond which the scour depth began to decrease with increasing velocity, and then eventually increase again towards the threshold depth. The data thus used in the analysis were taken at threshold conditions for clear-water scour because the scour holes that form under such conditions are found to be larger and deeper than those under live-bed scour conditions. According to Figure 7 in Melville (1992), $K_I = 1$ at threshold conditions, thus it can be said that effects of the flow intensity and thus the flow velocity was excluded from the analysis.

Ettema (1980) studied the influence that sediment size has on the scour depth for uniform sand around piers. He concluded that the scour depth is independent of the sediment size when the sediment is smaller than 1/50th of the width of the pier. Melville (1997) showed that this also held true for scour depths around abutments. Seeing that in practice and even in small-scale laboratory conditions, the abutment length is usually very long compared with the sediment size, Melville conducted his analysis for data that satisfied the condition $L_a / d_{50} \geq 50$. Melville also showed that this condition is applicable to both uniform and non-uniform sediment. Melville, however, chose only to apply his analysis to data collected for uniform sediment conditions as it is known that river beds consisting of graded or non-uniform sediment ($\sigma_g > 1.3$) produce lower scour depths than those consisting of uniform sediment (Raudkivi and Ettema, 1977). Melville excluded the affects of sediment size and gradation from his analysis of the maximum scour depth and thus assumed K_d and K_σ to be equal to unity. It should be noted that Melville only used the data for non-ripple forming sediment as the scour depths that develop for uniform ripple-forming sediment are less than those of non-ripple forming sand.

The effect of the approach geometry of the channel on the maximum scour depth at an abutment is included in the factor K_G. The value of K_G depends on the relative size, shape and roughness of the both the main channel and the flood plain channel, as well as the abutment length relative to the width of the flood plain. Unfortunately insufficient data was available to be able to quantify K_G and thus it was decided to set the value to unity. This is a conservative approach and is likely to result in excessively large scour depth predictions. The effect of the approach channel geometry was thus excluded from the analysis of scour depth around an abutment.

Melville based his analysis on the prediction of the maximum scour depth around vertical plate abutments aligned perpendicular to the flow, thus the effect of shape and alignment of the abutment could be excluded from the analysis. If the effects of the flow intensity, sediment size and gradation as well as the geometry of the upstream channel are also excluded from the analysis, the scour depth can be seen as independent of all influences except those of the approach depth (Y_1) and abutment length (L_a).

Melville (1992) plotted relationships between the equilibrium scour depth and the abutment length and the equilibrium scour depth and the approach flow depth. He derived the following equations that envelope nearly all the data:

$$y_s = 10Y_1, \text{ for } \frac{L_a}{Y_1} \geq 25 \text{ ("long" abutments)} \tag{2.47}$$

$$y_s = 2\sqrt{Y_1 L_a}, \text{ for } 1 < \frac{L_a}{Y_1} < 25 \text{ ("intermediate" abutments)} \tag{2.48}$$

$$y_s = 2L_a, \text{ for } \frac{L_a}{Y_1} \leq 1 \text{ ("short" abutments)} \tag{2.49}$$

Equation 2.49 shows that for a "short" abutment, in other words where the abutment only extends a short distance into the channel in relation to the depth of flow, the maximum scour depth scales with the abutment length and is independent of the approach depth. A study by Melville and Kwan (1994) showed that the principal vortex with its associated downflow component is primarily responsible for the development of the scour hole at the abutment. They also showed that for "short" abutments the principal vortex and downflow are concentrated inside the scour hole below the original bed level, thus rendering the downflow unaffected by changes in the approach flow depth. Melville (1997) stated that in deep flows, in other words at "short" abutments, the strength of the principal vortex and associated downflow at abutments are related to the transverse size of the abutment, thus rendering the scour depth dependent on the abutment length. Similar results can be seen for the scour depth around piers in relatively deep flows (Melville and Kwan, 1994). Melville and Kwan measured the velocity fields around a wing-wall abutment and concluded that the flow structure associated with the scouring process around an abutment is similar for that of piers of an equivalent shape to the abutment.

Equation 2.47 shows that for "long" abutments, in other words where the abutment extends a long distance into the channel in relation to the depth of flow, the maximum scour depth scales with the approach flow depth and is independent of the abutment length. One of the explanations that can be given regarding this result is by considering the effect that the "dead" water region, upstream of the abutment near the channel wall, has on the scour depth at the abutment. Kwan (1984) and Kandasamy (1989) (taken from Melville, 1997) found that the fluid within the region of "dead" water has no effect on the local scouring processes and, in fact, the outer limit of this "dead" water region demarcates the effective length of the abutment responsible for inducing local scouring. They also found that as the abutment length increases, the extent of the "dead" water region increases and thus the scoured region only extends part of the way along the abutment. Melville thus concluded that seeing that the scoured region does not extend right up to the channel wall, the maximum scour depth becomes less dependent on the abutment length, or in the case of a "long" abutment, independent of it.

Kandasamy (1989) offered another explanation for the independence of the scour depth on the abutment length for "long" abutments. He reported that at a "long" abutment, part of the flow that approaches the abutment is deflected parallel to the upstream abutment face and thus is ineffective in generating downflow ahead of the abutment. The scour depth therefore becomes proportionally reduced in terms of the abutment length and eventually becomes independent of it.

Finally, Ettema (1980) and Melville (1997) provided an explanation as to why the scour depth around a "long" abutment is dependent on the depth of flow. Ettema (1980), who considered local scouring effects around piers, explained that at shallow flows, the surface roller that forms upstream of the bridge pier interferes with the scouring action of the horse-shoe vortex as the two have opposite directions of rotation. As the flow depth increases, the interference is reduced until it eventually becomes insignificant. Melville (1997) showed this also to be relevant to "long" abutments, except that the roller interferes with the principal vortex upstream of the abutment, which is equivalent to the horse-shoe vortex at piers.

In practice, most abutments cannot be classified as either "short" or "long" and are in fact classified as having an "intermediate" length. The maximum equilibrium scour depth at abutments of "intermediate" length is influenced by both the abutment length and the approach flow depth, and is expressed by Equation 2.48. It should be noted that this equation is of a similar form to the equations 2.26 and 2.33, derived by Laursen (1962) and Lim (1997) respectively for the maximum equilibrium scour depth under clear-water conditions.

The effects of the abutment shape are included by the shape factor K_s, the values of which can be determined from Table 1 in Melville (1992). Melville (1992) determined that the importance of the shape of the abutment on the scour depth diminishes as the abutment gets longer because the effect of the shape on the channel bed is only felt at the end of the abutment. He also determined from consideration of the various shape factors that, for shorter abutments, the scour depth is reduced by streamlining the shape of the abutment. Melville thus recommended using adjusted shape factors K_s^* where

$$K_s^* = K_s, \text{ for } \frac{L_a}{Y_1} \leq 10 \tag{2.50}$$

$$K_s^* = K_s + (1 - K_s)\left(0.1\frac{L_a}{Y_1} - 1.5\right), \text{ for } 10 \leq \frac{L_a}{Y_1} \leq 25 \tag{2.51}$$

$$K_s^* = 1, \text{ for } \frac{L_a}{Y_1} \geq 25 \tag{2.52}$$

It should be noted that L_a / Y_1 = 25 is the limit of influence of the shape factor, in other words, the shape has no influence on the maximum scour depth for "long" abutments.

The effect of the alignment of the abutment relative to the flow is included by applying the alignment factor K_θ, the value of which can be read off from Figure 4 in Melville (1992). Melville (1992) found that the affect of the alignment on the maximum scour depth diminishes with the abutment length and thus recommended the following adjusted alignment factors:

$$K_\theta^* = K_\theta \text{, for } \frac{L_a}{Y_1} \geq 3 \tag{2.53}$$

$$K_\theta^* = K_\theta + (1 - K_\theta)\left(1.5 - 0.5\frac{L_a}{Y_1}\right)\text{, for } 1 \leq \frac{L_a}{Y_1} \leq 3 \tag{2.54}$$

$$K_\theta^* = 1 \text{, for } \frac{L_a}{Y_1} \leq 1 \tag{2.55}$$

In summary, the design equations proposed by Melville to predict the equilibrium maximum scour depth are as follows:

$$y_s = 10K_\theta Y_1 \text{, for } \frac{L_a}{Y_1} \geq 25 \text{ (“long” abutments)} \tag{2.56}$$

$$y_s = 2K_s^* K_\theta^* \sqrt{Y_1 L_a} \text{, for } 1 < \frac{L_a}{Y_1} < 25 \text{ (“intermediate” abutments)} \tag{2.57}$$

$$y_s = 2K_s L_a \text{, for } \frac{L_a}{Y_1} \leq 1 \text{ (“short” abutments)} \tag{2.58}$$

Ignoring the effect of sediment characteristics, lateral distribution of flow, and approach channel geometry, Melville has shown that for channels at the threshold flow intensity for clear-water conditions and of non-ripple forming uniform sediment, the maximum equilibrium scour depth at an abutment is a function of the abutment length and approach flow depth. Melville (1992) however warns the hydraulic engineer that the scour depth estimates obtained from this method will be inherently conservative and should be combined with engineering judgement when assessing the protection required against local scouring at an abutment.

2.6.5.4 Summary of the previous research on local scour depths around abutments

In consideration of the various approaches taken in the prediction of the scour depth around an abutment, it is apparent that the prevailing mode of sediment transport in the approach channel is a very important factor to consider when determining the parameters that can be seen to have the most influence on the local scour depth.

Under clear-water conditions, Laursen (1963) and Lim (1997) determined that the local scour depth around an abutment is dependent on the approach depth, the approach velocity, the geometry of the abutment and the sediment size. Zaghloul (1983) and Melville (1992), who excluded the effects of the sediment size on the scour depth from their analyses, drew the same conclusions for the other mentioned parameters. Although Melville excluded the effects of sediment size on the scour depth, he did recognise that the scour depth was reduced for non-uniform and/or ripple-forming sediment.

Laursen, Zaghloul and Melville also recognised that at threshold conditions under clear-water scour, the scour depth produced is a maximum and thus recognised the importance of considering this particular condition of scour when researching scour depths around abutments.

Ahmad (1953), Liu et al. (1961), Froehlich (1989) and Lim & Cheng (1998(a)) all concluded that under conditions of live-bed scour in the approach channel, the scour depth is dependent on the approach depth, approach velocity and geometry of the abutment. These findings were opposed by Laursen (1962) who found that the scour depth was in fact independent of the approach velocity and only dependent on the approach depth and geometry of the abutment. These findings by Laursen were also supported by research undertaken by Melville (1997) who stated that the dependence of the scour depth on the approach velocity as found by other researches was due to the lack of proper distinguishing between clear-water and live-bed scour.

2.7 Total scouring around abutments

Structures in rivers are exposed to both local and constriction scour. In most experimental studies performed around a structure in a river, the ratio between the obstructing length of the structure perpendicular the flow, and the approach width of the channel (contraction ratio) is kept very small (typically less than 0.1) in order to avoid the constriction effect on the local scour depth at the structure (Ballio & Orsi, undated). Cunha (1973), in fact, concluded that under clear-water conditions, the constriction effect on the local scour depth at an abutment can be considered negligible for contraction ratios, L_a / B_1, less than 0.09.

In practice, however, the obstructing length of the structure is frequently not small compared to the approach width, thus it can be expected that the average acceleration of the flow due to the contraction will affect the local acceleration of the flow around the structure.

It is the usual practice that when determining the total scour around a structure, the local scour and constriction scour depths are calculated separately and then added together (HEC-18, 2001), provided that they overlap (Hamill, 1999). For example, constriction scour may be added to the local scour around a pier or abutment to get the total scour in the vicinity of the structure, however the pier and abutment scour would not be added unless the two scour holes overlapped. This additive procedure to determine the total scour assumes that each component of scour occurs independent of the other, in other words, any mutual interaction is ignored. Investigations have shown, however, that this additive procedure might significantly overpredict the total scour at the structure (HEC-18, 2001; Ballio & Orsi, undated).

Ballio & Orsi (undated) performed an experimental analysis on the mutual interaction of local and constriction scour at an abutment by examining local scour at an abutment for different values of the contraction ratio (L_a / B_1). The aim of their investigation was to determine the effect that the contraction ratio has on the scouring process around an abutment and to evaluate the additive procedure typically used to calculate the total scour depth around an abutment.

The experiments were run at near threshold conditions. The abutments consisted of a plexi-glass prism with $L_a = 0.1$ m and $M_a = 0.4$ m, where M_a refers to length of the abutment parallel to the flow. The width of the channel was varied in order to attain various contraction ratios. Contraction ratios between 0.1 and 0.33 were mainly considered. One test was run for the contraction ratio of 0.5.

Experimental results showed that the scour patterns around the abutment, for the contraction ratios 0.1 to 0.3, under the same flow conditions, were geometrically similar, thus concluding that the effect of the various contraction ratios on the scour process is very limited. They observed that when the contraction ratio was increased by a factor of 3, in other words, from $L_a / B_1 = 0.1$ to $L_a / B_1 = 0.33$, there was only a 10% increase in the scour depth. The scour depth was seen to only be significantly affected for the contraction ratio of 0.5, where it was observed to be about 30% deeper than that for the other runs.

When comparing the experimentally measured values of the scour depths (inclusive of local and constriction effects) at the abutments to the calculated value obtained from the addition of the local and constriction components separately, Ballio & Orsi concluded that the simple addition of the separate scour components leads to a significant overestimation of the total scour depth (up to 300%). The reason for this is that under clear-water conditions, constriction scour equations predict the depth of scour based on the average transport condition in the contracted reach, in other words, the average point at which critical conditions for incipient motion is considered to be reached across the entire contracted area. When local scouring occurs around an abutment, however, the transverse area of the scour hole next to the abutment becomes much larger than the general area across the contraction after a relatively short time. Through the principle of continuity, the average velocity next to the abutment will decrease, within a short period of time, until the flow condition in the local scoured area reaches below the critical incipient motion condition. At this point, constriction scour will no longer take place around the abutment, although it will still be taking place in the rest of the contracted reach. It is therefore obvious that if the calculated constriction scour depth, which is obtained from considering the average transport conditions across the contraction, is added to the calculated local scour at the abutment, the total scour would be an overprediction of the true value. The assumption that the constriction and local scour depth can be linearly superimposed on one another is thus not conceptually sound.

2.8 Protection measures

Local scouring around fluvial structures has been known to cause the undermining of the foundations of the structure and subsequent failure, especially during flooding events. Thus one of the most important considerations to a hydraulic engineer is that of the protection of the river bed around fluvial structures against local scouring effects.

The most effective way to ensure that the structure is sufficiently protected from the effects of scour is to design the structure so that its foundations are well below the maximum level to which the bed would be scoured. Another measure that can be taken at the design stage is to design streamlined structures that are aligned so as to minimise the obstruction to the flow, for example, angling the structure downstream with respect to the flow.

With existing structures, however, that are found to be suffering from local scour effects, to deepen the foundations of the structure becomes an expensive and difficult operation. In this case, the most economical method of in-situ protection is the use of riprap (Hamill, 1999). This method of protection generally involves the pre-excavation of the area that is found to be influenced by local scouring and then the filling of the area with hard durable dense angular rock (riprap). The use of riprap as a protective measure has the advantage that it is cost effective (rocks in the area can be used), durable, easy to place, easy to repair and recoverable if the stones should be moved from their positions (Hamill, 1999). It should also be noted that if the use of riprap is included in the design stage of a structure, the foundations could be designed with shallower depths than those predicted by the various available equations (HEC-18, 2001).

Other less common forms of protection that can be used around an existing structure include the following:

i) Soil-cement mixtures using the soil around the structure. This method is used for very small structures only.
ii) Gabions, which involve the placement of stones in wire baskets.
iii) Sand and cement filled sacks. This method is used for very small structures only.

iv) Precast cellular concrete blocks. This is known to be an expensive method in comparison to the use of riprap.

v) Geotextile mattresses that consist of stones wrapped in geotextile material.

Chapter 3
Experimental Apparatus

3.1 Introduction

This chapter describes the apparatus used in the experimental investigation of the initial local scouring around a rectangular "long" contraction. A description of the flume in which the experiments were performed is given as well as the devices that were installed in the flume for the removal of turbulence and contaminants. The test area of the flume in which the experiments were performed is defined and the two PVC long contraction insert sections of varying opening ratios are described. The type of sediment used along the bottom of the flume is discussed including the method with which it was evenly dispensed into the flume. Finally, the apparatus employed for the measurement of the approach flow, temperature, approach depth and the extent of the scouring around the contraction is described in detail.

3.2 The flume

The experiments were conducted in a tilting flume of rectangular cross-section that was situated in the hydraulics laboratory at the University of Cape Town. The flume was approximately 18 m long, 610 mm wide and 550 mm deep (Figure 3.1). The floor and walls of the flume were made of glass. For these experiments the bed slope, S_o, was made equal to zero, in other words, the bed was horizontal. Parallel steel rails were located on top of the flume walls, which were stripped of paint, cleaned and polished. A thin layer of grease was also applied to the rails to protect the rails from corrosion.

Water was supplied to the flume via a constant head tank through a 150 mm diameter steel pipe into a steel stilling basin and thence into the flume. A butterfly valve situated on the inlet pipe was used to control the flow rate. A gate valve situated downstream was used to stop the supply of water into the flume whenever the same flow rate was required the following day. In this case, the butterfly valve was not closed.

At the downstream end of the flume the water flowed over a tailgate and into a sump, from whence it was returned to the constant head tank via two sump pumps. The tailgate was also used to adjust the depth of water in the flume and was operated via an electric motor.

There were various other additions made to the flume: a V-notch weir was installed downstream of the flume inlet for the measurement of the flow; sheets of wire gauze and a flow guide were installed for the removal of turbulence and straightening of the flow; two fine wire screens were installed to act as a filter for any contaminants in the flow; and a test area was prepared in which the long contraction insert section was positioned. These are discussed in more detail below.

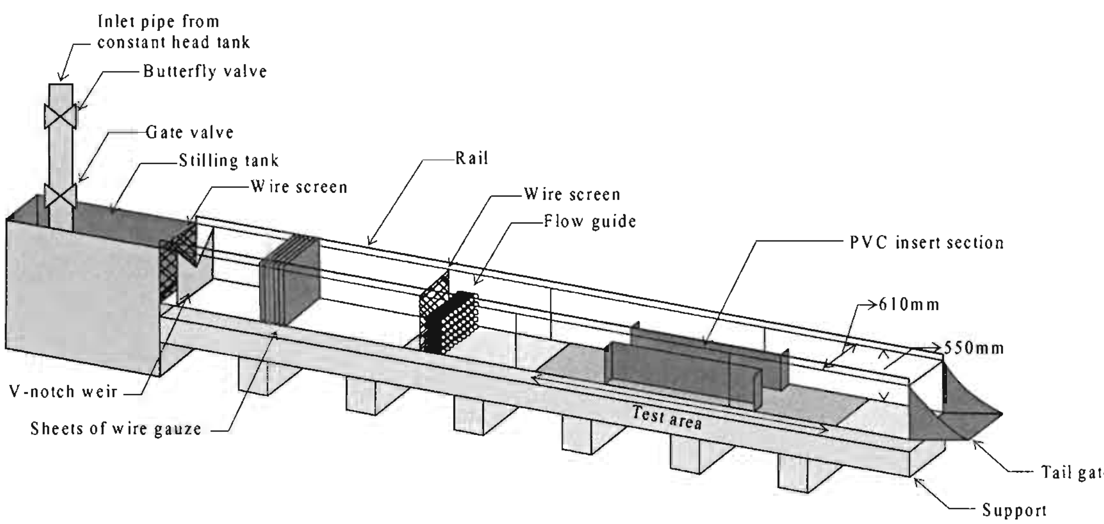

Figure 3.1: Diagram of the flume used in the investigation

3.3 Flow measurement

The flow measuring device used was a V-notch weir positioned immediately downstream of the flume inlet. The dimensions of the weir are given below in Figure 3.2. The V-notch weir was constructed from a steel plate of 6 mm thickness with a 90° notch angle. The weir was mounted on a wooden frame that was sealed to the sides of the flume with silicone.

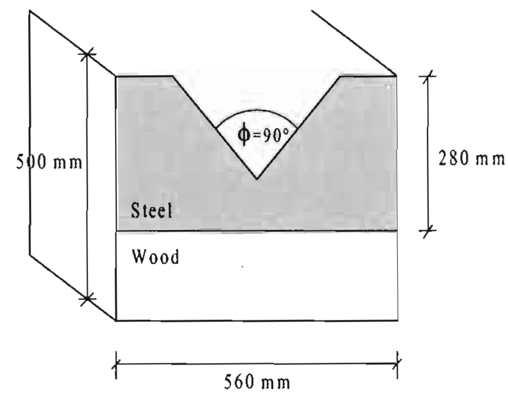

Figure 3.2: Diagram of the weir inserted into the flume

The equation of flow for a V-notch weir is as follows (Chadwick and Morfett, 1993):

$$Q = \frac{8}{15} C_d (2g)^{1/2} \tan(\phi) h_v^{5/2} \tag{3.1}$$

Where Q = flow rate (l/s)
C_d = coefficient of discharge
g = gravitational acceleration (9.81 m/s^2)
ϕ = angle of notch
h_v = overflow height upstream of the V-notch weir (m)

The coefficient of discharge was taken to be 0.58 as recommended by Beckerath (1992).

On applying the numerical values to the equation, the final equation becomes:

$$Q = 1370 h_v^{5/2} \tag{3.2}$$

The effective range of the weir was found to be 1 – 20 l/s.

3.4 Turbulence control

Large flow disturbances were created by the outflow of water from over the weir into the channel. Disturbances were also created by the interaction of the fluid with the boundary layers along the walls. These disturbances could cause the rotation of the sediment as it passed down the channel and the pulling of the sediment towards the sidewalls. The following measures were thus taken to reduce the turbulence in the flow and to ensure relatively straight streamlines near the test section area:

i) Several sheets of wire gauze were placed parallel to each other and to the flow just downstream of the weir. Not only did these sheets help dissipate the excess energy of the incoming flow, but they also created a surface on which air bubbles could adhere and thus be removed from the flow.

ii) A flow guide (Figure 3.3) was installed in the flume approximately 4.1 m upstream of the test area and 5.3 m from the long contraction insert section. This was seen to be sufficient area over which any disturbance to the flow would diminish before reaching the long contraction. The flow guide was comprised of LDPE irrigation pipes (150 mm long with an internal diameter of 20 mm) neatly piled on top of one another in such a way that the gaps between them were minimised. The flow guide was built up to a height of approximately 330 mm, in order to exceed the height of the insert section. A wooden platform, on top of which weights were placed, was placed on top of the pipes to ensure the stability of the flow guide.

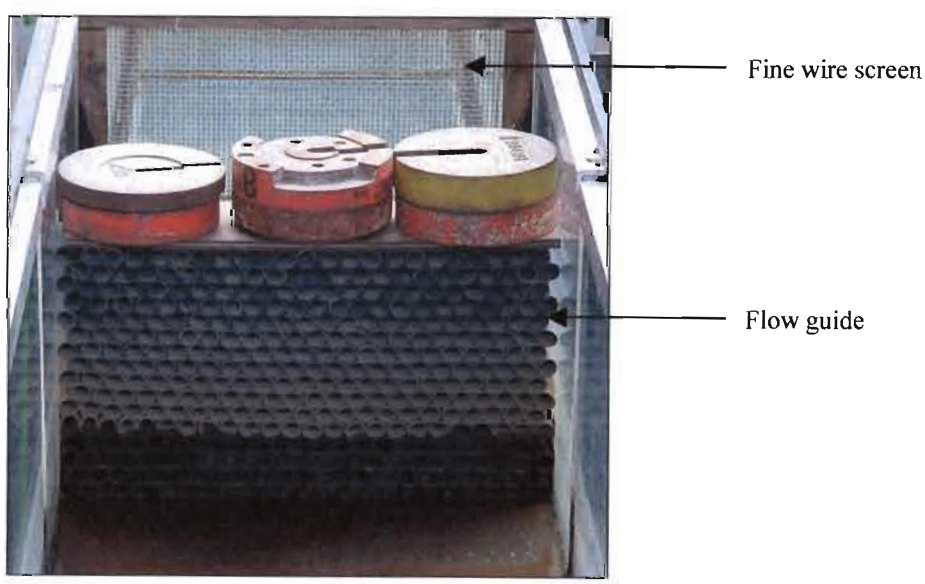

Figure 3.3: Photograph of the flow guide

3.5 Contamination control

The removal of contaminants, such as sand particles or suspended debris, from the flow was seen as necessary in order to prevent the movement of these contaminants through the test section during the running of the experiments as this could upset the behaviour of the sand. It was also found necessary to remove the sand from the sump so as to protect the pump impellers from abrasion. The following measures were thus taken:

i) To prevent the movement of contaminants carried by the flow through the test area, two fine wire screens were installed: one at the downstream end of the stilling basin and the other just upstream of the flow guide (see Figure 3.3). The screens acted as a filter for any particles present in the water.

ii) A "flow guidance structure" (Figure 3.4) was placed just downstream of the tailgate over the entrance of the sump. The walls of the structure were made of wood and the bottom from shade cloth. Not only did the "flow guidance structure" direct the fast moving flow from over the tailgate into the sump area, but also the cloth bottom provided an initial filter for sand moving through and out of the flume.

Figure 3.4: Photograph of the flow guidance structure

iii) The underdrain into which the water from the flume entered had two passages leading to the main sump from where the water was drawn up by the pumps. In order to prevent the sand from reaching the main sump, one passage of the underdrain was dammed up using sand filled bags while the other passage was intercepted by two wire screens covered with shade cloth. The underdrain therefore acted like a dam thereby allowing the sand to settle out, while water filtered by the shade cloth passed through the screens and entered into the main sump. In the cases where the flow was high, a plastic pipe was placed between the sand bags high up in the dam wall so as to prevent flooding.

3.6 Long contraction insert section

The test area in the flume started approximately 12.9 m downstream of the flume inlet and extended a further 3 m downstream. An insert section representing a rectangular "long" contraction was installed 1.2 m downstream from the start of this test area. The section could be correctly termed a "long" contraction because the length of the contracted reach parallel to the flow was made equal to the width of the approach channel. The contraction was described as rectangular because the entrance and exit corners of the contraction formed right angles.

The long contraction section consisted of six PVC walls: four walls, of the same dimensions, placed perpendicular to the flow to make up the upstream and downstream faces of the long contraction (L_c); and two walls placed parallel to the flow to make up the length of the contracted section (M_c). The long contraction was designed in this manner so that the opening ratio $((B_1 - 2\,L_c) / B_1)$ could be altered by simply interchanging the different walls, in other words, by varying the length L_c. Only two opening ratios were considered for use in this investigation, $\alpha_c = ¼$ and $\alpha_c = ½$. The PVC walls (15 mm thick × 300 mm height) were machined to precise tolerances so that when the sections were assembled, the joins between the different PVC walls were flush, and the heads of the countersunk screws used to join them were flush with the surface of the sections. This was to prevent any disturbance to the flow condition around the sections. The dimensions of the "long contraction" insert sections used in the experimental procedure are displayed in Figure 3.5.

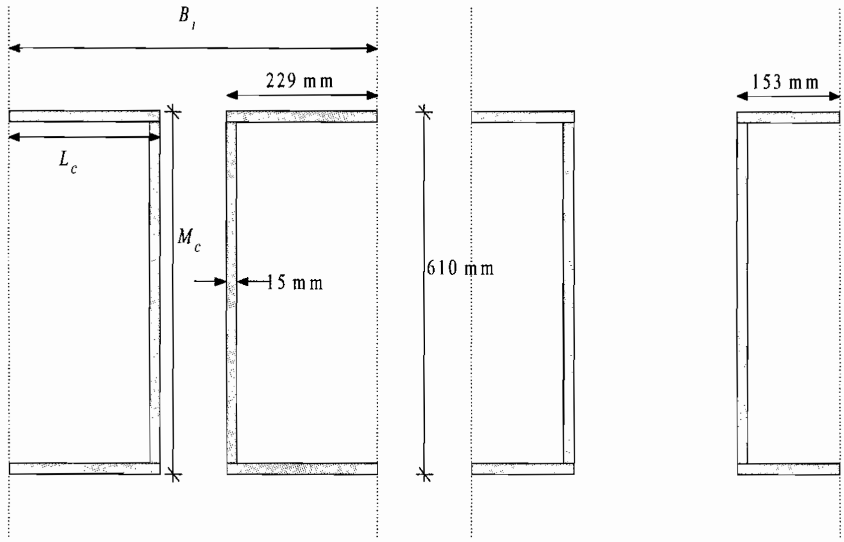

Figure 3.5: Plan view showing dimensions of the long contraction insert sections

Originally the insert sections were made out of varnished waterproof plywood. The use of the wood, however, proved to be problematic as it is a hydrophobic surface, and bubbles of air attached themselves to the insert section as well as the sand around it. These bubbles were seen to hinder the movement of the sand thus interfering with the experimental results. The use of PVC as the material for the insert section provided a smooth surface that was hydrophilic and thus did not attract the formation of bubbles. It was also easier to machine and to install, and its surface required no preparation with respect to waterproofing.

The PVC sections making up both sides of the long contraction were first assembled and then adhered to the bottom and the sides of the flume using silicone. The silicone also acted as a sealant preventing the movement of any water beneath the sections. A steel T-square was used to position the sections perpendicular to the surface of the flume. This also ensured that the upstream and downstream faces of the long contraction were positioned perpendicular to the direction of the flow, while the contraction length was parallel to the flow direction. The two assembled sections were placed opposite one another by using a steel ruler supported by a steel block that was held flush against the sides of the sections.

Although the bottom of the flume was made of glass, there were steel seams that ran across the bottom at regular intervals. This created a varying roughness along the bottom that could disturb the scouring processes around the insert section. It was thus decided to install a sheet of waterproofed hardboard ((7320 mm × 609 mm × 3 mm) along the bottom of the flume on top of which three sheets of glass, 2.44 m in length and 3 mm thick, were placed adjacent to each other. A glass surface was chosen as it is a hydrophilic surface and will not promote the formation of bubbles that could hinder the movement of the sand around the contracted section. This glass section extended from 5.5 m upstream of the insert section to approximately 1.2 m downstream of the section, in other words, to the end of the test area. The hardboard and glass sheets were glued to the bottom of the flume using silicone. Silicone was also placed between the edges of the hardboard and glass sheets and the side of the flume to prevent the entrance of any water. The silicone was left to dry after which it was trimmed using a sharp blade. The surface was then cleaned of any excess silicone using acetone. It was essential to ensure that all excess silicone had been removed from the glass surface as silicone is a hydrophobic surface and thus can promote the formation of bubbles.

3.7 Sediment

Quartzitic sand of the size range 600-850 μm was used in the experiments, with an average diameter of 725 μm. This sand range was chosen on the basis that it is reasonably uniform with a geometric standard deviation $\sigma_g < 1.3$ (Melville, 1997), non-ripple forming ($d_{50} > 0.7$ mm - Hamill, 1999; HEC-18, 2001; Melville, 1997) and satisfies the condition $L_c / d_{50} \geq 50$ (Melville, 1997).

The geometric standard deviation was calculated using Equation 2.11. As the exact percentage sizes of the sand range could not be calculated due to limited measuring apparatus, $d_{84.1}$ was taken to be 850 μm and $d_{15.9}$ to be 600 μm giving $\sigma_g = 1.19$ which represents a conservative value.

A similar problem was encountered when calculating the median diameter (d_{50}), which is used to determine whether or not the sand is ripple-forming. According to Yang (1996) the median diameter is calculated from the average of the $d_{15.9}$ and $d_{84.1}$ values. Taking the same approach as above, a conservative value of d_{50} was calculated and found to be 0.725 mm. The sand can thus be considered as non-ripple forming as it satisfies the condition $d_{50} > 0.7$ mm. Although this condition is only just satisfied, it was observed during the experimental process that no ripples formed in the sediment layer.

A thin layer of sand was spread evenly across the test area of the flume with the use of a custom made sand-spreader (Figure 3.5). The sand spreader consisted of a PVC bucket (1) with metal side plates (2) connected to a moveable metal frame (3). The frame was fitted with wheels that ran along rails on both sides on the flume. The PVC bucket was constructed with a spring-loaded gate (4), which was prevented from opening by a cam-bar (5). A push-rod (6) was connected to the cam-bar via a rotating pin, which, when pulled upwards, caused the cam-bar to move off-centre in an anti-clockwise direction, thus allowing the gate to open. A slot was machined in the push-rod so that in its locked position, the gate (7) opened a distance of 2.8 mm. The gap between the metal side plates and the spring-loaded gate was designed such that it was not too narrow that the swinging motion of the gate was restricted, nor too wide so that sediment became lodged in the gap thus hindering movement.

A reversible 12V DC motor (8), mounted on top of the spreader, provided a maximum speed of 64 rpm at 12V and controlled the movement of the device along the rails. The motor was controlled by a stabilised variable dual DC power supply providing 5V or 0-30V at 3A. The motor was connected to a 50 mm diameter drum (9) wrapped with a 3 m length of steel wire (10). The wire was attached to a bracket downstream of the test section on top of the flume. The spreader was pulled downstream across the test section through the rotation of the drum.

The sand-spreader was constructed so that it would pass over the insert section with a 10 mm clearance. Appendix A contains the engineering drawing of the sand-spreader.

(a) Oblique view

(b) Top view

Figure 3.6: Photographs of the sand-spreader

3.8 Depth measurements

The elevation of the water surface and the sand bed was measured using a Vernier Depth Gauge that was located along the centre line of the flume, and that travelled along the parallel horizontal rails located on top of the sidewalls of the flume.

Two Vernier Depth Gauges were used in the experiments. One for the measurement of the water depth and bed elevation at selected points across the test section, and the other to measure the water surface elevation in the stilling tank upstream of the weir in order to calculate the overflow height.

3.9 Temperature measurements

The temperature of the water was recorded during the experiments with an ordinary laboratory mercury thermometer.

3.10 Scour extent measurements

The aim of this thesis was to investigate the initial local scouring around a rectangular long contraction. This was accomplished by measuring the edge of the scoured region, in other words, the lateral extent of scour at various measuring points around the contracted section in the flume. It was essential that when measuring the lateral extent of the scour hole around the long contraction, the measuring apparatus would not interfere with the flow conditions around the structure, in other words, the apparatus could not extend into the depth of flow. A laser-pointer rig was thus built which could measure various scour positions effectively without causing a disturbance to the flow.

The laser-pointer rig (Figure 3.7) consisted of a laser-pointer (1) connected to an adjustable vernier rod (2) (allowing movement in the z-direction), which could move along a square iron bar (3) via four V-rollers (allowing movement in the x-direction) that were held in place by a thick steel plate (4). The V-rollers (5) were used to eradicate any play in the movement of the vernier across the iron bar. This was required as it was essential that the laser-pointer returned to precisely the same measuring points along the scour extent numerous times throughout the experiment. For the same reason, the laser-pointer was locked tightly into place using glue, so that the position of the light point on the bed would not change during any of the experiments. The iron bar was attached to a steel frame (6) that allowed the laser-pointer rig to move along the rails on either side of the flume via rollers (allowing movement in the y-direction).

A steel measuring tape (7) was extended across the laser-pointer rig above the square iron bar. An additional steel measuring tape (8) was also attached to the side of the flume along one of the rails. A pointer was attached to the top of the steel plate and to the side of the laser-pointer rig in such a way that they lined up precisely with the light point emitted from the laser pointer. This enabled the exact position of the light point to be expressed in terms of an x and y co-ordinate.

To achieve a better accuracy of measurement, the size of the light point emitted onto the bed surface from the laser-pointer had to be reduced. This was achieved by fitting a PVC cap (9) to the end of the laser-pointer. A fine hole was drilled in the centre of this cap. The size of the light point was thus reduced to an acceptable 1 mm point. A recess was machined into the cap to allow the laser to be switched on and off.

Appendix A contains the engineering drawing of the laser-pointer rig.

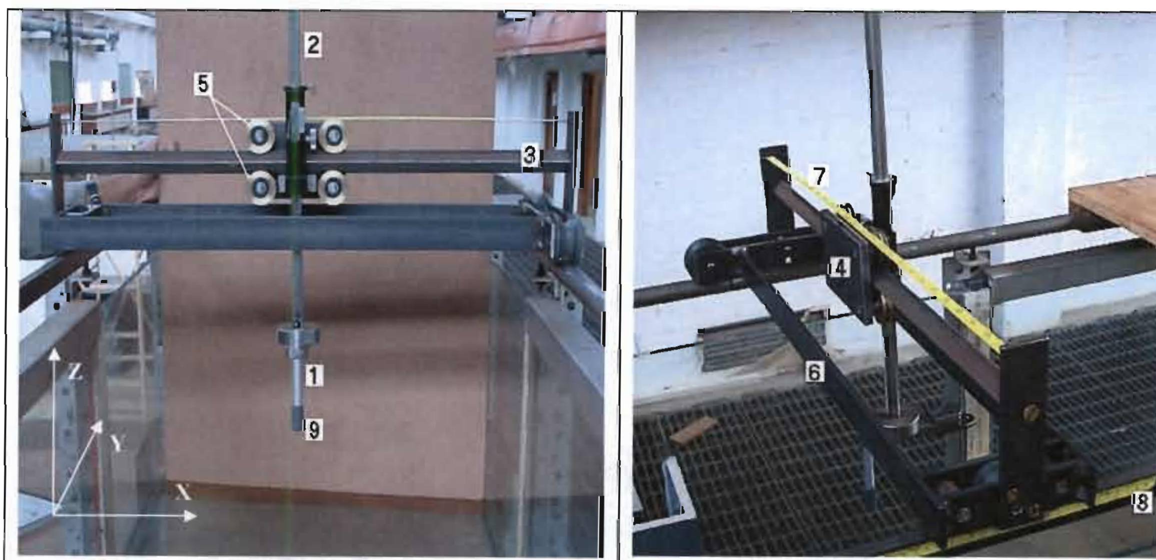

(a) Front View

(b) Oblique View

Figure 3.7: Photographs of the laser-pointer rig

Chapter 4
Experimental Method

4.1 Introduction

Experimental work was undertaken to investigate the initial local scouring around a rectangular "long" contraction in an open channel under clear-water scour conditions. The experiments involved the measurement of the lateral extent of scour at certain chosen measuring points both upstream and downstream of the long contraction. All of the experiments were performed in a rectangular laboratory flume under sub-critical flow conditions ($F_r < 1$). A thin even layer (approximately 1.6 mm) of uniform non-ripple forming quartzitic sand was placed on the bottom of the flume in order to set the roughness condition for the experiment. The removal of this sand also acted as an indicator of the scour.

This chapter describes both the experimental preparation and procedure for the experiments performed in this investigation. The preparation of the bed and the setting up of the experiments are described. This is followed by a description of the establishment of the flow rate and flow depths of the experiments, as well as the actual measurement procedure undertaken. Finally the selected measuring points at which the scour measurements were taken are also described in detail.

4.2 Experimental preparation

4.2.1 Preparation of the bed

A layer of sand was laid over the test area in the flume, starting 1.2 m upstream of the long contraction and extending 3 m through the contracted section and further downstream. The function of the sand layer was to set the roughness condition for the experiment and to indicate scour.

Initially the sand was distributed across the dry test section by hand, but this created a sand layer of varying thickness. This is comparable to a sand layer containing bed forms, which is associated with ripple-forming sediment. It was necessary, however, that the sand be non-ripple forming as it is known that the local scour depth (and thus scour extent) around a structure will be less for a bed of uniform ripple-forming sediment than that of uniform non ripple-forming sediment. A smooth bed would also limit disturbances to the scouring process. It should be noted that an attempt was also made at distributing sand into the flume by hand just upstream of the long contraction while the water in the flume was flowing. This proved unsuccessful, however, as the sand was washed away quickly by the rapidly accelerating flow around the contraction. A large amount of sand would thus have to be used around the upstream face of the long contraction in order to achieve an adequate definition of the scour pattern.

It was for the above reasons that the sand-spreader described in Section 3.7 was used to ensure an evenly distributed thin layer of sand throughout the test section. Also by using the sand spreader, consistency in the experimental set-up could be achieved. This was important as in this investigation comparisons of the measured scour extent values were required to be made between the different experiments.

4.2.1.1 Sieving of the sand

To obtain the size range of the sand chosen for use in the experimental process, namely 600-850 μm, the sand was passed through two sieves of the different mesh sizes, which were placed on top of each other and vibrated on a vibrating table. The sand that passed through the 850 μm sieve but was retained on the 600 μm sieve was used during the experimental process.

4.2.1.2 Thickness of the sand layer

The thickness of the sand layer was made thick enough to cover the bottom of the flume, but thin enough so as to reduce the time required for the extent of the scour around the long contraction to reach equilibrium. This was especially true for the measuring points downstream of the long contraction section. The most effective sand thickness was found to be about twice the diameter of the largest sand grain (850 μm).

4.2.1.3 Steps using the sand-spreader

i) The rails of the flume were examined to ensure that they were free of water or sediment. This was required to ensure that no sand adhered to the wheels of the spreader, causing the sand-spreader to vibrate while depositing the sand, resulting in a rippled bed.

ii) The 5V power supply was connected in reverse polarity to unwind the steel wire wrapped around the drum, so that the spreader could be moved to the desired position just upstream of the test area, in other words, approximately 1.2 m upstream of the contracted section.

iii) The interior of the bucket was examined to ensure that it was dry. The opening was also checked to ensure it was completely clear, and that no sediment was lodged between the side plates and the spring-loaded gate of the bucket.

iv) The sand spreader was closed by pushing the lever downwards to its furthest position. The bucket was then filled with clean, dry sand up to a marked level.

v) The DC motor was then provided with an input voltage of 30V so that the spreader could be pulled forward over the test section.

vi) As the sand-spreader reached the beginning of the test area, the lever of the sand-spreader was pulled upwards so that the gates of the bucket opened and sand was released at a constant rate over the full width of the flume.

vii) When the sand-spreader reached the end of the test section, in other words, approximately 1.2 m downstream of the contracted section, the gates of the bucket were closed by pushing the lever downwards completely, and the motor controller was deactivated.

It should be noted that a small build up of sand occurred along the upstream face (perpendicular to the flow) of the long contraction. This build up was not removed as this could lead to different conditions on either side of the contraction as well as between the different runs. Therefore, for the sake of consistency, the sand was left as it was. This could imply that any scouring in the area adjacent to the upstream faces of the contraction would take longer to stabilise than had it been the same thickness as the surrounding sand. It should also be noted that a thin sand-less strip existed along the downstream face of the long contraction. This area was filled in with a light layer of sand so that the scour extent could be indicated along this face.

4.2.2 Selection of flow and depths

To ensure that that clear-water scour conditions existed around the upstream face, within the contracted reach, and downstream of the contraction section, the depth in the contracted reach was considered as the limiting depth. This is because, for a particular flow rate, the velocity within the contracted reach would be greater than that in the approach channel owing to the reduction in area (continuity). Thus if sediment movement within the contracted reach was negligible so that clear-water conditions existed downstream of the contraction, it would automatically imply that the movement of the sediment in the approach channel to the contraction would also be negligible. This results in clear-water conditions around the upstream face and within the contracted reach of the contraction. The flow rates and approach depths chosen to be used in the experimental process were thus limited by the lowest possible depth within the contracted reach below which live-bed conditions would exist in the region downstream of the contraction, and the height of the long contraction section which was 300 mm. Conditions were also chosen so that a sufficient amount of scouring would occur in the region downstream of the contracted section. All of the experiments were performed under sub-critical flow conditions. The calculation process undertaken for the selection of the flow and depths is discussed in Chapter 5 and selected results are presented in Chapter 6.

4.2.3 Filling flume once the sand has been spread

Once a thin, even layer of sand had been laid across the test section, the bed surface elevations were measured at certain intervals upstream of the contracted section, and the flume was carefully filled with water to the approximate depth of flow selected for that particular experiment. These preparations were made the night before the running of the experiment such that the time taken to set up the actual conditions of the experiment on the following day would be greatly reduced. The following procedure was followed:

i) The Depth Gauge Vernier was employed to measure the elevation of the bed at 15 mm intervals from the upstream face of the long contraction to the upstream end of the test section (1.2 m upstream of long contraction).

ii) The tailgate was then closed so that the flume could be filled.

iii) As the test area was slightly raised above the remainder of the flume bed due to the installation of the hardboard and glass, the lower sections were first filled with approximately 30 litres of water. This was necessary to ensure that when the water started to flow from the upstream, it would not accelerate over the edge of the test area, thus causing a disturbance to the sand bed.

iv) The pumps were primed and switched on.

v) The butterfly valve was opened slowly to allow a very small flow of water into the flume (approximately 0.03 *l*/s). This was necessary to limit the scouring around the long contraction before the conditions for the experiment had been set up.

vi) This flow rate was maintained for approximately 30 minutes until there was a flow depth of about 30 mm in the flume.

vii) The flow was then increased to 1.0 *l*/s to allow the water to flow into the flume until the depth of flow was approximately 10 mm less than the required depth for the experiment.

viii) The butterfly valve was closed, and the pumps were switched off.

4.3 Experimental procedure

4.3.1 Establishment of the flow rate and flow depth

The flow of the water in the flume and the depth of flow in the contracted region of the long contraction were established using the following procedure:

i) The Depth Gauge Vernier was placed over the centre of the contracted section of the long contraction and set to the required depth by adding the necessary depth of flow to the previously measured bed elevation at that point.

ii) The Depth Gauge Vernier upstream of the V-notch weir was also set to the required height above the invert of the weir in order to mark the desired flow.

iii) The butterfly valve was then opened slowly to allow a low flow through the flume.

iv) As the water surface in the flume approached the required depth, the tailgate was slowly lowered so that the depth of flow remained just above the required depth for the experiment.

v) The flow was then repeatedly increased in conjunction with the lowering of the tailgate until the desired flow had been reached. This was achieved when the surface of the water upstream of the weir just touched the bottom point of the Depth Gauge Vernier.

vi) Once the required flow had been reached, the tailgate was then lowered slightly to the desired depth which was indicated by the water surface just touching the bottom point of the Depth Gauge Vernier.

vii) The time at which the correct flow and depth had been reached was recorded.

viii) The water surface elevations were measured above the same positions where the bed elevation measurements were taken using the Depth Gauge Vernier.

It should be noted that scouring frequently started around the contracted section before the desired depth and flow had been reached, but as the flow was always maintained above the required depth, the bed could not have scoured to a larger extent that when it was at its desired depth, and thus this method was considered acceptable for the purpose of this investigation.

4.3.2 Measurement procedure

4.3.2.1 Measuring points

The lateral extent of the scour was measured at the following measuring points (MP) as shown in Figure 4.1 below:

i) MP 1: Furthest point of the scoured region upstream of the contracted section towards the side-walls of the flume.

ii) MP 2: Most upstream point of the scour region, almost in line with the upstream inner corners of the contracted section.

iii) MP 3: Scour position in line with the upstream faces of the long contraction.

iv) MP 4: Scour position at the edge of the scoured region located approximately centrally within the contracted reach of the contracted section.

v) MP 5: Scour position located at half the width of the contracted reach (½ b_c) downstream of the downstream inner corners of the contracted section.

vi) MP 6: Scour position located $1b_c$ downstream of the downstream inner corners of the long contraction.

vii) MP 7: Scour positions located ¼ b_c downstream of the downstream inner corners of the long contraction.

To determine the lateral extent of the scour at each measuring point, two measurements were taken on either side of the centre-line (line of symmetry) of the flume and averaged. This method was undertaken so as to eliminate the impact of asymmetry introduced by the section. See Section 5.4 for a more detailed discussion on the averaging of the scour extent values.

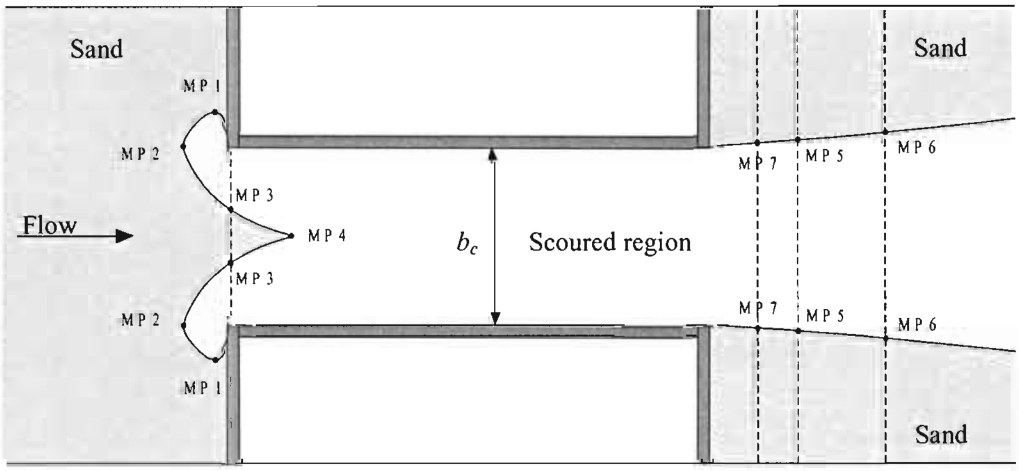

Figure 4.1: Diagram showing the measuring points (MP 1-7)

4.3.2.2 Experimental measurements

The measurements of the scour extent around the contraction were undertaken in the following manner:

i) The co-ordinates of the four inside corners of the long contraction were recorded using the laser-pointer rig. These co-ordinates acted as the reference points from which the scour extent measurements were offset.

ii) After the first hour of the experiment, the co-ordinates of the scoured region corresponding to the various chosen measuring points were measured using the laser-pointer. The temperature was then recorded. This process was repeated hourly over the entire test period.

It should be noted that before the co-ordinates of the extent of scour at the various measuring points were taken for each hour, the light beam of the laser pointer was lined up with a pre-established target point. This ensured that the laser-pointer rig was returned to the exact location of the chosen measuring points where the progression of the scour was being measured.

iii) At the end of the test period, the butterfly valve was closed and the pumps were turned off reducing the flow to zero.

iv) The full scour pattern around the long contraction was recorded by means of a sketch.

v) The tailgate was then lowered allowing the water in the flume to run out.

vi) The sand in the test section was then removed, dried out and resieved to remove any contaminants that may have been present. The sand could then re-used.

vii) The flume was flushed out and then swept clean to remove any sand, contaminants or dust.

viii) The flume was then left to dry out.

It should be noted that although the majority of the experiments were run over a continuous 12-hour period, some of the experiments were run over longer (13-15 hours) or shorter periods (6 hours) during the initial trial and error process of the experimental procedure. The experiments run over the longer period were in fact run over two days. The measured scour values obtained from the 6-hour and two-day runs were considered and some of the experiments were selected to be used in the analysis (See Section 5.5).

Chapter 5

Calculation Method

5.1 Introduction

This chapter provides a detailed description of the various calculation procedures that were used in this investigation. The boundary between clear-water and live-bed conditions is defined for the purpose of this thesis. A step-by-step description of the calculation procedure used to determine the experimental conditions for which clear-water conditions would occur throughout the contraction is then laid out.

The procedure used to extrapolate the scour measurements to the equilibrium values is then presented. Finally, the calculation procedure used in the analysis of the results of the experiments is described. A dimensional analysis approach was undertaken to identify the possible parameters that might have an influence on the initial local scouring around a long contraction.

5.2 Definition of clear-water/live-bed conditions for the purpose of this thesis

One of the most important aspects of this investigation was the distinction between clear-water and live-bed conditions. Clear-water scour is defined in the literature as occurring when no sediment is supplied from the approach channel to the scoured region, in other words, the particles along the bed upstream of the scoured region are at rest (Komura, 1966; Zaghloul, 1983; Breusers & Raudkivi, 1991; HEC-18, 2001). Live-bed conditions, on the other hand, exist when there is a general movement of particles along the bed in the approach channel thus resulting in a sediment input into the scour region (Raudkivi, 1998; Breusers & Raudkivi, 1991). It is important to distinguish between the two scour conditions as it has been shown in previous research to have a significant effect on the development of the local scour hole around the structure, as well as on the choice of parameters to be used to describe the scouring process.

It is common practice in the literature to make use of a simplified incipient motion model, particularly in terms of the critical average flow velocity (Hamill, 1999; Lim, 1997; Melville, 1992 & 1997; Raudkivi, 1986; Graf, 1998) and the critical bed shear stress (Laursen, 1962 & 1963; Komura, 1966; Breusers & Raudkivi, 1991; Raudkivi, 1998). Basically, if the average flow velocity or bed shear stress upstream of the scoured region is greater than the critical value, live-bed scour conditions exist, and if they are less than or equal to the critical value, clear-water conditions exist. This approach in defining incipient motion and thus the existing scour condition, however, has been seen to be problematic due to the highly stochastic nature of the movement of particles at incipient motion conditions. Theoretically, particle movement can take place under any flow condition, thus in order to compare meaningfully the results of local scouring around structures for conditions of clear-water and live-bed scour, a critical intensity of motion, *I*, needs to be defined.

Clear-water conditions assume no movement of particles upstream of the scoured region. In practice, however, clear-water scour conditions could be more accurately described in terms of a negligible movement of particles along the bed. This negligible movement can be compared to Kramer's (1935) definition of "weak" motion, which he defined as being the movement of a few or several of the small particles at isolated areas along the bed such that the number of particles moving across 1 cm^2 area could be visually counted. Shvidchenko & Pender (2000) defined "weak" movement as occasional particle movement at some locations along the bed and associated this movement with an intensity of motion of $I = 10^{-4}\,s^{-1}$ (one of 10 000 particles is entrained every second). On the other hand, live-bed scour can be described in terms of the general movement of sediment particles along the bed upstream of the scoured area. According to Kramer (1935), "general" movement of particles along a bed refers to when all the particles up to and including the largest particles are in motion at all locations of the bed. Shvidchenko & Pender (2000) described "general" movement as the frequent movement of particles at many locations along the bed and associated this movement with an intensity of motion of more than $I = 10^{-2}\,s^{-1}$ (one of 100 particles is entrained every second).

Considering the above definitions of the movement of sediment, it was decided for the purpose of this thesis to define the dividing line between clear-water and live-bed conditions as corresponding to an intensity of motion $I = 10^{-3}\,s^{-1}$ (one of 1000 particles is entrained every second). This intensity of motion can be seen to broadly correspond with Kramer's (1935) definition of "medium movement" of sediment which refers to the condition at which the motion of the particles of mean diameter is too large for them to be visually counted, but not strong enough to result in an appreciable sediment discharge. Therefore when the sediment upstream of the scoured region has an intensity of motion below $I = 10^{-3}\,\mathrm{s}^{-1}$, it can be said that scour conditions tend more towards that of clear-water where the maximum scour extent will be reached at static equilibrium. At any intensity of motion above $I = 10^{-3}\,\mathrm{s}^{-1}$, it can be said that scour conditions tend more towards that of live-bed where the maximum scour extent will be reached at dynamic equilibrium.

5.3 Calculation of the conditions of the experimental procedure

In this laboratory investigation the flow rate and depth of flow were chosen such that clear-water conditions existed around the upstream face, within the contracted reach and downstream of the long contraction. Clear-water conditions were chosen as it has been shown in the literature that the maximum scour depth occurs under conditions of clear-water scour, and thus most of the available research only considers this condition. Also, it was desired that constriction scour did not occur in the contracted section of the long contraction so that only local scour effects on the bed around and downstream of the long contraction could be investigated. Lastly, clear-water conditions were chosen for convenience, as this condition was easier to model.

To ensure that clear-water conditions existed for the various chosen flows and depths, the approach developed by Armitage (2002) to describe incipient motion was used. This approach is based on the Movability Number (u_* / v_{ss}) and the particle Reynolds Number (Re_*). This approach was chosen as Armitage derived a plot of the Movability Number versus the particle Reynolds Number in which he defined curves of varying intensities of motion. The curve representing $I = 10^{-3}\,\mathrm{s}^{-1}$ was chosen as the boundary between live-bed (above the curve) and clear-water (below the curve) scour conditions. It should be noted that although the experiments in this investigation fell within the transitional boundary zone ($3 < Re_* < 70$), the experiments could be seen to fall wholly within the turbulent boundary zone as defined by Armitage. In his approach, Armitage defined turbulent conditions to occur for $Re_* > 6.23$.

Incipient motion criteria based on one-dimensional flow does not take into account the influence of the side-walls of the channel. A side-wall correction was thus required to be made to the laboratory results. The side-wall correction was incorporated by Armitage (2002) in his approach through the use of the "Einstein method" (Einstein, 1942; Shen, 1962; Chien and Wan, 1999), the Darcy-Weisbach equation, and the Barr (1975) approximation of the Colebrook-White equation (Colebrook & White, 1937). Three assumptions are pivotal when using this method (Armitage, 2002):

i) The cross-section of the channel may be divided into three zones, one producing the shear along the bed and the other two producing the shear on the walls. The boundaries between the zones are considered as surfaces of zero shear and are not included in the wetted perimeters.

ii) The formulae for open channel flow are applicable to each zone as though it was a channel by itself.

iii) The average velocity and energy slope in each zone are equal to the average velocity (U) and friction slope (S_f) for the whole section.

The following steps were used in the calculation procedure of the Movability Number and the particle Reynolds Number:

i) A flow rate and flow depth was selected.

ii) As a first approximation, the cross-sectional area affected by the bed (A_b) was deemed by Armitage (2002) to be delimited by the bed, two lines 45° to the bed drawn from each corner, and the included water surface (Figure 5.1a). The initial approximation of the cross-sectional area affected by the walls (A_w) was thus the remainder of the area. An initial estimate of the hydraulic radius associated with the wall zones, which is defined as $R_w = A_w / P$, could then be calculated based on a first approximation of the cross-sectional area affected by the walls and the wetted perimeter associated with the walls, $2Y$.

The above approach to determine an initial estimate of R_w is only relevant where the depth of flow (Y) is less than half the width of the flume (B_f). In the case where $Y \geq B_f / 2$, however, the initial approximation of the cross-sectional area affected by the bed becomes delimited by the bed and the two lines 45° to the bed drawn from each corner that intersect at a height of $B_f / 2$ (Figure5.1b). The initial approximation of the cross-sectional area affected by the walls will thus also change accordingly.

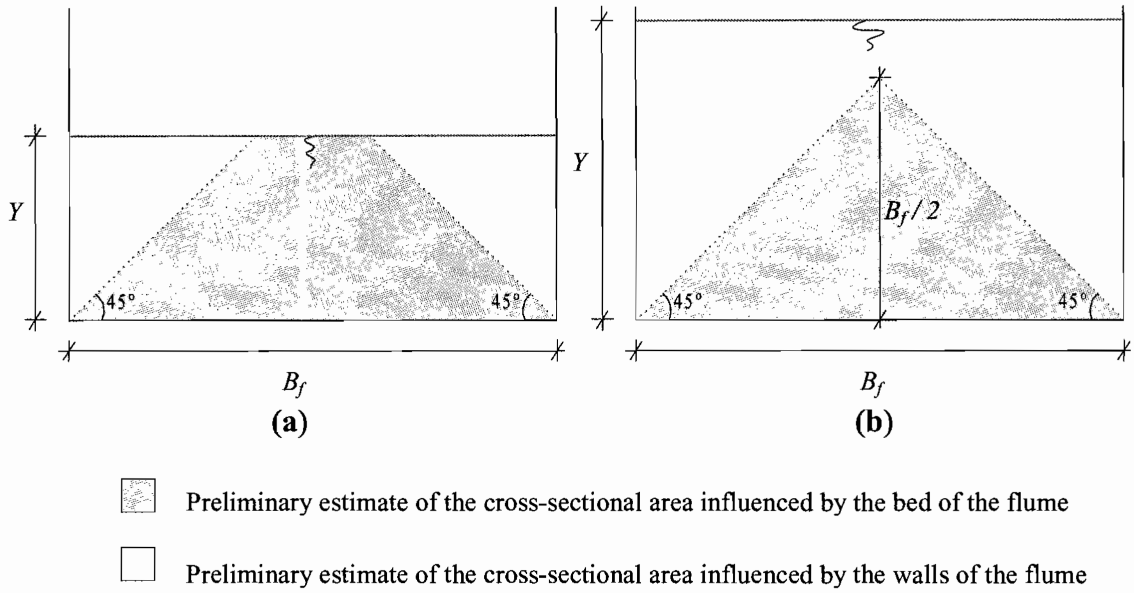

Figure 5.1: Diagram showing the preliminary estimate of the cross-sectional areas influenced by the bed and walls of the flume for (a) $Y < B_f / 2$ and (b) $Y \geq B_f / 2$

Based on the above deductions, an initial estimate of the hydraulic radius associated with the wall zones may thus be obtained from the following equations:

$$R_w = \frac{Y}{2} \quad \text{, for } Y < \frac{B_f}{2} \tag{5.1}$$

and

$$R_w = \frac{B_f}{2} - \frac{B_f^{\,2}}{8Y} \quad \text{, for } Y \geq \frac{B_f}{2} \tag{5.2}$$

iii) The hydraulic radius associated with the bed zone, R_b, was then calculated from R_w for any value of Y using the following equation derived by Einstein (1942):

$$R_b = Y\left(1 - 2\frac{R_w}{B_f}\right) \tag{5.3}$$

iv) The flow Reynolds Numbers for both the wall (Re_w) and the bed (Re_b) zones were then calculated using the following equations:

$$Re_w = \frac{R_w U}{\nu} \tag{5.4}$$

$$Re_b = \frac{R_b U}{\nu} \tag{5.5}$$

v) The Colebrook-White formula approximated by Barr (1975) allows the computation of the Darcy-Weisbach friction factor, λ_f, in pipes. Armitage (2002) further adapted Barr's equation with the use of the identity $d_p = 4R$ (where R refers to the hydraulic radius of the channel), so the equation would be applicable to open channel flow. The equation adapted from Barr is as follows:

$$\frac{1}{\sqrt{\lambda_f}} \approx -2\log\left\{\frac{k_r}{14.8R} + \frac{1.49336}{Re}\right\} \tag{5.6}$$

where Re = flow Reynolds Number $= \dfrac{RU}{\nu}$

The friction factors applicable to the wall λ_{fw} and the bed λ_{fb} were thus calculated by inserting the relevant parameters into the above equation. The roughness height, k_r, for the bed region was taken as the average of the two mesh sizes (600 and 850 µm) used in the sieving process of the sediment, in other words, 725 µm. The roughness height of the glass wall region was taken as 0.005 mm (Armitage, 2002).

vi) The friction slope can be determined using the Darcy-Weisbach equation:

$$S_f = \frac{\lambda_f U}{8gR} \tag{5.7}$$

Seeing, however, that the friction slope in each zone is equal to the friction slope for the whole section, the following identity holds true:

$$\frac{\lambda_{fb}}{R_b} = \frac{\lambda_{fw}}{R_w}$$

(5.8)

If Equation 5.8 was satisfied, the initial estimation of R_w was correct. If the equation was not satisfied, however, a higher or lower value of R_w was estimated (guided by the outcome of the above identity) and steps iii) to vi) were repeated until the equation was satisfied to the nearest 1 mm on the estimate of R_w.

vii) Once the correct values of λ_{fb} and R_b had been calculated, S_f was calculated using Equation 5.7. The shear stress u_* could thus be calculated using the following formula:

$$u_* = \sqrt{gR_bS_f}$$

(5.9)

viii) The settling velocity was calculated using the equation derived by Cheng (1997):

$$v_{ss} = \frac{v\left(\sqrt{25 + 1.2d_*^{\,2}} - 5\right)^{1.5}}{d}$$

(5.10)

In Equation 5.10 the dimensionless particle size, d_*, was calculated from:

$$d_* = \left(\frac{\Delta g}{v^2}\right)^{1.3} d$$

(5.11)

where the relative submerged density, Δ, was calculated from the equation:

$$\Delta = \frac{(\rho_s - \rho)}{\rho}$$

(5.12)

The kinematic viscosity, v, was calculated using the equation presented by Yang (1996):

$$\nu = \frac{1.79\times10^{-6}}{\left(1.0+0.0337T+0.000221T^2\right)} \tag{5.13}$$

where T is the temperature in degrees Celsius.

ix) The Mobility Number, u_* / v_{ss}, could thus be calculated whilst the particles Reynolds Number was calculated from:

$$Re_* = \frac{u_* d}{\nu} \tag{5.14}$$

x) The Movability Number and the particle Reynolds Number for the selected rate of flow and depth was plotted on the Liu-type diagram devised by Armitage (2002) (Figure 5.2). If the calculated point lay below the line defined by $I = 1\times10^{-3}\,\mathrm{s}^{-1}$, clear-water conditions were considered to exist and the chosen flow and depth was acceptable for use in the experimental process. If the point, however, lay above the line, live-bed conditions were considered to exist and the chosen flow and depth had to be disregarded and another flow and depth selected.

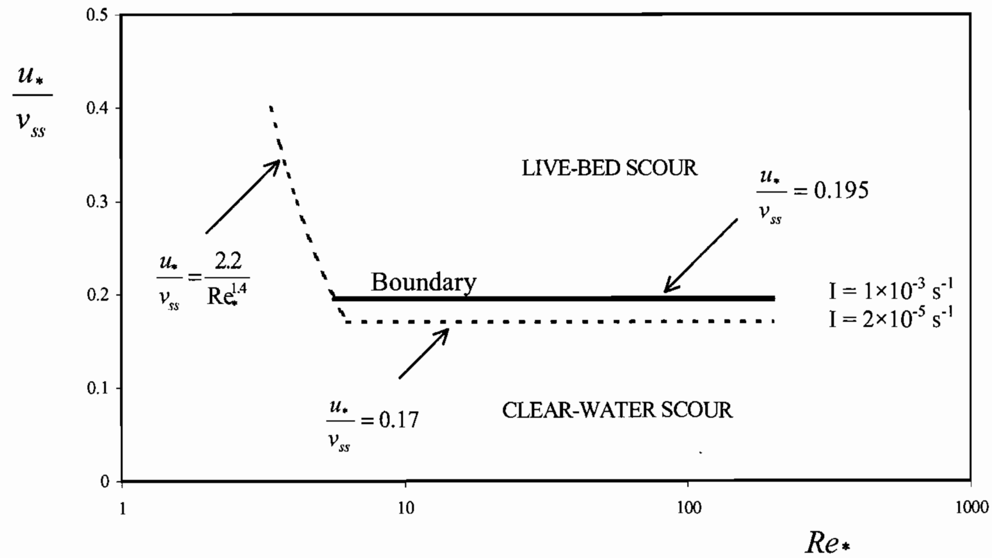

Figure 5.2: Graph showing the boundary between clear-water and live-bed conditions (adapted from Armitage (2002))

The above described process for the calculation of the Movability Number and particle Reynolds Number was performed for the contracted region of the long contraction section only. The reason for this is that if at a particular flow rate the intensity of motion of the sediment within the contracted reach is below $I = 1\times10^{-3}\,\mathrm{s}^{-1}$, then it would automatically imply that the sediment in the approach channel to the contraction would also have an intensity of motion less than $I = 1\times10^{-3}\,\mathrm{s}^{-1}$ (due to the larger geometry of the channel). Clear-water conditions would therefore exist throughout the long contraction, in other words, around the upstream face, within the contracted reach and downstream of the contraction. Also by ensuring an intensity of motion below $I = 1\times10^{-3}\,\mathrm{s}^{-1}$ within the contracted reach, this would eliminate complications caused by constriction scour.

5.4 Calculation of the average lateral extent of scour (scour extent), w_{save}, for each measuring point

At every hour during an experimental run the co-ordinates of the scour extent at the various measuring points on either side of the contracted section were measured using the laser-pointer rig. These co-ordinates were then entered into an Excel spreadsheet and the actual scour extent calculated by comparing the measured values to the chosen reference values (origins of the contracted section). The scour extent values corresponding to the same measuring points on either side of the long contraction were then averaged to obtain the final scour extent values at these points for each hour over which the experiment was run. The contracted section was designed to be symmetrical about the centre-line of the flume, thus it is expected that symmetrical scour patterns would result. The averaging of the scour extent value was however found to be necessary due to slight asymmetries in the scour pattern around either side of the section.

5.5 Selection of experiments to be used in the analysis

Once the averaged scour extent values had been calculated, it was then necessary to relate these averaged scour values in terms of an equilibrium scour value. In this investigation, the experiments were originally run over a duration of 6 hours. It was observed, however, that for most of these runs, the lateral extent of the scour at the downstream measuring points was not close to stabilising within this period, making it very difficult to predict the equilibrium scour extent values. It was therefore decided for these experiments to include only the data obtained for the upstream measuring points where equilibrium conditions prevailed, and to exclude the data for the downstream measuring points. It was then decided to run the experiments over a period of two days (13 – 15 hours with a break in-between). It was observed that for some of the experiments, the starting of the pumps on the second day caused a sudden increase in the scour extent values at all of the measuring points after which the scour values immediately stabilised. Since it was thought that the sand might have become over-scoured in the process, these experiments were excluded from use in the analysis. Finally it was decided that the experiments would be prepared on the first day and run for a continuous 12 hour period on the second day. All of the experiments run over a 12 hour period were included in the analysis.

5.6 Calculation of the equilibrium scour extent, w_s

In determining the value of the equilibrium scour extent at the selected measuring points around the contracted section, two different methods were employed at the measuring points upstream (MP 1,2,3) and downstream (MP 5,6,7) of the contraction.

5.6.1 Upstream measuring points

Owing to the strong vortical action and accelerating flow around the upstream face of the contracted section, the light point emitted onto the bed in this region from the laser-pointer rig was sometimes diffracted by the uneven water surface and did not accurately locate the scour edge. In these instances, the measurements taken by the laser-pointer could only provide an indication as to whether areas of the scoured region around the upstream face had in fact reached equilibrium within the experimental period. If it was found that equilibrium had been reached, the values of the scour extent at the various measuring points were measured using the laser pointer rig after the experiment had been stopped, in other words, under conditions of zero flow. These measurements were then entered into the Excel spreadsheet to determine the average scour extent values. The resulting averaged values were thus considered as representative of the equilibrium scour extent value. If it was found that equilibrium had not been reached within the experimental period, the scour extent values for the experiment were disregarded from the analysis.

5.6.2 Downstream measuring points

In the region downstream of the contracted section, the disturbance to the beam of light from the laser pointer rig by the flow was negligible. The averaged scour extent values obtained for the downstream measuring points could therefore be used with confidence for the prediction of the equilibrium scour extent values, had equilibrium conditions not been reached within the duration of the experiment.

For the downstream measuring points, equilibrium was considered to be reached when the averaged scour extent values were within 0.5 mm of one another for at least 3 consecutive hours. If equilibrium had in fact been reached, the scour extent values within 0.5 mm of one another were simply averaged to determine the final equilibrium value.

For the case where the averaged scour extent did not reach equilibrium within the experimental period, a curve represented by the following exponential function

$$w_{save} = a\left(1 - \exp^{-bt}\right) \tag{5.15}$$

was fitted to the data, where w_{save} is the averaged scour extent, t is time, and a and b are constants. This function was selected as its form closely approximates the observed temporal development of the scour extent which can be seen to initially increase rapidly and thereafter slowly approach an asymptotic value (maximum equilibrium scour extent, w_s).

Statistica Version 5.0 was used to fit this function to the data. A non-linear estimation procedure was selected in which the exponential function was specified. The following estimation methods: quasi-Newton, Simplex, Simplex quasi-Newton, Hooke-Jeeves, Hooke-Jeeves quasi-Newton, Rosenbrock, Rosenbrock quasi-Newton, were employed to fit the curve to the data. The curve given by the estimation method that was judged to best fit the data was selected to give the maximum equilibrium value of the scour extent (Figure 5.3). For an infinite time, the asymptotic equilibrium scour extent value is given by the constant a in Equation 5.15.

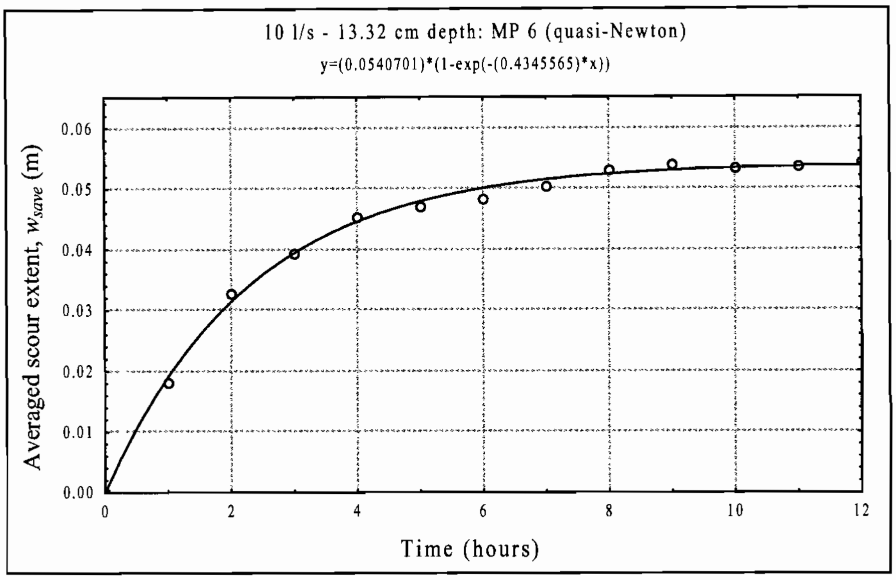

Figure 5.3: Example of a best-fit curve to the scour data at one measuring point

Sand scoured from the upstream area and the contracted region of the long contraction moved through the area downstream of the long contraction before being washed away by the flow. This sand migration affected the averaged scour extent values at the downstream measuring points by causing a reduction in their values until the sand had cleared and the scouring process could continue unhindered. This presented a particular problem for the lower flows where it took longer for the sand to clear. In the cases where the averaged scour extent values were affected by the migrating sand over a significant period of time, Statistica often underestimated the equilibrium scour values (Figure 5.4). Under these circumstances, the disturbed scour data was disregarded from the data set to give a better approximation of the maximum equilibrium scour extent value (Figure 5.5).

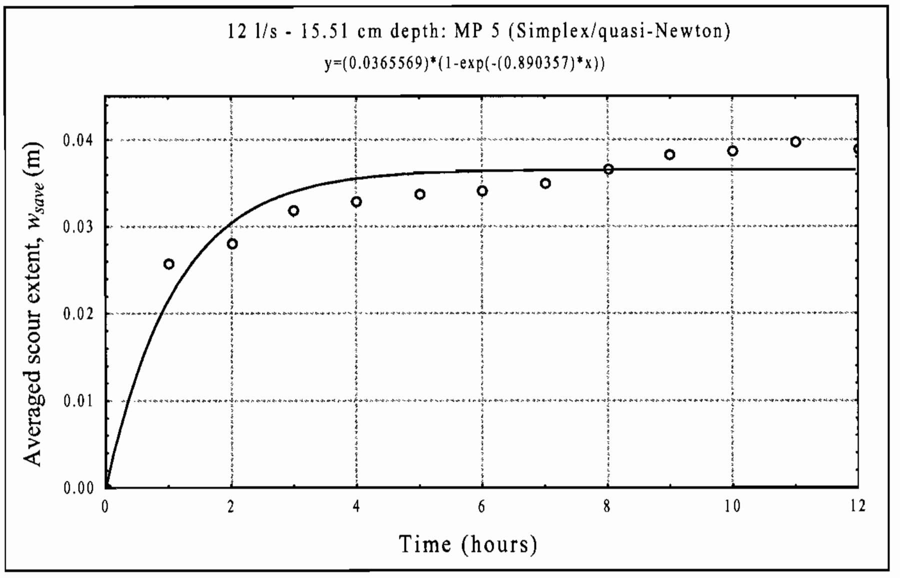

Figure 5.4: Figure showing an example where Statistica underestimated the equilibrium scour extent value

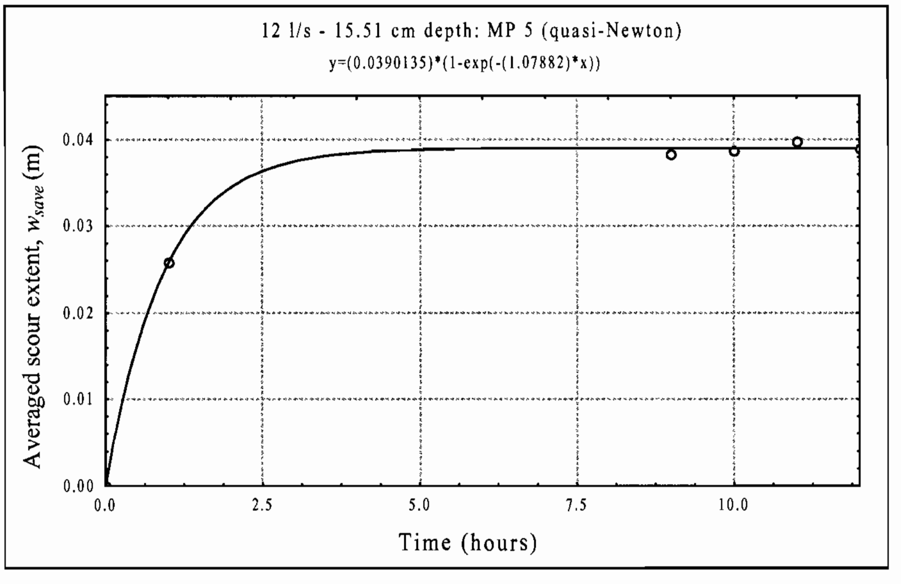

Figure 5.5: Figure showing an example where disturbed scour values were excluded to obtain a better approximation of the equilibrium value

If the averaged scour extent values appeared to be fluctuating throughout the experimental period (Figure 5.6), the original data set was not altered when using Statistica to predict the maximum equilibrium scour extent value.

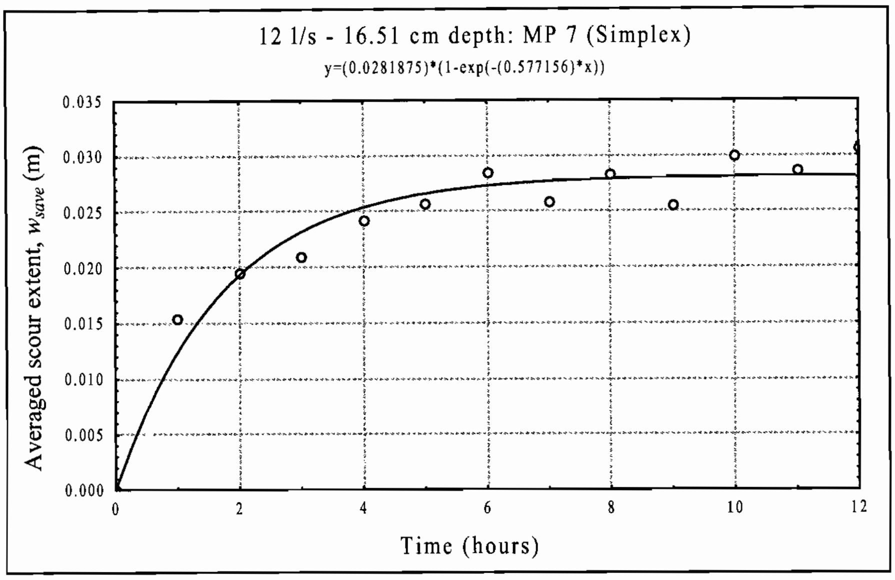

Figure 5.6: Diagram of fluctuating scour data between the 5th and 12th hour

On occasion the data set was so poor that Statistica could not be used to predict the maximum equilibrium scour value with confidence (Figure 5.7). These averaged scour extent values at the various measuring points were thus excluded from the analysis.

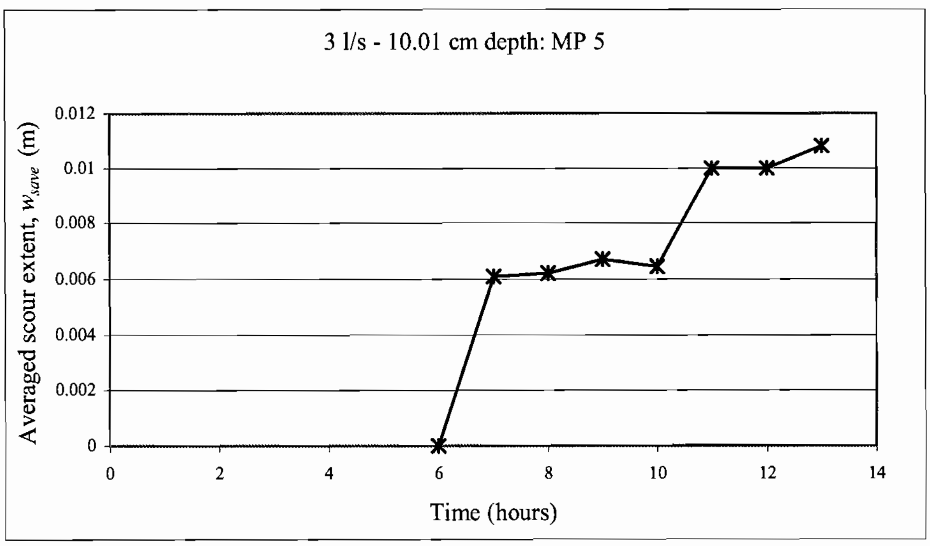

Figure 5.7: Example of a scour extent data set that could not be used to predict an equilibrium scour value

5.6.3 Shifting of the origin of the curve

If scouring did not occur within the first hour of the experiment (Figure 5.8(a)), all the data representing the zero scour extent values were excluded from the data set except for the last zero scour value corresponding to the origin of the curve plotted by Statistica (Figure 5.8(b)).

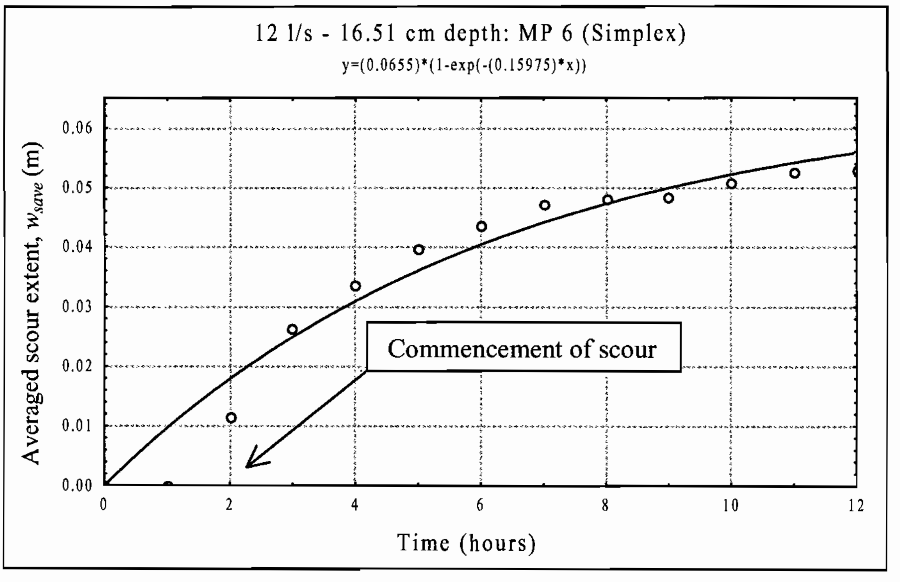

(a)

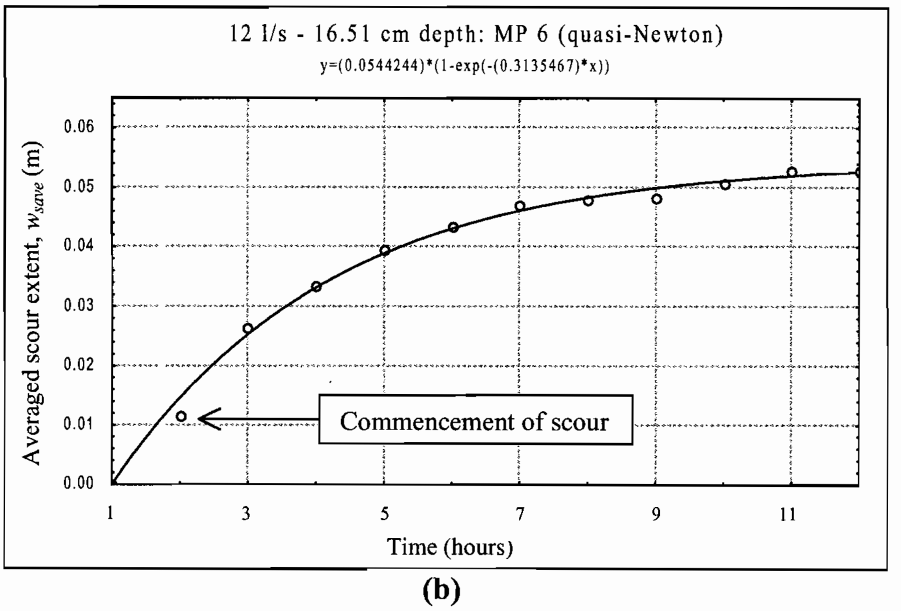

(b)

Figure 5.8: Example showing the effect of excluding the zero scour extent values (b) from the original data set (a)

5.6.4 Disturbances to the averaged scour extent values

The averaged scour extent measurements at the scour measuring points were disregarded from the analysis if there was an obvious disturbance to the scouring process. A disturbance was considered to have occurred if the average scour extent suddenly increased by greater than 10% of the previous averaged scour value during the running of the experiment and then immediately stabilised. This indicated that the area had become over-scoured, in other words, had scoured beyond its equilibrium value (Figure 5.9). Such disturbances could have been caused by contaminants, for example, sand particles or floating debris being carried in the flow; a sudden surge in the pumps; a sudden lowering of the tailgate; or particles might have become interlocked and thus were scoured away earlier than had they been single particles.

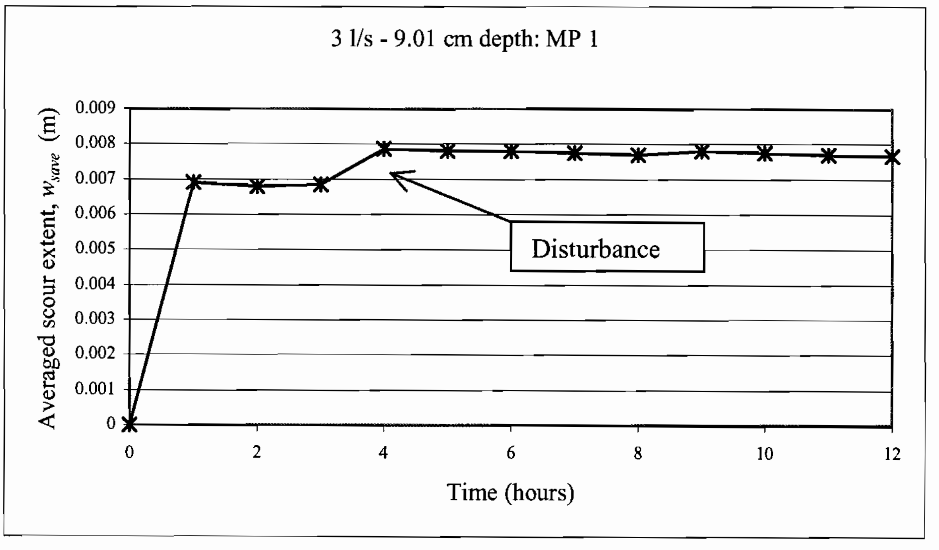

Figure 5.9: Figure showing an example of a disturbance

The scour extent values were also disregarded if the averaged scour extent values stabilised immediately within the first hour of the run (Figure 5.10). It was not expected that the scour extent should stabilise within such a short duration and therefore these values were disregarded as it was uncertain if over-scouring had occurred. This scouring behaviour could have resulted from the tailgate being lowered too quickly during the set up of the experimental process, thus resulting in a sudden increase in the flow velocity around the contracted section. This is especially true for the upstream measuring points where the acceleration of the flow through the contraction is the most severe.

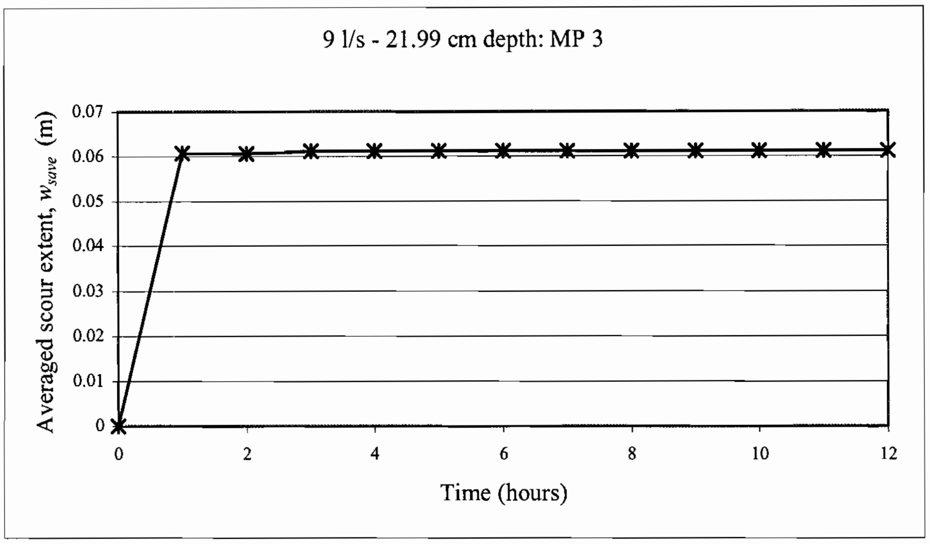

Figure 5.10: Figure showing an example where the scour extent values stabilised immediately within the first hour

It should be noted that in some of the experiments run over a two-day period (13-15 hours), the average scour extent suddenly increased at some of the measuring points as a result of the starting of the pumps on the second day (Figure 5.11). The scour extent values at these points were disregarded if the average scour extent value exceeded 10% of the previous scour value and immediately stabilised.

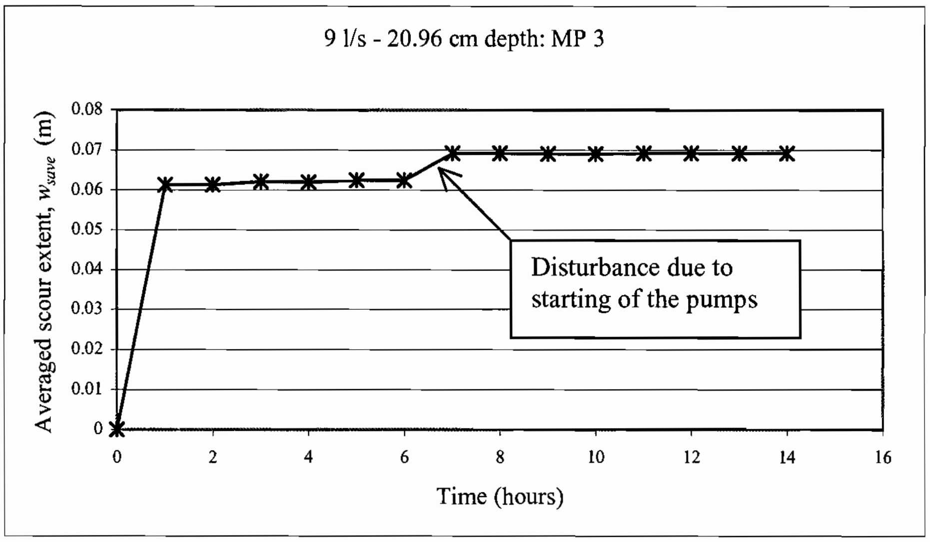

Figure 5.11: Figure showing example where scouring process was disturbed by the starting of the pumps on the second day of the experiment

If, however, the scour extent continued to increase after the disturbance occurred and appeared to be stabilising at a later period in the experiment (Figure 5.12), the scour value at this point was used in the investigation.

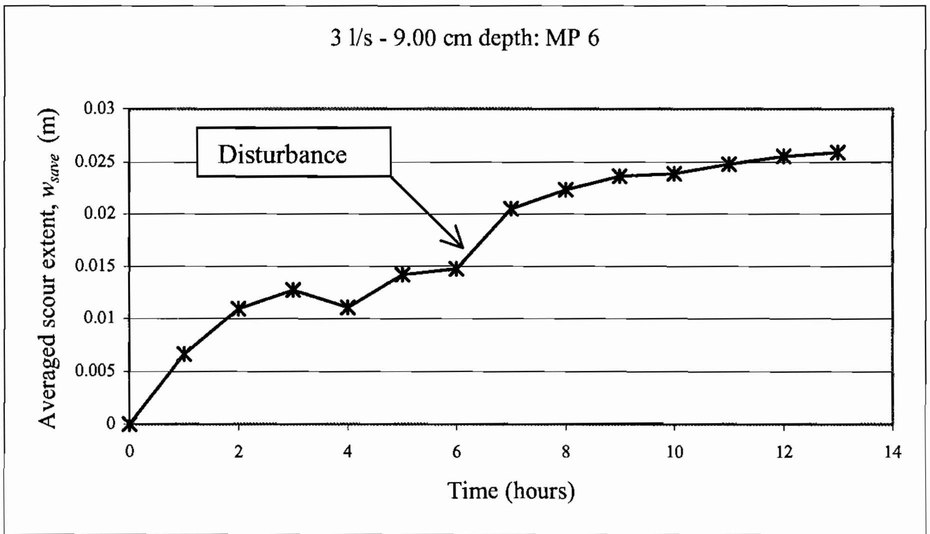

Figure 5.12: Figure showing an example of an averaged scour data set that would be accepted for use after a disturbance

5.7 Dimensional Analysis

Dimensional Analysis was used to determine dimensionless groups that could be used in the interpretation of the data. In this investigation, only the influence of the approach Froude number, Fr_1, the dimensionless approach depth, Y_1, and the opening ratio, α_c, on the lateral extent of scour was considered.

5.7.1 Parameters considered in Dimensional Analysis

The maximum equilibrium scour extent around a "long" contraction was seen as a function of the following parameters (adapted from Melville (1992) for scour depths, y_s, around abutments):

$$w_s = f(\rho, v, U, Y_1, \rho_s, d, \sigma_g, L_c, M_c, Sh_c, Al_c, G_c, B_1, g) \tag{5.16}$$

where ρ and v are the fluid density and the kinematic viscosity; U is the average approach flow velocity; Y_1 is the approach flow depth; ρ_s is the sediment density; d is the sediment size; σ_g is the geometric standard deviation of the sediment; L_c is the length of the upstream face of the long contraction perpendicular to the flow; M_c is the length of the contracted section of the long contraction parallel to the flow; Sh_c and Al_c are the shape and alignment of the long contraction; G_c is the cross-sectional shape of the approach channel; B_1 is the width of the approach channel; and g is the gravitational acceleration.

Applying a dimensional analysis to Equation 5.16 and assuming the following:

i) A constant relative density of the sediment.
ii) The absence of viscous effects.
iii) Uniform, $\sigma_g < 1.3$, non-ripple forming sediment that satisfies the condition $L / d_{50} \geq 50$ (Melville, 1992), in other words, the sediment size has no influence on the extent of the scouring around the long contraction.
iv) A constant shape and alignment of the contracted section.
v) A constant cross-sectional shape of the approach channel.

results in the following dimensionless relationships

$$\frac{w_s}{\lambda} = f\left(Fr_1, \frac{Y_1}{\lambda}, \alpha_c, \beta\right) \tag{5.17}$$

where λ = scaling factor to non-dimensionlise the length parameters
Fr_1 = approach Froude number = $U / \sqrt{(gY_1)}$
α_c = opening ratio = $((B_1 - 2\,L_c) / B_1) = b_c / B_1$
β = length to width ratio = M_c / B_1

Melville (1992), who investigated the maximum equilibrium scour depth around abutments, showed that for "short" abutments ($L_a / Y_1 \leq 1$) the scour depth scaled with the length of the abutment perpendicular to the flow, L_a, and that for "intermediate" abutments ($1 < L_a / Y_1 < 25$) the scour depth scaled with $\sqrt{Y_1 L_a}$. In this investigation, when the ratios of the length of the upstream face of the long contraction perpendicular to the approach flow (L_c) to the approach depth (Y_1) were calculated, the experiments fell under both the "short" and "intermediate" categories as described by Melville with values ranging between 0.92 and 2.75. Thus according to Melville's findings either scaling factors $\lambda = L_c$ or $\lambda = \sqrt{Y_1 L_c}$ could both be appropriate for this investigation. Although the majority of the data fell under the "intermediate" category, the simpler scaling factor L_c, which does not include the additional parameter of approach depth that varies for each data point, was selected to be used in the investigation. In addition, it is unknown whether the findings of Melville can actually be related to scour extents around a long contraction. Equation 5.17 thus becomes

$$\frac{w_s}{L_c} = f\left(Fr_1, \frac{Y_1}{L_c}, \alpha_c, \beta\right) \tag{5.18}$$

5.7.2 Calculation method to determine the influence of Fr_1, Y_1 on the lateral extent of scour

For each of the chosen measuring points, three-dimensional plots were produced of dimensionless equilibrium scour extent (y-axis) versus dimensionless approach depth (x-axis) with each data point having a unique value of approach Froude number (z-axis) (See Figure 5.13). Separate plots were produced for the two values of opening ratio, in other words, α_c = ½ and ¼.

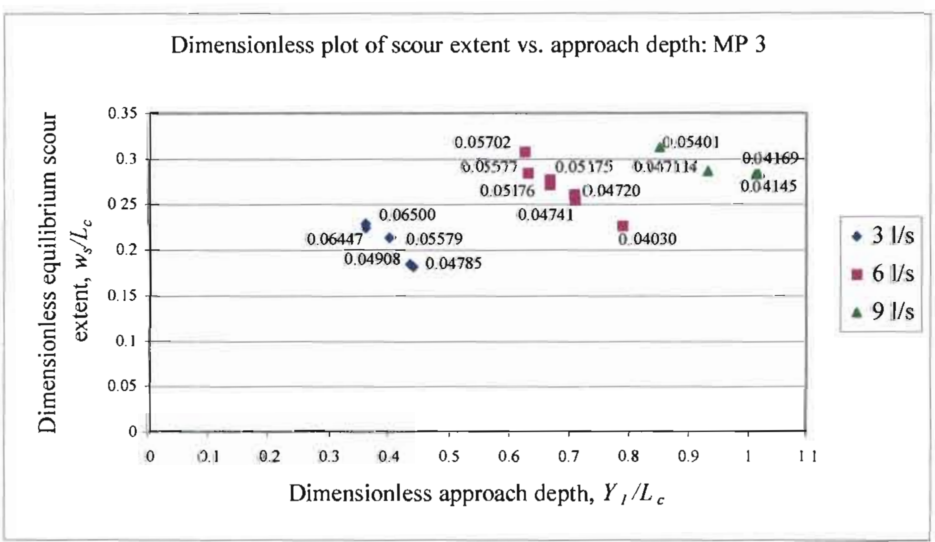

* values next to data points represent the corresponding approach Froude numbers

Figure 5.13: Example of a dimensionless plot of scour extent versus approach depth at MP 3 for α_c = ¼

In order to provide an estimate of the intermediate values of approach Froude number between the measured data points, interpolation was employed.

High-order polynomials are frequently used for interpolation. The problem with high-order polynomials, however, is that they sometimes produce undesirable fluctuations as these polynomials are forced to fit the data exactly. Thus small errors in the data can have an undesirable effect on the interpolated values. This method of interpolation was thus not considered in this investigation as the data sets were small and there was considerable measurement error. Instead, low-order algorithms were used as these would provide smoother interpolated curves between the data sets. Two algorithms were considered: the quadratic polynomial interpolation which fits a second-order polynomial between at least three data points; and the cubic spline interpolation which fits third-order polynomials for each interval between the individual data points with continuous derivatives at the end point of the intervals. Statistica Version 5.0 (non-linear estimation) was used to produce the interpolated curves.

As the cubic spline algorithm considers each data point, it is more of an exact interpolator than quadratic polynomial interpolation and was therefore used initially in order to give a more accurate indication of possible outlying data points. It was found necessary to determine and exclude outliers as due to the sparse data sets, the algorithms are very sensitive and any outlying data point can result in interpolated curves which may misrepresent the data. An example of the identification and removal of an outlying data point can be seen in Figure 5.14. The data point corresponding to $Fr_1 = 0.057022$ was identified as an outlier using cubic spline interpolation (Figure 5.14(a)) and removed from the original data set to give curves that are more representative of the data (Figure 5.14(b)). It should be noted that care was taken not to remove data points without considerable justification.

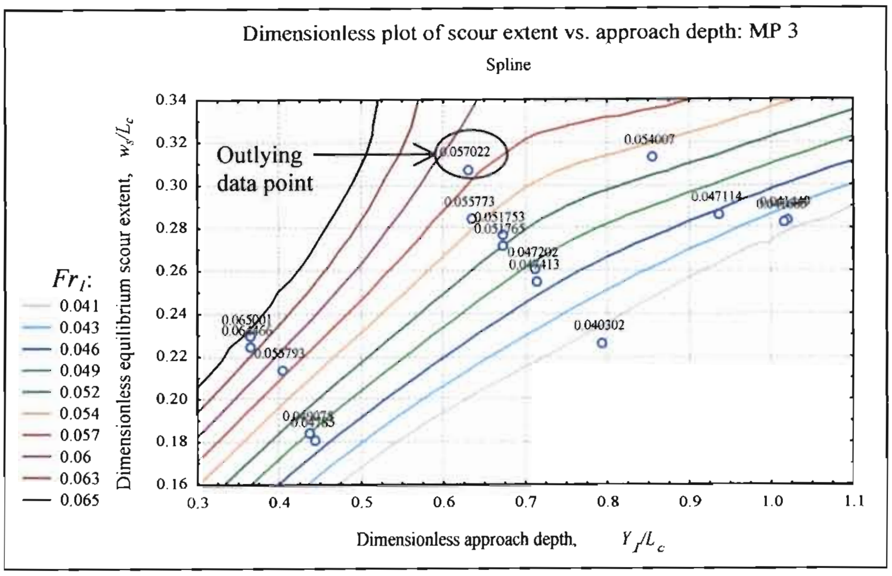

(a)

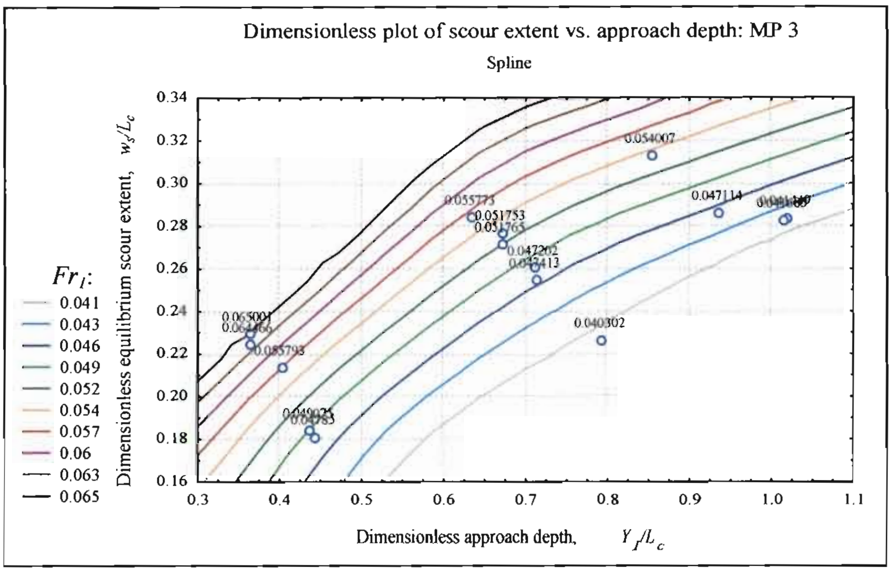

(b)

Figure 5.14: Figure showing the influence of the removal of an outlying data point on the interpolated curves

Once the obvious outlying data points were removed, quadratic interpolation was then employed to produce the final interpolated curve to be used for the analysis (Figure 5.15). In the case of sparse data sets, quadratic interpolation produces very similar curves to that of cubic spline interpolation, except the curves are smoother which is more desirable for this investigation.

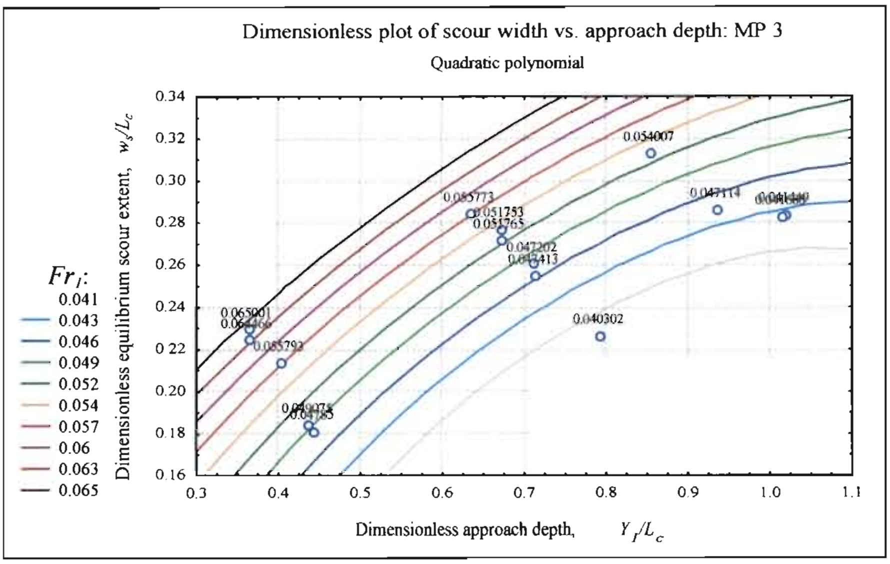

Figure 5.15: Figure showing interpolated curves using the quadratic polynomial interpolation

The interpolated curves of dimensionless scour extent versus dimensionless approach depth that were produced for the two opening ratios were then used to determine the particular influence of the approach Froude number and approach depth on the scour extent around the contracted section.

In order to determine the influence of one particular parameter on the scour extent around the long contraction, namely, either the approach Froude number, the approach depth or the opening ratio, all other parameters must be held constant. Thus when considering the effect of the approach Froude number on the dimensionless equilibrium scour extent, a particular value of dimensionless approach depth was chosen at a particular opening ratio. All the approach Froude number values and the corresponding dimensionless equilibrium scour extent values were then read off for the chosen dimensionless depth, and a plot of dimensionless scour extent versus approach Froude number was determined.

When considering the effect of the approach depth on the equilibrium scour extent, an approach Froude number was chosen at a particular opening ratio from which all the dimensionless approach depth values with the corresponding dimensionless equilibrium scour extent values were determined. A dimensionless plot of scour extent versus the approach depth was thereafter produced.

5.7.3 Calculation method to determine the influence of the opening ratio α_c on the lateral extent of scour

When investigating the influence of the opening ratio on the lateral extent of scour around the contraction, the approach as described in Section 5.7.2 could not be followed. The reason for this is that due to time constraints only two opening ratios were considered in the experimental investigation, thus by fixing both the approach depth and approach Froude number in order to determine the corresponding scour extent values, only two points would be determined. If only two points were plotted on a graph of dimensionless scour extent versus opening ratio, no definitive conclusion regarding the influence of the opening ratio on the scour extent could be reached with any confidence. It was thus decided to present the influence of the opening ratio on the scour extent around a long contraction by producing a two-dimensional plot of the ratio of the equilibrium scour extent to the approach depth (y-axis) versus the approach Froude number (x-axis) for the various chosen measuring points. The data points were plotted for both opening ratios, α_c = ½ and ¼ on the same set of axes and a best-fit line was plotted through them. This would allow the determination of the influence of the two opening ratios on the scour extent for the same approach conditions, in other words, for the same values of approach depth and approach Froude number.

Chapter 6

Development of the initial local scouring around a rectangular long contraction

6.1 Introduction

The aim of this investigation is to provide information on the initial phase of local scouring around a rectangular "long" contraction under clear-water scour conditions. This was achieved by considering the influence of various parameters on the lateral extent of scour around the contraction. These parameters were identified as being the approach Froude number, the approach depth and the opening ratio.

In order to have a good understanding of the resulting relationships between the initial local scour and the identified parameters, it is vital to have a good understanding of the development of the initial local scouring process around the contracted section. This is also an important consideration when comparing the results of this investigation to the findings in literature that considers the development of local scour depths around abutments.

It has been shown in previous research that the scour condition upstream of the scoured region, whether it be clear-water or live-bed scour, is an important consideration in the investigation of local scouring around structures. Not only has it been shown that the scour condition affects the spatial and temporal development of the local scoured region around the structure, but it also determines the important parameters that can be considered to have the most influence on the local scouring process. Thus, the first part of this chapter defines the boundary between clear-water and live-bed conditions for the purpose of this investigation.

The second part of the chapter then goes onto describe the existing vortex systems that are responsible for local scouring around the contraction, and the manner in which they influence the development of the scoured region.

Lastly, the influence that the vortical structures have on the initial scouring process around the long contraction under clear-water/live-bed scour conditions is investigated. More attention is given to the behaviour of the scour under clear-water conditions, as this was the desired condition selected for this investigation.

6.2 Thesis definition of clear-water/live-bed scour conditions

In this investigation it was decided that the boundary between live-bed and clear-water scour conditions would be defined in terms of an intensity of motion, I, due to the stochastic nature of sediment transport along a bed especially around threshold conditions. The value chosen was $I = 1\times10^{-3}\,\mathrm{s}^{-1}$, which represents the limiting intensity of motion of the sediment in the approach channel to the scoured region below which clear-water conditions, and above which live-bed conditions, were deemed to exist (Section 5.2).

Figure 6.1 shows the scatter of data points representing the average conditions in the contracted section for the experiments conducted in this investigation. The conditions in the contracted reach of the long contraction were selected so that the intensity of motion of the sediment within the reach would be less than $I = 1\times10^{-3}\,\mathrm{s}^{-1}$. Table 6.1 shows the experiments that were used in this investigation for both opening ratios.

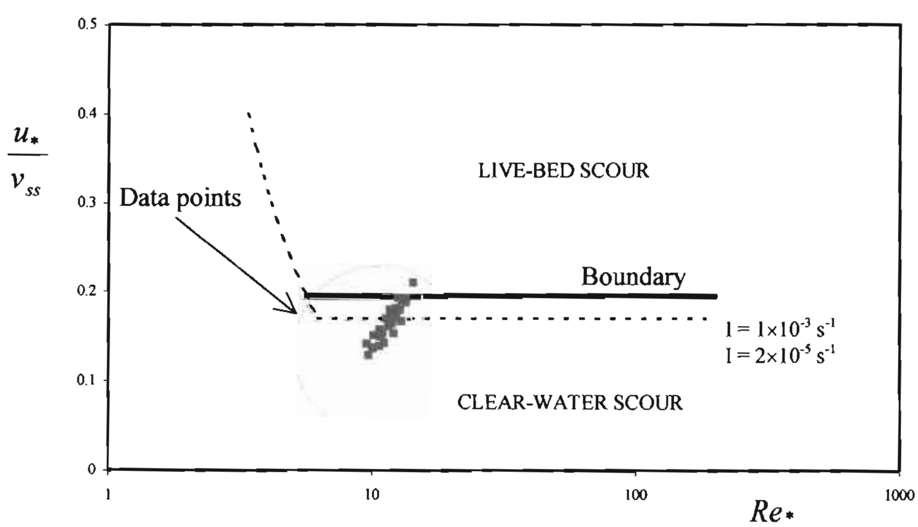

Figure 6.1: Graph of Movability Number (u_* / v_{ss}) versus the particle Reynolds Number (Re_*)

Opening ratio α_c	*Flow rate* (*l/s*)	*Depth in Contraction* (*mm*)	U_* / v_{ss} (*contraction*)	Re_* (*contraction*)	I s^{-1} (*contraction*)
¼	3	79.9	0.181	11.83	1.14E-04
		80.4	0.177	11.98	6.80E-05
		90	0.159	10.80	4.17E-06
		90.1	0.157	10.93	3.02E-06
		99.3	0.143	9.67	3.74E-07
		100.1	0.139	10.25	1.95E-07
	6	140.2	0.194	13.68	8.41E-04
		141.5	0.194	12.71	8.41E-04
		149.7	0.182	12.50	1.52E-04
		150.4	0.180	12.75	1.10E-04
		160.6	0.168	12.12	1.70E-05
		160.6	0.171	11.46	2.70E-05
		180.5	0.152	10.26	1.45E-06
	9	***190.1**	**0.211**	**14.46**	**1.20E-02**
		209.6	0.191	13.14	5.49E-04
		210.5	0.189	13.60	3.80E-04
		219.9	0.181	12.95	1.16E-04
		230.6	0.171	12.28	2.83E-05
		230.2	0.173	12.31	3.53E-05
½	8	105.2	0.165	12.02	1.03E-05
		115.3	0.150	10.81	1.17E-06
		125.1	0.137	10.15	1.52E-07
	10	125.4	0.168	13.09	1.62E-05
		135.2	0.154	12.27	2.18E-06
		145.3	0.144	11.26	4.26E-07
	12	145.2	0.174	12.52	4.05E-05
		155.1	0.162	11.71	6.98E-06
		165.1	0.152	10.95	1.52E-06

* Experiment for which constriction scour occurred within the contracted reach

Table 6.1: Table of the conditions (in the contracted reach) of the experiments chosen for use in the investigation

One experiment (9 l/s with contraction depth of 19.01 cm) was performed where the intensity of motion within the contracted reach was $I = 1.2\times10^{-2}\,\mathrm{s}^{-1}$, in other words, where live-bed conditions could be deemed to exist in the region downstream of the contraction. It was therefore also expected for this experiment that constriction scour would have occurred within the contracted reach, as an intensity of motion of $I = 1.2\times10^{-2}\,\mathrm{s}^{-1}$ implies a general movement of sediment. In order to have a clearer understanding of this phenomenon, the equilibrium scour extent values at MP 4 were plotted against the Movability Number (u_* / v_{ss}) for all of the experiments with the opening ratio α_c = ¼. It should be noted that u_* / v_{ss}=0.195 corresponds with $I = 1\times10^{-3}\,\mathrm{s}^{-1}$, and thus can also be used to define the boundary between clear-water and live-bed scour conditions. MP 4 was chosen as it was the only measuring point located within the contracted reach, and its scour extent value is the measure of the distance between its location and the upstream face of the long contraction. The results can be viewed in Figure 6.2 below.

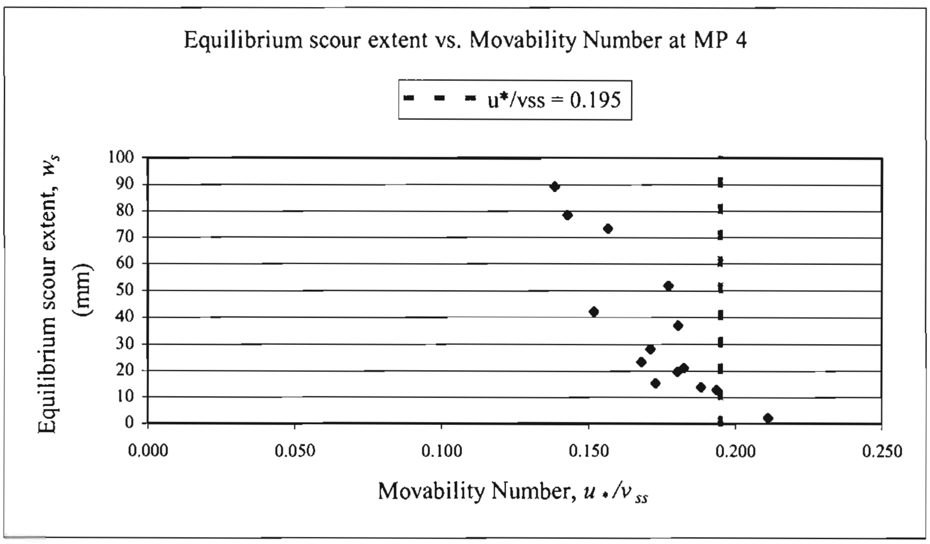

Figure 6.2: Figure of equilibrium scour extent versus the Movability Number for MP 4 and α_c= ¼ (The dashed line represents the boundary between clear-water (left) and live-bed (right) conditions for the region downstream of the contraction.)

It can be clearly seen from Figure 6.2 that for the experiment associated with live-bed conditions downstream of the contraction (u_* / v_{ss}=0.211), the difference in location between the scour extent at MP 4 and the upstream face of the long contraction is almost zero (2.1 mm), in other words, the contracted reach appeared to be completely cleared of all sediment. For all of the other experiments associated with clear-water scour conditions downstream of the contraction ($u_* / v_{ss} < 0.195$), the scour extent at

MP 4 ranges from a minimum of 13 mm to a maximum of 89 mm. Seeing that only a thin layer of sand existed within the contracted reach (average thickness of 1.6 mm), it is to be expected that all the sand would be removed if constriction scour existed. This was the exact result that was achieved for the only experiment performed where the intensity of motion within the contracted reach was greater than $I = 1\times10^{-3}\,\mathrm{s}^{-1}$. Seeing that constriction scour within the contracted reach is associated with live-bed conditions in the region downstream of the contraction, it can thus be said that the assumption made in this thesis that the intensity of motion $I = 1\times10^{-3}\,\mathrm{s}^{-1}$ defines the boundary between clear-water and live-bed scour appears to be reasonable.

6.3 Development of the lateral extent of scour around a long contraction and the associated coherent structures

In this investigation it was observed that the spatial and temporal development of the lateral extent of scour differed for the region around the upstream face of the long contraction and that downstream of the contracted section. This can be seen to be due to the differing vortex systems responsible for the scouring in the two regions. In the following discussion, the development of the scoured region around the upstream face and downstream of the long contraction are thus considered separately.

6.3.1 Development of the lateral extent of scour around the upstream face of the long contraction

In the following discussion on the development of scour around the upstream face of the long contraction, reference will be made to the measuring points (MP 1-4) that define the scoured region under consideration. Figure 6.3 displays these relevant measuring points.

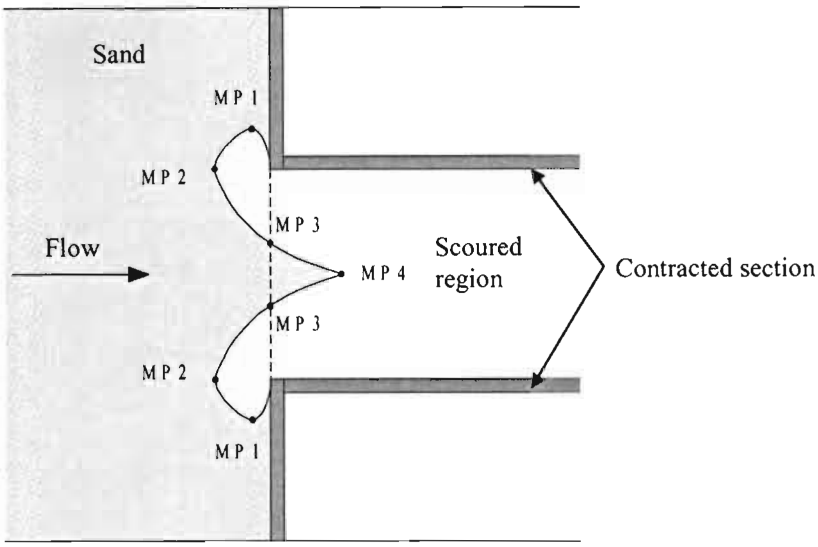

Figure 6.3: Upstream scour measuring points

Two main vortices were identified as being responsible for local scouring around the upstream face of the long contraction, these being the corner vortex that formed at the inner corners of the entrance to the contraction, and the principal vortex which formed a short distance upstream of the entrance.

Owing to the sudden decrease in the velocity along the boundary between the "dead water" region upstream of the blocked sides of the long contraction and the faster flowing water in the main channel, an increase in pressure occurs creating a vertical downflow and the subsequent formation of what is known as the "principal vortex". The principal vortex can be described as being elliptical in shape and having a horizontal axis of rotation parallel to the bed. In previous research, which considers the depth of scour around abutments, the principal vortex was recognised as being the primary scouring agent. In these cases the principal vortex was found to be confined within the scour hole beneath the original bed level and was thus protected from the oncoming flow. In the case of this investigation, however, which does not allow for an increase in the depth of scour, the principal vortex is in fact exposed to the oncoming flow, which may cause a reduction in strength of this vortex and thus its dominant role in the scouring process.

For all of the experiments conducted in this investigation, scouring was observed to commence almost immediately at the inner corners of the entrance to the long contraction in the form of small circular regions. This is in fact characteristic of the corner vortex (vertical axis of rotation) that is known to originate from the upstream inner corner of the contracted section. The circular scouring regions then rapidly elongated downstream into the contracted reach of the long contraction (Figure 6.4(a)) while increasing in size both laterally and longitudinally (Figure 6.4(b) and (c)). This too is characteristic of the behaviour of the corner vortices which then generally break away from the inner corners of the contraction to form the wake vortices.

Scouring continued in this fashion until the two developing scour regions on either side of the contraction met at a point (corresponding to MP 4) that was approximately located centrally between the two sides of the contracted reach (Figure 6.4(d)). This scour shape can be explained by the overlapping of the paths followed by the wake vortices. The point then began to migrate upstream due to the sand being scoured away from either side of the scoured region. For the smaller opening ratio, $\alpha = ¼$, the point migrated rapidly upstream to a short distance downstream of the upper inner corners of the contraction (13-89 mm) (Figure 6.5(a)), whereas for $\alpha = ½$, the point extended quite a distance into the contracted region (169-220 mm) (Figure 6.5(b). This behaviour can be explained by considering the formation of the corner vortices and their associated wake vortices.

The vertical corner vortex forms at the inner corners of the entrance to the contraction due to the sudden convergence of the streamlines as the flow accelerates around the corners and into the contraction (Figure 6.6). This sudden convergence at the inner corners creates steep velocity gradients that in turn cause low pressure and the subsequent formation of the vortices. For the smaller opening ratio, the convergence of the streamlines around the inner corners is more severe than for the larger opening ratio, thus resulting in the formation of corner vortices of higher vorticity. Also for the smaller opening ratio, it is logical that the paths of the vortices should overlap at a shorter distance downstream of the inner corners of the contraction in comparison to the larger opening ratio, due to the narrower width of the contracted region.

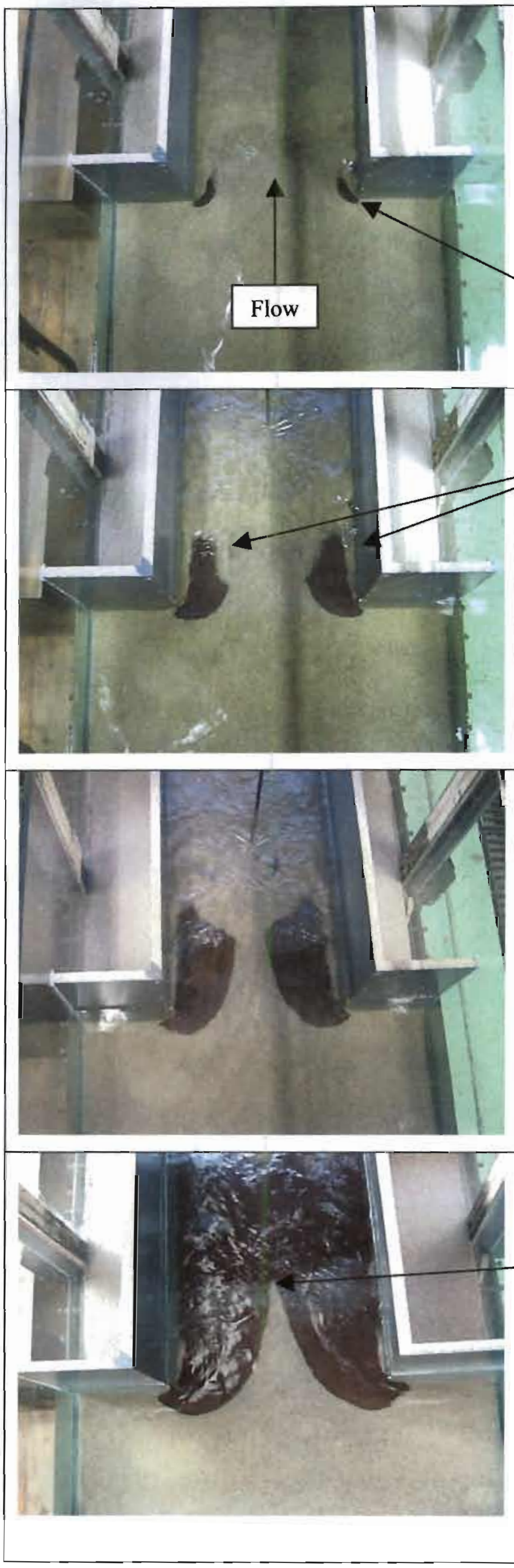

Figure 6.4: Photographs of the scour development around the upstream face

(a) Point at which scouring commences as small circular regions

(b) Scoured region increases both laterally and longitudinally around the inner corners

(c)

(d) Point of overlap of the scoured regions

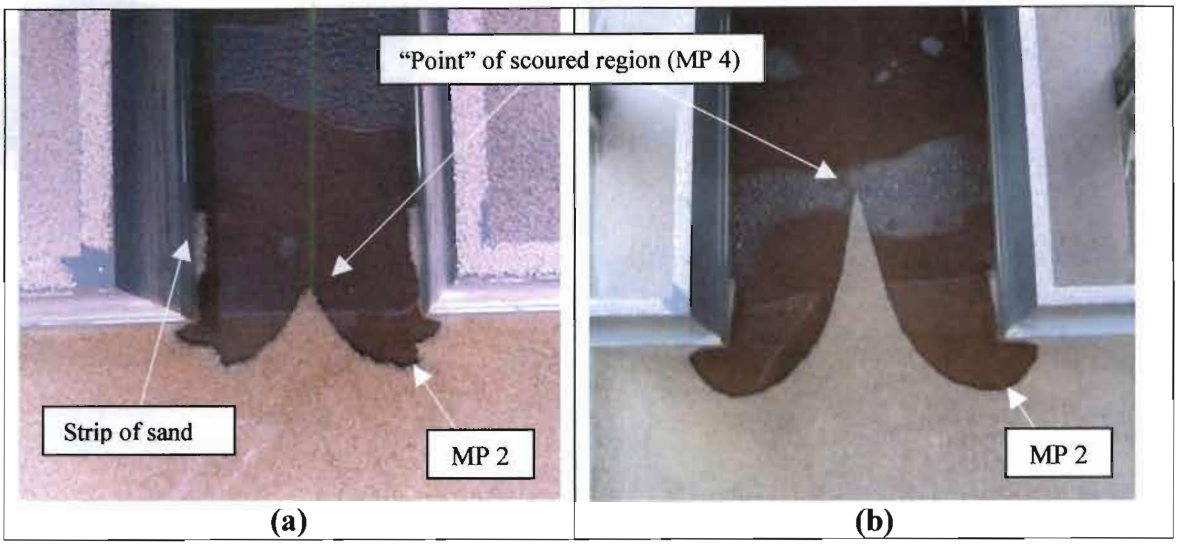

Figure 6.5: Photographs showing the scour pattern around the upstream face for (a) α_c = ¼ and (b) α_c = ½

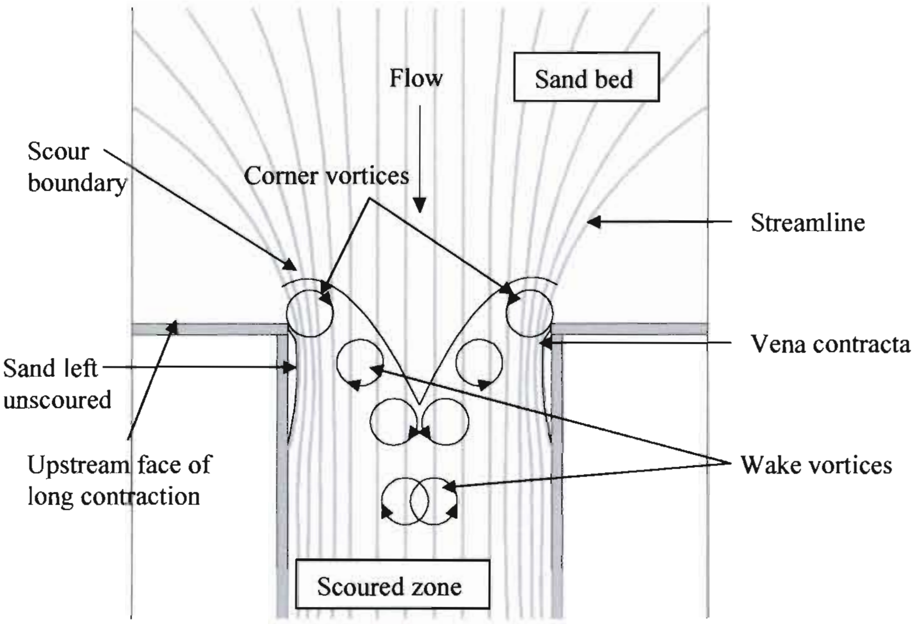

Figure 6.6: Corner vortices with the associated wake vortices

It should be noted that a strip of sand was left intact a short distance downstream of the entrance to the long contraction against the side-walls throughout the experiments (see Figure 6.5(a),(b) and Figure 6.6). This marks the vena-contracta of the flow accelerating through the opening of the contracted section.

It was observed that the upstream edge of the scoured region corresponding to MP 2 increased in size in the upstream direction and appeared to almost form into a point (Figure 6.5(a)). This additional scouring in the upstream direction was seen to be due to the influence of the principal vortex on the bed. It therefore appears that although the corner vortices might be more important than the principal vortex when it comes to the initiation of the local scouring, the principal vortex also plays an important role in the scouring process at MP 2. For the smaller opening ratio, α_c = ¼, it was observed that the scoured edge at MP 2 increased in an upstream direction to a greater extent than for the larger opening ratio, α_c = ½. This is evident by the typical resulting shapes of the scoured regions (at equilibrium conditions) for the two opening ratios that can be seen in Figure 6.5.

In the case of the larger of the two opening ratios tested (α_c = ½) the principal vortex was observed to have a minimal influence on the scouring process around the upstream face of the long contraction in comparison to the influence of the corner vortices. This can be explained by considering the formation of the principal vortex. Although the principal vortex forms along the whole length of the boundary between the dead water region upstream of the contraction and the fast-flowing water in the main channel, the principal vortex is relatively weak further upstream of the long contraction increasing in size and strength as it approaches the upper inner corners of the contracted section (Figure 6.7). The reason for this is that the strength of the principal vortex increases with increasing flow velocity. As the flow velocity increases, the pressure gradient that forms along the boundary between the dead water region and the fast-flowing water in the main channel becomes steeper thus causing a stronger downflow and subsequent vortex. It is thus not surprising that the principal vortex would have more of an influence on the scoured region for the smaller opening ratio, as the convergence of the streamlines through the smaller opening is more severe than for the larger opening ratio, thus resulting in higher velocities.

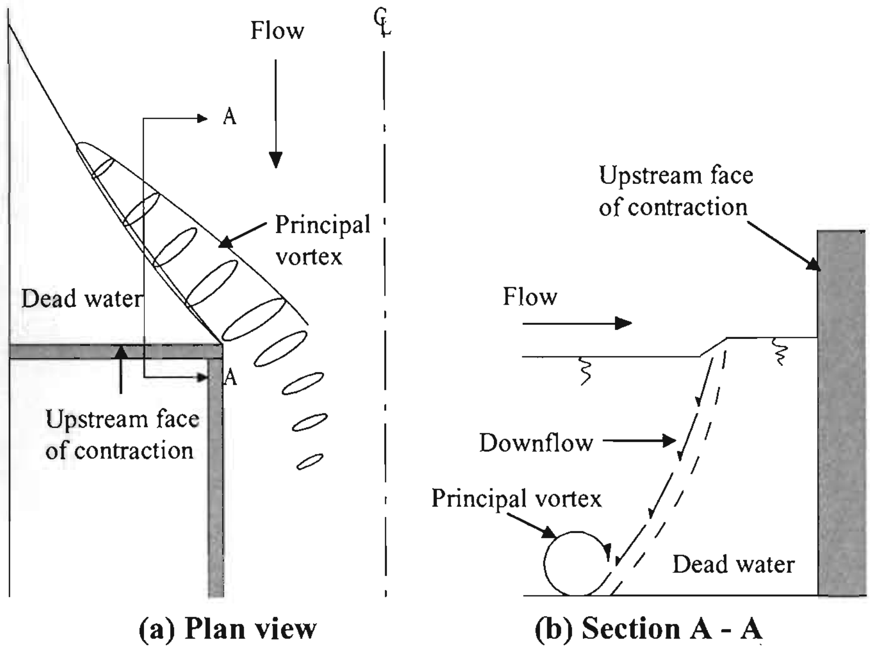

Figure 6.7: Plan (a) and side view (b) of the principal vortex upstream of left side of long contraction

The influential role of the principal vortex on the scoured region for the two opening ratios can also be determined by considering the temporal development of the scoured region around the upstream face of the contraction. In general for the upstream measuring positions MP 1-3 and for the two opening ratios considered, scouring was observed initially to increase rapidly within the first hour of the experiment and then to slow down as it approached a limiting value, in other words, the equilibrium scour extent value. Figure 6.8 is a typical example of the temporal development of the scoured region around the upstream face of the contracted section for MP 2 ($\alpha_c = ¼$).

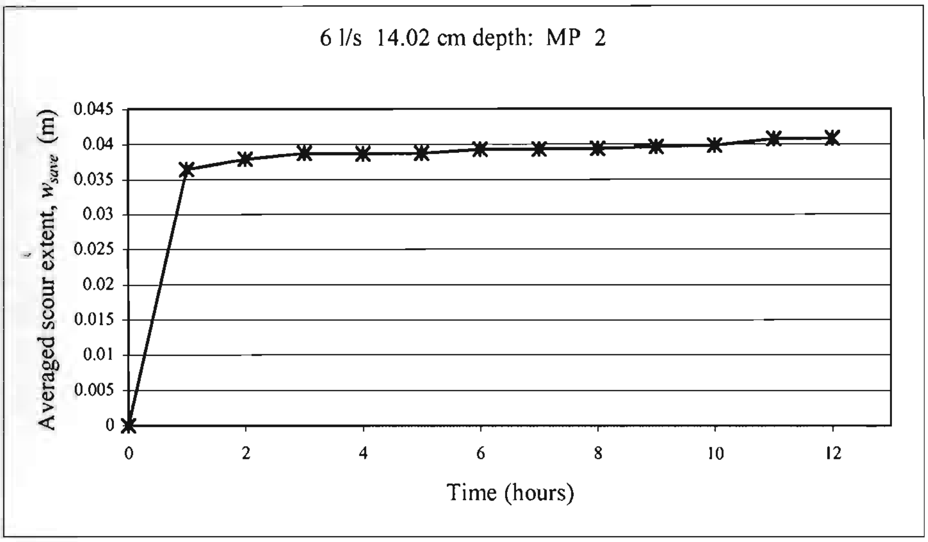

Figure 6.8: Figure showing the temporal development of the lateral extent of scour at MP 2 for α_c = ¼

The average percentage of the equilibrium scour extent values scoured within the first hour of the experiments for the upstream measuring points MP 1, 2 and 3 as well as the average time taken to reach equilibrium (t_e) are presented in Table 6.2.

	α_c = ¼		α_c = ½	
	***% scour in first hour* (%)**	**t_e (hours)**	***% scour in first hour* (%)**	**t_e (hours)**
MP 1	89	5	75	9
MP 2	86	6	79	10
MP 3	93	5.5	93	9

Table 6.2: Table showing the average percentage of the equilibrium scour extent value scoured in the first hour of the experiment and the time taken for the scour to reach equilibrium for MP 1-3

The percentage of the equilibrium scour extent achieved during the first hour of testing at MP 2 appeared to be larger for the smaller opening ratio (86%) as opposed to the larger opening ratio (79%). This can be explained by the fact that MP 2 was influenced by both the corner vortex and the principal vortex and that the principal vortex appeared to be stronger (developed at a faster rate) and thus more influential on the scour extent for the smaller opening ratio. At MP 3, the percentage of the equilibrium scour extent that occurred within the first hour of the experiments (93%)

was observed as the same for both opening ratios. This can be explained by the fact that MP 3 was predominantly influenced by the corner vortex for both opening ratios. Although the temporal behaviour of scour at MP 1 should have resembled that of MP 3, seeing that this point was also predominantly influenced by the wake vortex, it shows a much lower percentage of scour within the first hour for the larger opening ratio. This is explained by the influence of the build-up of sand along the upstream face of the contracted section caused by the use of the sand spreader. It should also be noted that although the average equilibrium time for MP 1 is shown in Table 6.2 to be 5 hours, there was considerable variation in the time taken to reach equilibrium. Two values in fact had to be excluded from the calculation of the average equilibrium time, as equilibrium conditions were not even realised on these two occasions.

Information is not presented for MP 4 in the above table due to the erratic progression of the scour at this point, which often failed to reach equilibrium within the duration of the experiment. This inconsistent behaviour can be explained by the fluctuations in the velocity at this point associated with the shedding vortices as well as the turbulent mixing that occurred as a result of the wake vortices interacting with each other.

By considering the spatial and temporal development of the scoured region around the upstream face of the long contraction, it can thus be said that the corner vortex plays more of a dominant role than the principal vortex in the scouring process around a long contraction for the larger opening ratio $\alpha_c = ½$ (Figure 6.9(a)). For the smaller opening ratio $\alpha_c = ¼$, however, it appeared as though both the corner vortex and the principal vortex played influential roles on the scoured region (Figure 6.9(b)).

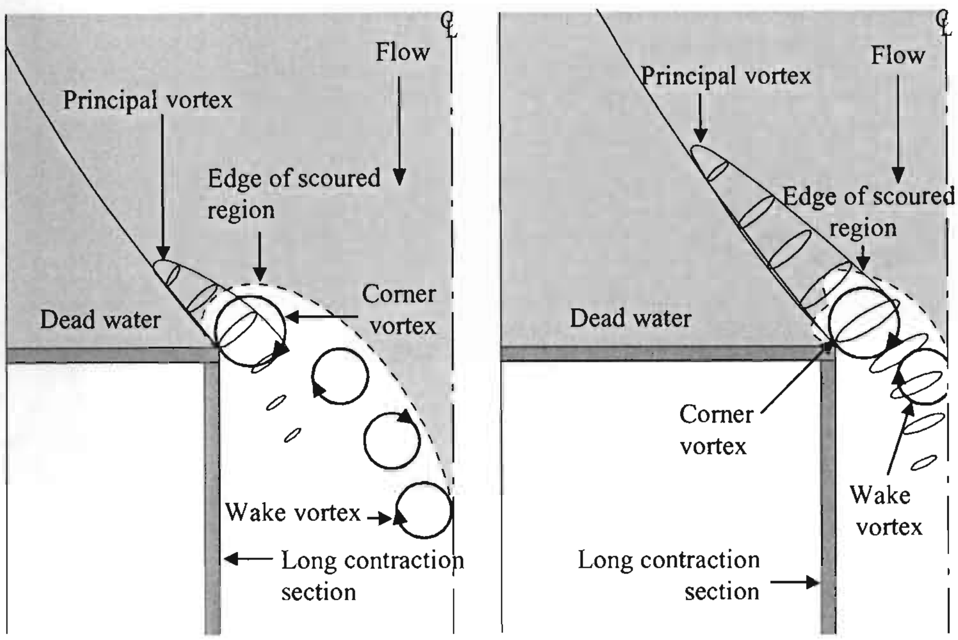

(a) $\alpha_c = ½$ (b) $\alpha_c = ¼$

Figure 6.9: Dominant vortices responsible for the local scour extent around the upstream face of the long contraction for the two opening ratios

It was however noticed that on average the measured equilibrium scour extent at MP 2 was only half the equilibrium scour extent at MP 3 (see Table 6.3). This was true for all of the experiments, except for the experiments conducted for a flow rate of 3 *l*/s (opening ratio α_c = ¼), where the scour extent at MP 2 was observed to be approximately only one third of the scour extent at MP 3.

	Flow	w_s(MP 2) / w_s(MP 3)
$\alpha_c = ¼$	9	0.47
	6	0.46
	3	0.33
$\alpha_c = ½$	12	0.55
	10	0.54
	8	0.48

Table 6.3: Table showing the ratio of the extent of scour at MP 2 to the extent of scour at MP 3 for opening ratios α_c = ¼ and α_c = ½

The size proportions of the scour extents displayed in Table 6.3 are typical of the scour pattern that would be caused by the corner vortex that forms at the inner corners of the contracted section and moves towards the centre of the flume as it is shed. Although the principal vortex does show an influence on the scour extent at MP 2 (especially for the smaller opening ratio) it appears as though the vortex is not strong enough to show a significant influence on the scour extent in comparison to the corner vortex. In the literature considering scour depths around abutments, the scoured region extends just as much upstream from the inner corners of the abutment than it does laterally. This is because the principal vortex, which forms upstream of the abutment, was recognised as being the dominant scouring agent. In the case of this investigation, however, the influence of the principal vortex is reduced due to the fact that, unlike for the case in the literature, the principal vortex is exposed to the approach flow, which appears to weaken it.

Another vortex that has not yet been mentioned but is known to exist in the upstream region is the "bow-wave" or "roller". As with the principal vortex, this vortex forms along the same boundary between the dead water region upstream of the long contraction and the fast-moving flow of the main channel and has a horizontal axis of rotation parallel to the bed (Figure 6.10). Unlike the principal vortex, however, the roller forms along the surface and rotates in the opposite direction to the principal vortex. The existence of this vortex was evident by the observed rise in the water surface upstream of the long contraction. This rise in water surface corresponds to the velocity head of the oncoming flow that is a maximum at the surface. The flow is forced upwards and back onto itself to form the roller. As for the principal vortex, the roller gains in strength as it nears the corners of the entrance to the contraction where it comes into contact with both the principal and corner vortices. The influence that this vortex has on the scouring along the bed is dependent on its degree of interaction with the two latter vortices responsible for the scouring. Seeing that the roller forms along the surface, this degree of interaction is also dependent on the depth of the flow.

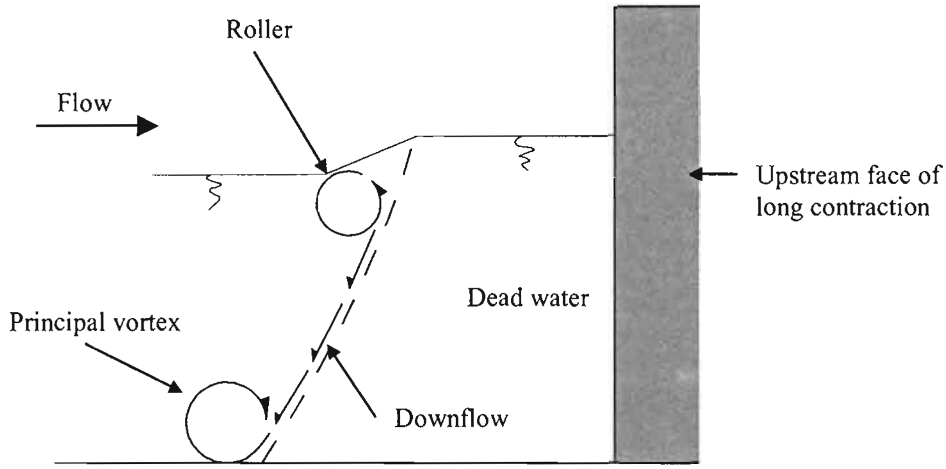

Figure 6.10: Diagram of the bow-wave or roller

6.3.2 Development of the lateral extent of scour in the region downstream of the long contraction

In the discussion on the development of scour downstream of the long contraction, measuring points MP 5 - MP 7 are of relevance. The positioning of these measuring points is shown in Figure 6.11.

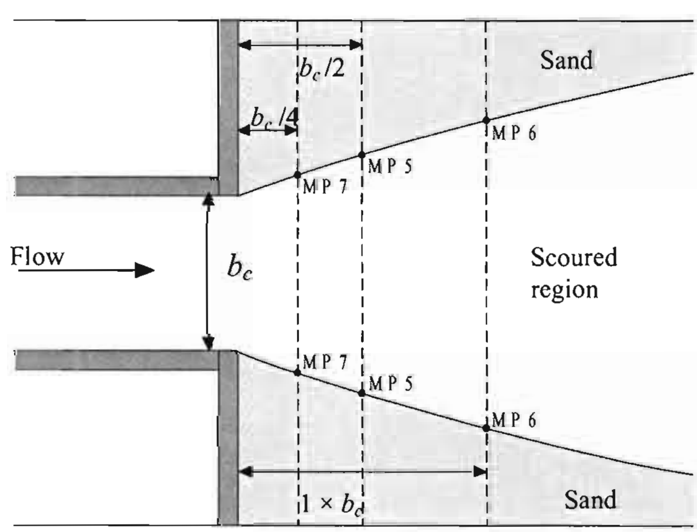

Figure 6.11: Downstream scour measuring points

For the area downstream of the long contraction, scouring was observed to commence as small scoured regions that formed a short distance in front of the corners of the exit to the contraction. These slowly extended laterally and more rapidly longitudinally to form scour regions in the shape of elongated lobes (Figure 6.12(a)). These scoured lobes extended further upstream until they became attached to the inner corners of the contraction.

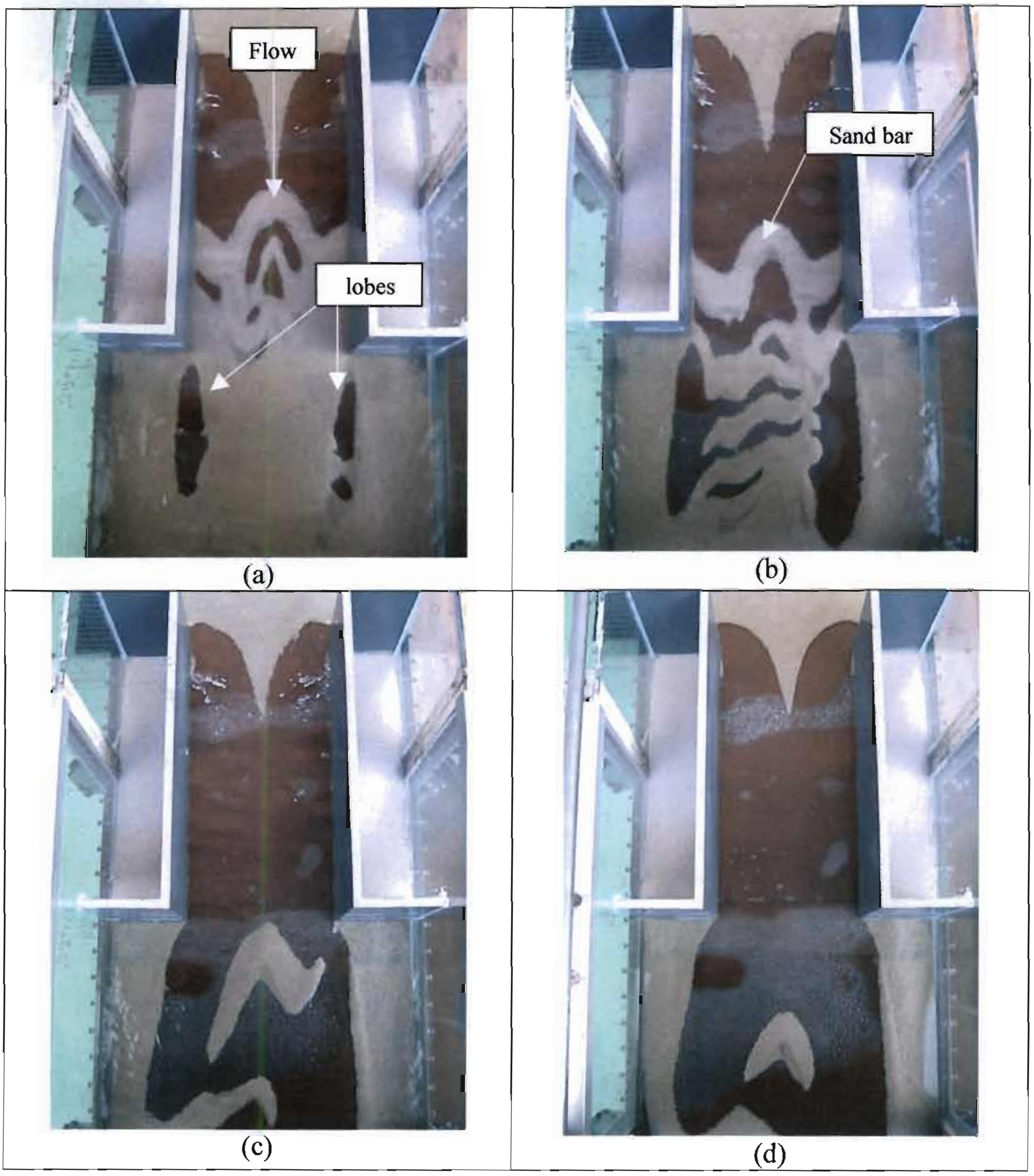

Figure 6.12: Photographs of the scour development downstream of the long contraction

This behaviour of the scour can be seen to be characteristic of vertical wake vortices that are shed from the downstream inner corners of the contracted section (Figure

6.13). These vortices are known to form as a result of the sudden expansion of the flow from the contracted region as it enters into the downstream region. The flow path of the water does not immediately adhere to the walls of the channel, instead it gradually expands before joining the walls at some point downstream. This causes the formation of relatively still areas (dead water region) downstream of the long contraction. The boundary between this dead water region and the faster moving water towards the centre of the channel creates a shearing action and the consequent formation of the wake vortices. The strength of these vortices diminishes as they move further downstream until they eventually dissipate into the general turbulence.

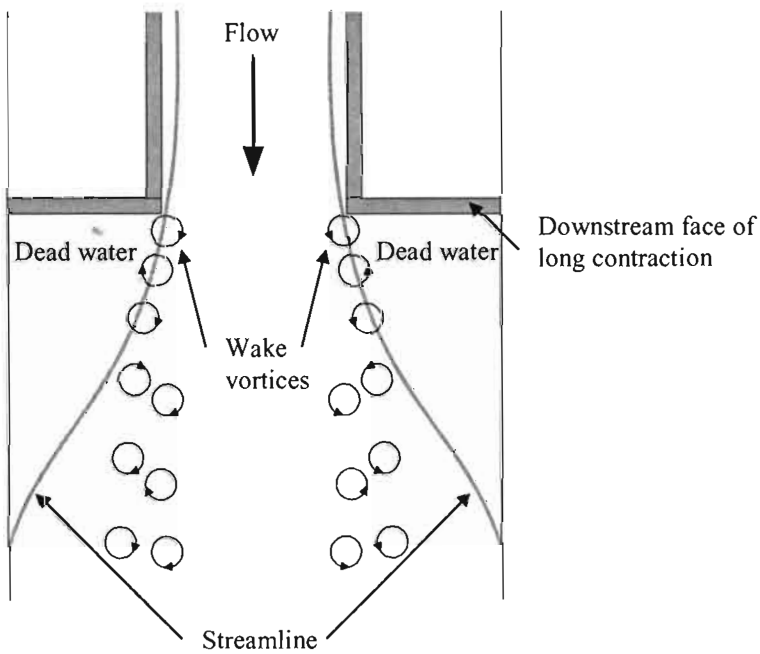

Figure 6.13: Wake vortices responsible for scouring in the region downstream of the contracted section

The area of sand between the expanding lobes was observed to be progressively scoured away by the fast moving, turbulent flow from the contracted region that also carried with it the excess sand from the contracted region (Figure 6.12(b)). The migrating sand from the contracted region was observed to move towards the downstream area in the form of "sand bars". Upon entering into the downstream area the sand bars appeared to attach themselves to the area around the exit. At this stage sand began to be scoured away from the outer edges of the sand bar towards the centre of the flume. Occasionally sand from the bar also moved along the outer edges of the lobes especially along the areas in close proximity to the downstream corners of the contracted section. The bar remained at this position until one side became detached, after which it was more easily washed away by the flow (Figure 6.12(c)). This process would then begin for the next migrating sand bar until eventually all the sand from the contracted reach was cleared away, leaving only clearly defined strips of sand in front of the downstream faces of the long contraction (Figure 6.12(d)). Owing to the fact that the conditions of the experiments were chosen such that no constriction scour occurred within the contracted reach, it can thus be said that the sand removed from the contracted reach occurred solely due to local effects of the long contraction on the flow. It is believed that the vortices shed from the upstream inner corners of the contraction retained a significant proportion of their strength throughout the contracted reach due to the fast moving flow within the contraction. These vortices were seen to enter into, and to cause scouring to the central region of the area downstream of the long contraction, before eventually diminishing due to the deceleration of the flow.

It should be noted that for all of the downstream measuring points, in other words, MP 5, MP 6 and MP 7, and for both opening ratios, the scour extent reached about 50% of the equilibrium scour value within the first hour of the experiment (Figure 6.14). In most cases the equilibrium scour extent value had to be forecast using Statistica as it was found that only 8 of the 19 experiments performed for opening ratio α_c = ¼ appeared to reach equilibrium in the downstream area, whilst none did for α_c = ½, within the 12 hours over which experiments were run.

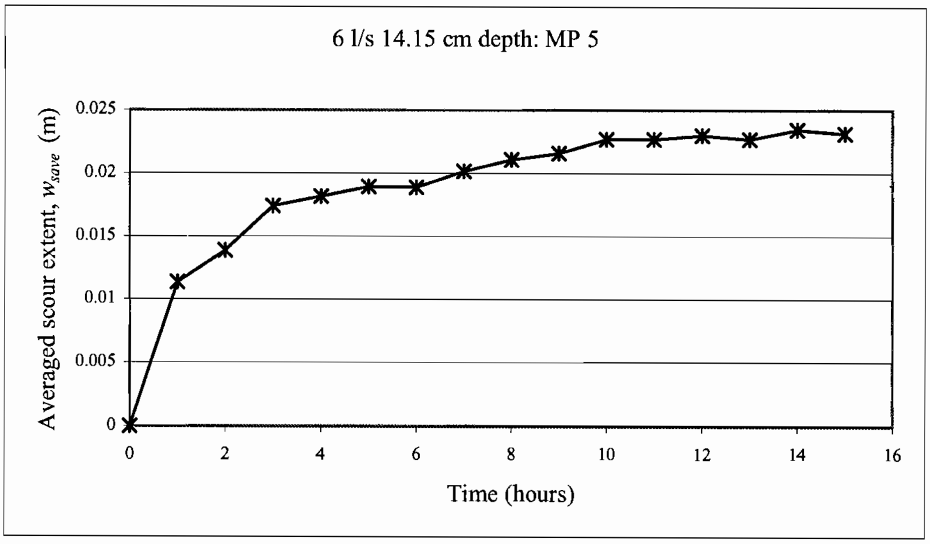

Figure 6.14: Figure showing the temporal development of the lateral extent of scour at MP 5 for α_c = ¼

This contrasts with the temporal development of the scoured region around the upstream face of the contraction. For the upstream scoured region it was observed that on average the percentage of the equilibrium scour extent value scoured within the first hour of the experiment was approximately 90% for α_c = ¼ and 80% for α_c = ½. The upstream scoured area was also generally observed to reach equilibrium conditions within the duration of the experiment. This contrasting temporal behaviour between the upstream and downstream scoured regions could imply that the strength of the corner vortices (with the associated wake vortices) that form at the corners of entrance to the contracted section is greater than that of the wake vortices that form at the corners of the exit to the contraction. This is a reasonable argument as it is expected that for the same approach velocity, the resulting velocity gradients around the entrance corners of the contracted section due to the strongly converging flow will be steeper than those that form at the exit corners along the shear boundary between the fast-flowing water of the main channel and the dead water regions in front of the section. A steeper velocity gradient implies the formation of a stronger vortex.

6.4 Development of the lateral extent of scour around a long contraction under live-bed/clear-water conditions

Although the flow rate and depth of flow for each experiment were chosen such that clear-water scour conditions theoretically existed throughout the contraction, the strong vortical action within the contracted reach transported the sand through the contracted section into the region downstream. Therefore, although the experimental procedure was designed for clear-water scour, the downstream region initially experienced conditions of live-bed scour until the sand had been completely removed from the downstream region by the flow. If the contraction had been long enough to ensure that the additional applied power due to the vena-contracta and the wake vortices within the contracted reach had died away before the exit of the contraction, clear-water conditions would have in fact prevailed throughout the experimental process.

MP 7 was observed to be the most influenced by the migrating sand from the contracted reach due to its close proximity to the downstream inner corners of the contracted section. MP 5, which is the next downstream measuring point after MP 7, typically showed influences of both live-bed and clear-water scour conditions. MP 6, which was the furthest measuring point downstream of the contraction, generally showed little influence of the migrating sand.

In considering the influence that these conditions of scour have on the scour extent around the long contraction, the temporal development of scour around the upstream face and downstream of the contracted section needed to be examined and compared with that found in the literature.

When considering scour depths around abutments, the equilibrium scour depth under clear-water conditions is reached when the flow velocity in the scour hole decreases (due to the increasing area) to a point where the flow can no longer remove the sediment from the scoured hole. For live-bed conditions, the equilibrium scour depth is reached when the sediment from the approach flow is transported into the scour hole at the same rate as the sediment being transported out. Because the sediment layer used in these experiments was only an average of 1.6 mm thick, the increase in depth of the scoured region was unlikely to have any influence on the velocity in the proximity of the scoured areas. Thus conditions of equilibrium under the various scour conditions could be seen as being quite different from those for scour depth considerations.

Under conditions of clear-water scour, which is known to exist around the upstream face of the contraction, scouring is caused by the high velocities associated with the vortices in the region, namely the corner vortex and the principal vortex. It can be seen in Table 6.2 that the majority of the scour occurs within the first hour of the running of the experiment. This is due to the high vorticity located in the centre of the vortices that have an immediate scouring effect on the bed of the flume. This vorticity decreases towards the outer limit of the vortex and thus the influence of the vortex on the bed will also decrease towards its outer limits until the vortex can be seen to no longer affect the bed. This would explain why after the large initial scour, the lateral extent of the scour then slowly increased outwards until it reached an equilibrium value. The extent of scouring can thus be seen to depend on the strength and size of the vortices. The strength and size of the vortices in turn depends on the acceleration of the flow. The corner vortex at the inner corners of the entrance to the contraction comes into existence as a result of the strongly converging streamlines at these locations as a result of the acceleration of the flow through the opening of the contraction. The principal vortex forms as a result of the vertical pressure gradient and associated downflow that occurs between the dead water region upstream of the contraction and the flow in the main channel. The greater the acceleration of the flow towards the opening of the contracted section, the steeper the pressure gradient and resulting vortex. It is thus obvious that under clear-water conditions, the equilibrium scour extent will depend on the velocity of the approach channel. This is also the conclusion that was drawn when considering scour depths around an abutment under clear-water conditions, although the reasoning is different.

Figure 6.15 shows the typical temporal behaviour of the local scour depth with time around an abutment under clear-water and live-bed scour. From this figure it can be seen that under clear-water conditions the local scour depth approaches its maximum value asymptotically and can be observed to take a longer time to reach this equilibrium value than under conditions of live-bed scour. In the literature it is even argued whether the equilibrium scour depth is ever realised under clear-water conditions.

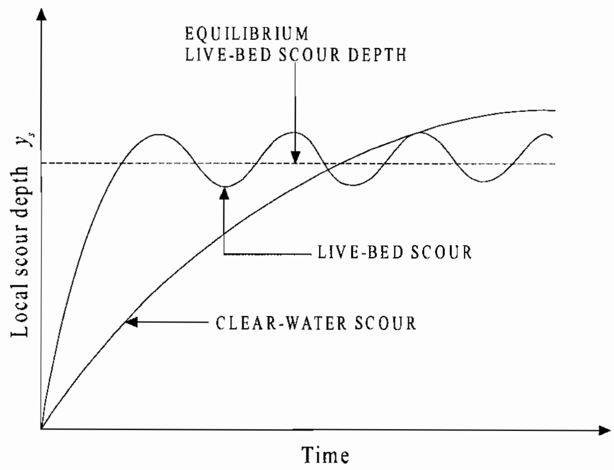

Figure 6.15: Figure showing the temporal behaviour of local scour around an abutment under clear-water and live-bed scour conditions

In this investigation, as with scour depths, it was observed that under clear-water scour conditions the equilibrium scour extent was approached asymptotically (see Figure 6.8). It was also observed that the equilibrium scour extent value often appeared to be reached within the experimental duration (12 hours). By considering Table 6.2, it can be seen that that the average time taken for the equilibrium scour to be reached around the entrance for the smaller opening ratio ($\alpha_c = ¼$) is less than the time taken for the larger opening ratio ($\alpha_c = ½$). This implies that the time taken to reach equilibrium conditions under clear-water conditions is dependent on the strength of the vortices responsible for the scour which in turn is dependent on the velocity gradient of the flow. For the smaller opening ratio, acceleration of the flow through the opening of the contraction was more severe than for the larger opening ratio thus resulting in a stronger convergence of the streamlines and the consequent formation of larger and stronger vortices.

Conditions of live-bed scour, which is defined as occurring when there is a continuous supply of sediment into the scoured region from the approach channel, were only observed at MP 7 of the scoured region downstream of the contraction. This was manifested by the fluctuations in the scour extent values when considering the temporal development of the scour. Figure 6.16 below is a typical example of the temporal behaviour of the scour at MP 7.

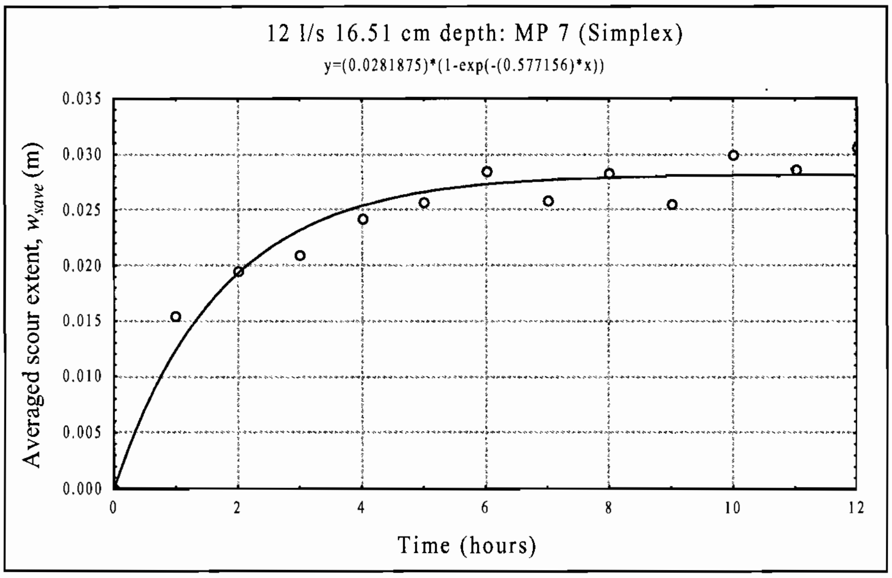

Figure 6.16: Figure showing the temporal development of the lateral extent of scour at MP 7 for α_c = ½

In the case of scour depths around abutments, the fluctuations that were observed in the scour depth (Figure 6.15) were explained in the literature as being caused by the migration of bed forms through the scour hole. In the case of this investigation, however, the observed fluctuations in the scour extent could rather be seen as a result of the erratic paths followed by the wake vortices as they are shed from the exit corners of the contraction. This erratic behaviour of the vortex streets can result in fluctuations in the instantaneous velocity along the channel bed, which is continuously being supplied with sand from the constricted reach, consequently resulting in fluctuations in the scouring process. It appears in Figure 6.16 that the scour extent values are fluctuating around an average scour value that can be viewed as being the equilibrium value.

Previous researchers observed that the time taken for the scour depth to reach equilibrium is less under conditions of live-bed scour than for conditions of clear-water scour (see Figure 6.15). In the case of this investigation, however, it was observed that for the measuring points downstream of the contraction, the time taken to reach equilibrium conditions was longer than that for the upstream measuring points and in most cases beyond the duration of the experiment. This was especially true for the measuring points affected by the sand from the contraction (MP 7 and MP 5). The reason for this is that it has been established above that the time taken to reach equilibrium conditions is dependent on the strength of the vortices responsible for the scour. The wake vortices shed from the downstream inner corners of the contracted section and into the downstream area could be seen as weaker than the vortices in the upstream region for the same approach conditions.

Live-bed conditions only existed throughout the duration of the experiment if the sand from the contracted reach was not completely cleared away from the downstream region. In the case where the sand was washed away, clear-water conditions would prevail. This mixture between scouring under live-bed and clear-water conditions was most evident at MP 5. MP 5 was seen to be less affected by the moving sand from the contracted reach in comparison to MP 7, as most of the sand that was observed to move along the edges of the scoured region was removed by the wake vortices further upstream. Figure 6.17 shows a typical example of the behaviour of the scour extent under both conditions of scour.

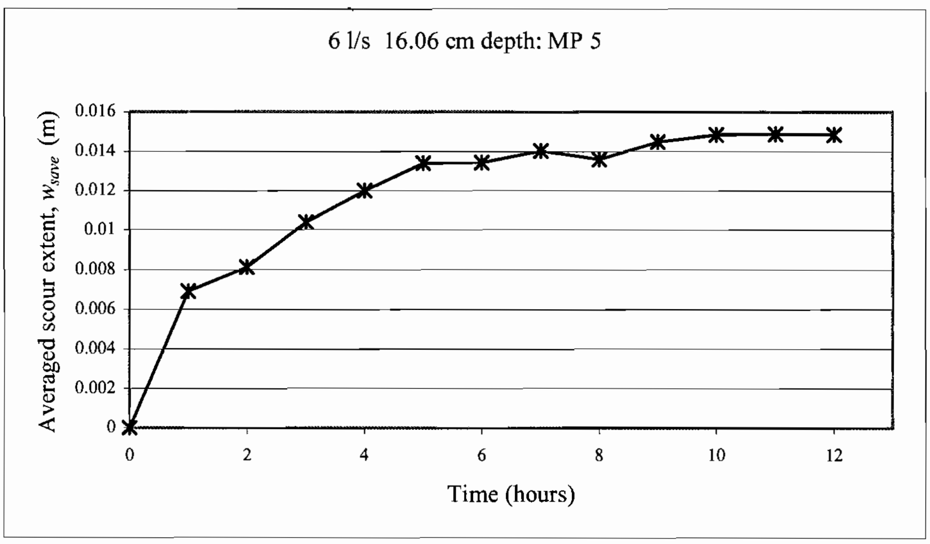

Figure 6.17: Figure showing the temporal development of the lateral extent of scour at MP 5 for α_c = ¼

From Figure 6.17 it can be seen that at first the scouring began under clear-water conditions as the scour lobes began to form (0 - 4th hour). As the experiment progressed, however, the scour extent began to become affected by migrating sand (5th – 8th hours) and was observed to fluctuate about what appeared to be an average scour extent value. This behaviour is indicative of live-bed scour conditions. From hours 8 to 9, the scour extent was then observed to increase after which it appeared to be stabilising at a higher scour extent value (10th – 12th hour) than that observed between the 5th and 8th hour. From the 8th hour the downstream area was cleared of sand and thus conditions of clear-water scour once again prevailed. It thus appears from the behaviour of the scour that the equilibrium scour extent value under live-bed conditions is lower than the equilibrium scour extent value under clear-water conditions. This could be explained by the fact that under live-bed conditions some of the sand scoured away by the wake vortices was replenished by the small amount of sediment transport that was taking place. This behaviour is close to the behaviour of the local scour depth under clear-water and live-bed conditions (for uniform ripple-forming sediment) as shown in the literature. In Figure 6.18, it can be seen that the equilibrium scour depth is a maximum under clear-water conditions after which, under live-bed conditions, the scour depth begins to gradually decrease.

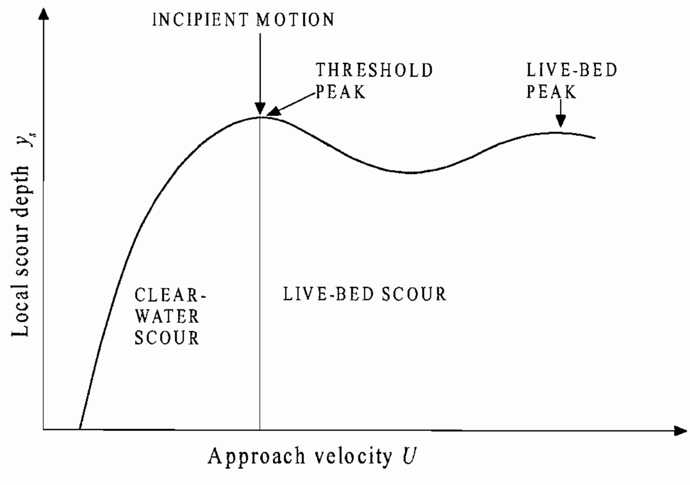

Figure 6.18: Figure showing the behaviour of the local scour depth with approach velocity around an abutment under clear-water and live-bed scour conditions for uniform non-ripple forming sediment

Chapter 7

Influence of the approach Froude number, approach depth and opening ratio on the initial local scouring around a rectangular long contraction

7.1 Introduction

Dimensional Analysis was employed to identify the candidate parameters that have the most influence on the scouring process around the contraction. These were found to be the approach Froude number, Fr_1, the dimensionless approach depth, Y_1 / L_c, and the opening ratio, α_c. In this investigation the influence of the sediment size and shape of the contraction was excluded from the analysis. The equilibrium scour extent values as well as the approach depth were rendered dimensionless by the scaling factor $\lambda = L_c$.

In this chapter the resulting relationships between the approach Froude number and approach depth on the scour extent around the contraction are presented and discussed. The influence of these two parameters on the scour extent are considered separately for the two opening ratios used in the experiments, α_c = ½ and ¼. The influence of the opening ratio on the lateral extent of scour is then presented and discussed.

For all of the results presented, only measuring points MP 2, MP 3 and MP 6 were considered. Reasons for this choice are presented in this chapter. Mention is also given to the data points that were identified as outliers and thus removed from the data sets that were used in the analysis.

The results obtained from the experimental process were compared to those found in the literature concerning the investigation of local scour depths around abutments. Although this investigation considered a long contraction and not an abutment, local scouring around a long contraction can be seen as a variant of local scouring around an abutment (Laursen, 1962). It was also believed that the scour depth could be related to the lateral extent of the scour through the angle of repose of sediment in water. In order to verify the latter assumption, likely scour depths were deduced from the experimentally measured scour extents around the contraction and compared to the scour depths predicted by published equations. The scour depths derived by Laursen (1963) and Lim (1997) were used in this comparison.

The data sets available for the analysis were limited due to a limited time available for experimentation. Also, experimental work will always be prone to some degree of error. For these reasons, the findings in this investigation are aimed more at understanding the process of initial scour formation around a long contraction rather than providing values for design purposes.

7.2 Measuring positions chosen for analysis

In the investigation into the influence of the various parameters on the scour extent around a long contraction, measuring points MP 1, MP 4, MP 5 and MP 7 were excluded from the analysis, in other words, only MP 2, MP 3 and MP 6 were considered (see Figure 4.1 for clarification of the MP positions).

The scour extent measurements at MP 1 were excluded from the analysis due to the build up of the sand layer along the upstream face of the contracted section as a result of the operation of the sand spreader. It was observed that this build up of sand influenced the temporal development of the scour.

The scour measurements at MP 4 were excluded from the analysis as the scouring process at this point was observed to be erratic. This was attributed to the interaction of the wake vortices that were shed from the inner corners of the entrance to the contraction. It was also observed that the scour extent at MP 4 often failed to reach stable conditions within the duration of the experiment.

MP 5 (b_c downstream of the contraction) and MP 7 (b_c / 4 downstream of the contraction) were excluded from the analysis as the scouring process appeared to be disturbed by the migrating sand from the upstream region and contracted section of the long contraction. Scouring at these measuring points exhibited behaviour typical of live-bed scour conditions. This was especially evident at MP 7, which was the closest measuring point to the corners of the exit to the contraction.

7.3 Removal of outlying data points

For opening ratio α_c = ¼, possible outlying data points for MP 2, 3 and 6 were identified with the aid of cubic spline interpolation. It was decided that for MP 2, 3 out of the 19 data points would be removed. These were for the following experiments: 6 *l*/s with approach depth 14.48 cm, 6 *l*/s with approach depth 15.45 cm, and 9 *l*/s with approach depth of 21.54 cm. For MP 3, only 1 out of the 16 data points was removed. This point was for 6 *l*/s with approach depth 14.48 cm, which is the same experiment that was identified as problematic for MP 2. For MP 6, 3 out of the 16 data points were identified as outliers and removed. These were for the following experiments: 3 *l*/s at approach depth 9.27 cm, 6 *l*/s at approach depth 14.61 cm, and 9 *l*/s at approach depth 23.45 cm.

For opening ratio α_c = ½ it was evident that there was a problem with the experiment utilising 8 *l*/s at an approach depth of 14.30 cm as all the data corresponding to this experiment had to be scrapped from the analysis. Just one other point was removed for MP 3 which was for 10 *l*/s at an approach depth of 13.55 cm.

It was obvious by looking at the data sets that these points were clear outliers and were influencing the interpolated curves representing the approach Froude number. The scouring process around the contraction was found to be very sensitive to any disturbance that might have occurred during the duration of the experiment as the scour extent only increases by very small amounts (sometimes only fractions of a millimetre) every hour, especially when it was close to reaching a stable value. Any sudden disturbance to the scouring process such as large particles in the flow being carried over the test section, a sudden surge in pressure in the pumps, or perhaps the tailgate being lowered too quickly at the start of the experiment will cause a large error in the scour extent value. Also a problem might have occurred when the experiment was run over a two-day period, as it is unlikely that the exact flow conditions could be replicated on the second day thus causing error. It is interesting to see that the downstream measuring points appeared to be the only points affected when the experiments were run over two days.

7.4 Influence of the approach Froude number on the scour extent around a long contraction

In the following section, the results showing the influence of the approach Froude number on the scour extent around a long contraction are presented separately for both opening ratios α_c = ¼ and ½. A brief description of the procedure leading up to the results for the two opening ratios is also given. The results are then followed by a detailed discussion.

7.4.1 Results for Approach Froude number for opening ratio α_c = ¼

In order to determine the relationship between the approach Froude number and the scour extent around a long contraction for an opening ratio α_c = ¼ (see Section 5.7.2 for calculation method), a dimensionless approach depth of 0.7 was chosen to be kept constant. This value of dimensionless approach depth was chosen as it provided the maximum number of data points of the approach Froude number with the corresponding value of dimensionless scour extent to be used in the analysis. The two latter values were read off from the graphs of w_s/L_C versus Y_1/L_C (with interpolated curves of Fr_1) for MP 2, 3 and 6 and the results presented in a plot of w_s/L_C versus Fr_1. These results can be viewed in Figure 7.1.

It was noticed in the results that for the various measuring points the dimensionless scour extent values appeared to be increasing at an increasing rate with increasing values of the approach Froude number towards the end of the plots. This was especially evident for MP 2 and MP 3. This is an unlikely trend as it is expected that the extent of scour should increase at a decreasing rate with increasing approach Froude number. This is due to the geometrical constraints of the structure and the channel, as well as the limitation of the size to which the vortices can develop. It was thus considered whether the problem could be caused by distortions due to the sparsity of the data. For this reason, the data points of the experiment for which live-bed conditions were deemed to exist in the region downstream of the contraction (Fr_1 = 0.054007) were included back into the data sets. The resulting plots of the dimensionless scour extent versus the approach Froude number are shown Figure 7.2. It should be noted that the dimensionless depth of 0.7 was once again held constant.

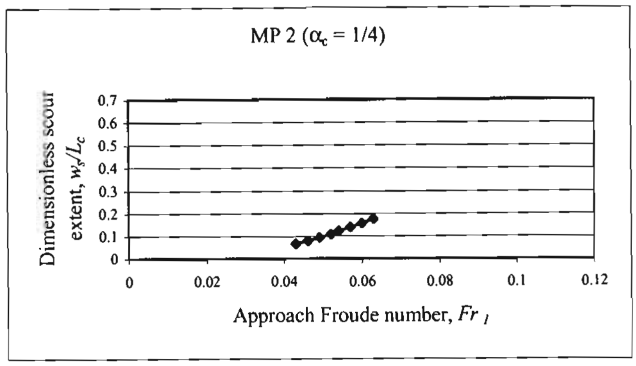

(a)

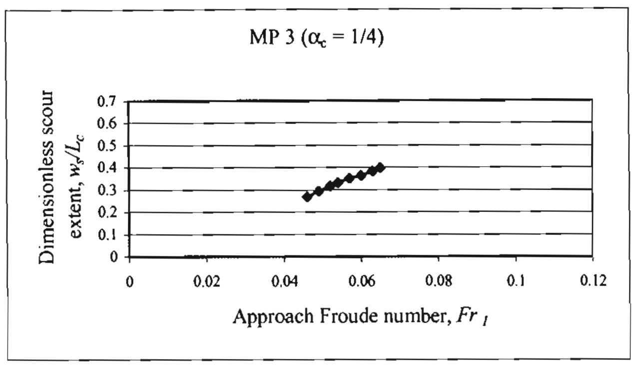

(b)

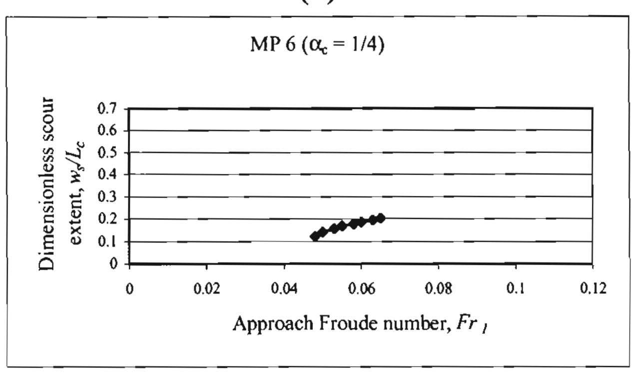

(c)

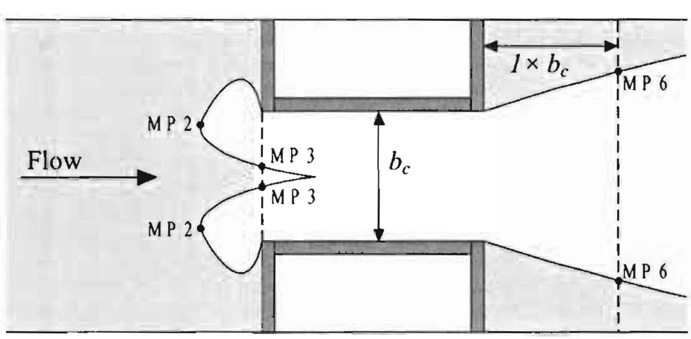

Figure 7.1: Results showing the influence of the approach Froude number on the scour extent around a long contraction for α_c = ¼, Y_1 / L_c = 0.7

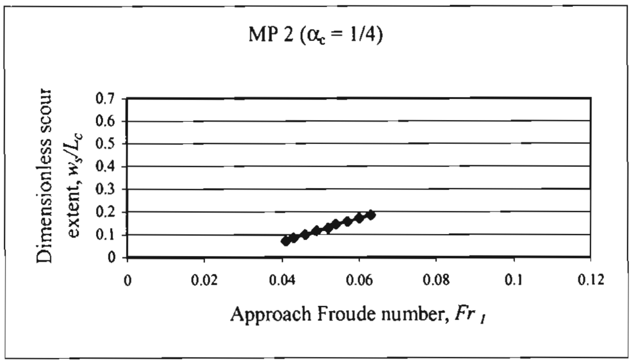

(a)

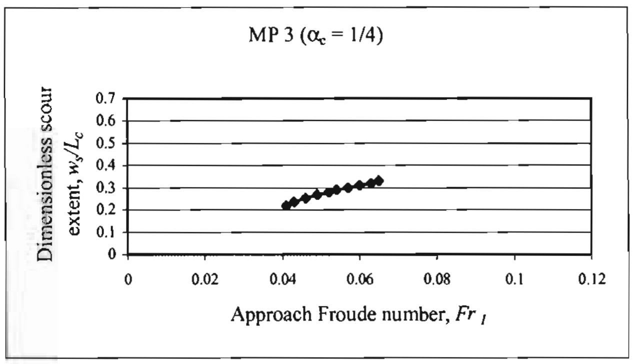

(b)

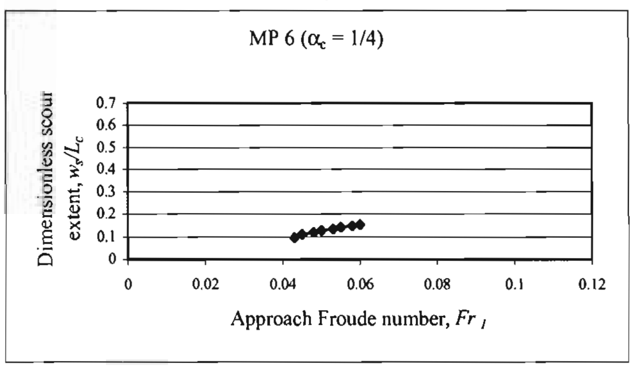

(c)

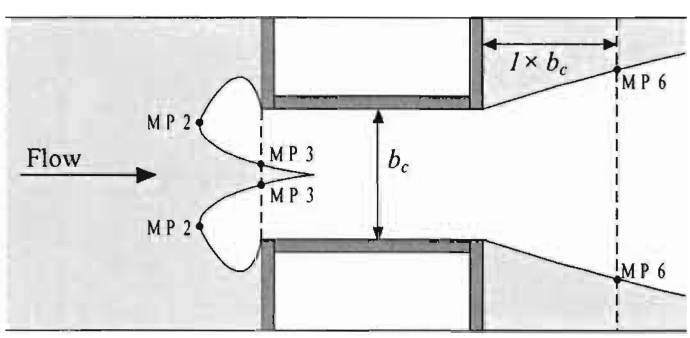

Figure 7.2: Results showing the influence of the approach Froude number on the scour extent around a long contraction for α_c = ¼, Y_1 / L_c = 0.7 where data point corresponding to Fr_1 = 0.054007 has been included into the data set

The inclusion of the point representing Fr_1 = 0.054007 into the data set produced curves that appear to be more representative of the relationship between the approach Froude number and the dimensionless scour extent. The differences seen in the plots of Figures 7.1 and 7.2 were as a result of the "flattening out" of the interpolated curves representing Froude number in the plots of dimensionless scour extent versus dimensionless approach depth. This effect is clearly illustrated in Figure 7.3 for MP 2 for which it was the most drastic.

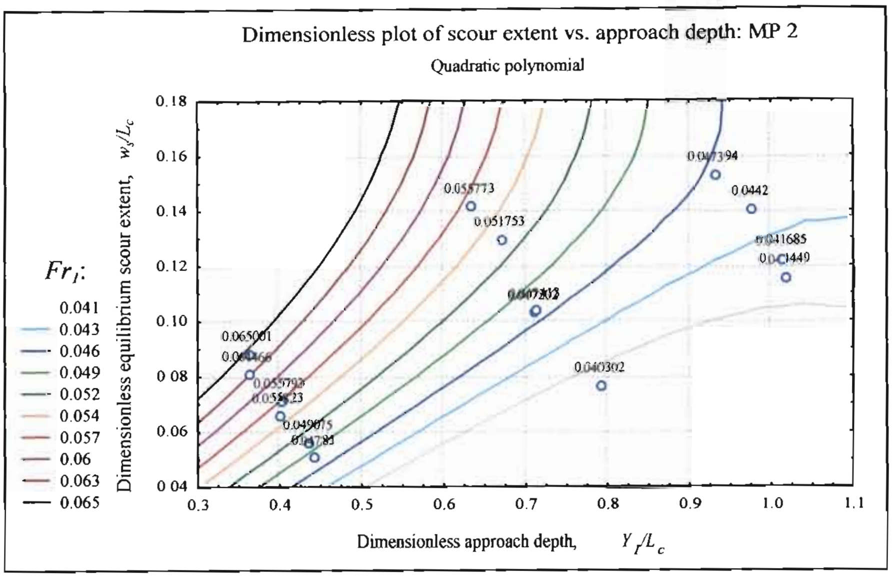

(a)

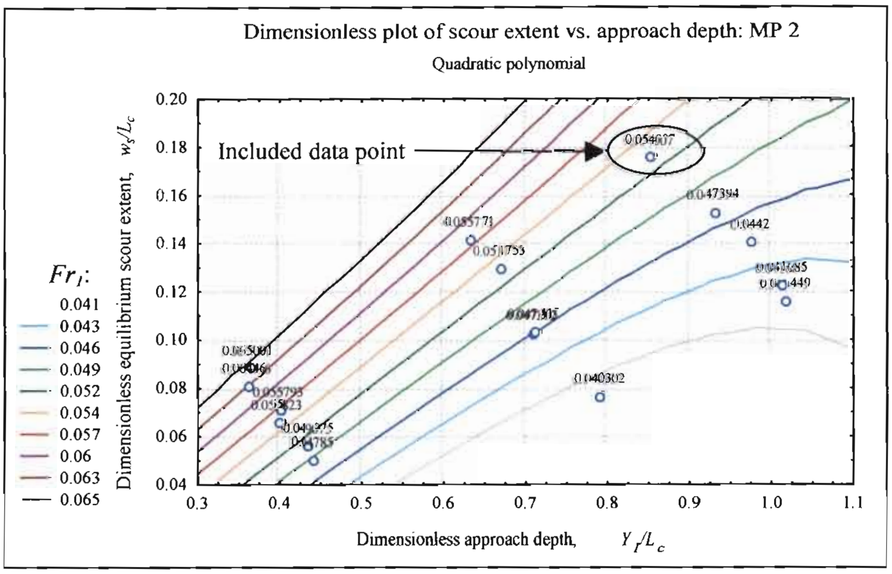

(b)

Figure 7.3: Figure showing behaviour of interpolated curves (a) before the inclusion of point Fr_1 = 0.054007 and (b) after the inclusion of point Fr_1 = 0.054007 into the data set

The resulting interpolated curves can be considered to be more representative of the true situation, as if a data point was added to the data set instead of the point representing $Fr_1 = 0.054007$, which had the same flow rate but which just fell below the limiting intensity of motion, the approach Froude number of that point would be even less, thus causing the curves to flatten out even more.

Although the inclusion of the point representing $Fr_1 = 0.054007$ into the data set appeared to show a better numerical result between the dimensionless scour extent and the approach Froude number, it still remained that it was associated with constriction scour within the contracted reach. This implies the existence of live-bed scour conditions in the downstream region of the contraction. It was however observed that the contracted reach and downstream region of the contraction was cleared of sand within the first few hours of the experiment, after which clear-water conditions could be deemed to exist in the downstream region. The only measuring point affected throughout the experiment by the constriction scour within the contracted reach was MP 4, and this point was excluded from the analysis. Although MP 3 is in line with the upstream face of the contraction, it was assumed that the local effects were more dominant than the constriction scour at this point and thus could be used in the analysis.

Seeing that there was negligible movement of sediment in the approach channel, it could thus be said that clear-water conditions existed for all of the measuring points (except for MP 4) considered for this experiment. This assumption is confirmed in Figure 7.4 which shows that for the downstream measuring point MP 5, the scour extent was seen to be the greatest in comparison to the other runs of the same flow rate (9 *l*/s) that were performed under clear-water conditions. This behaviour is indicative of clear-water scour conditions in which the scour extent can be seen to scale with the velocity of the approach flow which was the greatest for the experiment under question.

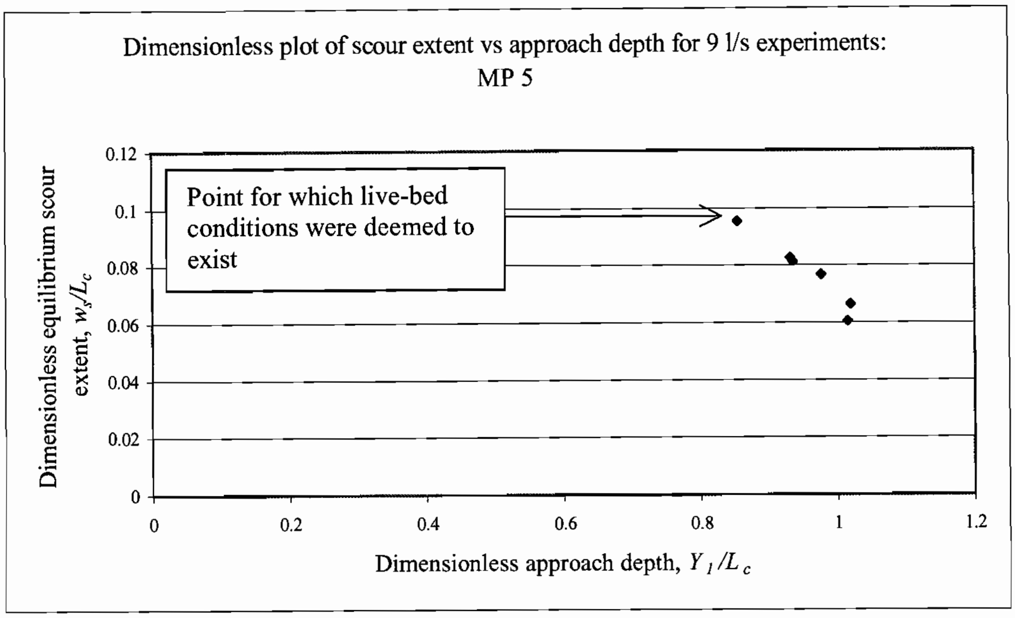

Figure 7.4: Figure showing dimensionless scour extent vs dimensionless approach depth at MP 5 for experiments with a flow rate of 9 *l*/s

It should be noted that although it can be considered that clear-water conditions occurred throughout the contracted section, this is somewhat artificial here. Live-bed scour conditions existed but there was simply a lack of material to be transported by the flow. These special cases of clear-water scour, however, have been found to occur in nature when the river bed becomes vegetated to a point that the movement of material is prevented.

The following discussion on the influence of the approach Froude number on the lateral extent of scour around a long contraction will thus only consider the results presented in Figure 7.2. It should be noted that the range of the approach Froude numbers considered in this discussion are small due to the limitations experienced in setting up the conditions for each experiment. The flows and depths chosen were limited by ensuring that constriction scour did not occur within the contracted reach, in other words, clear-water conditions prevailed throughout the contraction; that the depths did not exceed the height of the long contraction; and that the conditions were such that a sufficient amount of scouring occurred at the measuring points downstream of the long contraction. The resulting plots were not extended for approach Froude numbers greater or less than the existing values, as it was unsure what the behaviour of the line would be for the other values.

7.4.2 Discussion on results obtained for approach Froude number for opening ratio $\alpha_c = ¼$

From Figure 7.2 it can be seen that in general the dimensionless scour extent around a long contraction increases for increasing values of approach Froude number. This phenomenon can be logically explained by the fact that the approach Froude number is a function of the approach velocity. It has been shown in Chapter 6 that the equilibrium scour extent is dependent on the strength of the vortices responsible for the scour. These were seen to be the corner vortex and the principal vortex in the upstream region and the shedding wake vortices in the downstream region of the contraction. The strength (vorticity) of the vortices in turn can be seen to be dependent on the velocity gradients, the steepness of which depends on the approach velocity. It can thus be logically deduced that the scour extent under clear-water conditions would increase with increasing approach velocity and thus with increasing values of the approach Froude number.

It also appears from the plots in Figure 7.2 that none of the graphs would pass through the origin. This finding is expected as the approach velocity would have to reach a minimum value before the velocity gradients within the flow become steep enough to form vortices strong enough to entrain the sediment.

It is expected that the dimensionless scour extent should increase at a decreasing rate with the increase in approach Froude number due to the geometrical limitation of the structure and the channel, and the limitation of the size to which the vortices can develop. This result can be seen for both MP 3 (Figure 7.2(b)) and MP 6 (Figure 7.2(c)). For MP 2 (Figure 7.2(a)), however, the dimensionless scour extent appeared to be increasing almost linearly with the approach Froude number. The possible reason for this could be due to the fact that both the corner and the principal vortex, and their interactions at this point, might have a significant influence on the resulting lateral extent of scour. The principal vortex increases in strength towards the inner corners of the upstream face of the long contraction, thus at low approach Froude numbers (low velocities), the influence of the principal vortex on the bed would only occur very close to the corners of the entrance to the contracted section. It is also at these corners that the corner vortex forms, and thus perhaps the corner vortex would have a dominating influence on the bed rather than the principal vortex at low velocities. As the approach Froude number (velocity) increases, however, the principal vortex gains in strength and will begin to scour further upstream along the boundary between the dead water region and the fast-flowing water in the main channel. It is thus possible that the corner vortex would have less of an influence on the scouring ability of the principal vortex for increasing velocity. This could explain the approximate linear relationship between the scour extent and the approach Froude number in comparison to the other two measuring points. It would be expected, however, that eventually the scour extent should start to increase at a decreasing rate owing to geometrical restrictions, but perhaps the data set is not large enough for this effect to be shown.

From Figure 7.2(c) it can be seen that the dimensionless scour extent at MP 6 increases at a lesser rate with the approach Froude number than for the upstream measuring points. This is an expected result because if the approach Froude number were to be increased, it is reasonable to assume that the upstream vortices, which form as result of the strongly converging flow through the opening of the contraction, would be of a higher vorticity than the downstream wake vortices that form as a result of the shearing action between the dead water region downstream of the contraction and the fast-flowing water in the main channel. It is also known that as these downstream wake vortices move further downstream from the corners into the flow, they diminish in strength due to the deceleration of the flow. Seeing that MP 6 is located at a distance of one times the width of the opening of the contraction from the downstream corners, it is expected that the vortices would have decreased in strength when reaching this point.

The literature (Laursen, 1962; Zaghloul, 1983; Melville, 1992 and Lim, 1997) reports that the scour depth increases with increasing approach velocity around abutments under clear-water scour conditions. Seeing that the approach Froude number is a function of the approach velocity, the findings in the literature can be seen to be similar to the findings in this investigation of the scour extent around a long contraction.

7.4.3 Results for approach Froude number for opening ratio $\alpha_c = ½$

In order to determine the influence of the approach Froude number on the scour extent around a long contraction for an opening ratio of α_c = ½ (see Section 5.7.2 for calculation method), a dimensionless approach depth of 0.95 was chosen to be held constant. This value of dimensionless approach depth was chosen as it provided sufficient data points of the approach Froude number with the corresponding value of dimensionless scour extent to be used in the analysis. These values were read off the graphs of w_s/L_c versus Y_1/L_c (with interpolated curves of Fr_1) and plots of w_s/L_c versus the Fr_1 were produced for MP 2, 3 and 6. These results can be viewed in Figure 7.5. It should be noted that the data points of the experiment associated with live-bed conditions in the region downstream of the contraction were included in the analysis for reasons as described in the above Section 7.4.1.

7.4.4 Discussion on results obtained for opening ratio $\alpha_c = ½$

From Figure 7.5 it can be seen that as for opening ratio α_c = ¼, the dimensionless scour extent generally appears to be increasing with increasing values of the approach Froude number. This was explained in Section 7.4.3 to be as a result of the increase in the strength of the vortices responsible for scouring with increasing approach velocity under clear-water scour conditions. The graphs in Figure 7.5 also do not appear to pass through the origin. This is an expected result as there must be a limiting approach velocity beyond which the vortices will become strong enough to be able to begin scouring the bed.

For the upstream measuring points, MP 2 (Figure 7.5(a)) and MP 3 (Figure 7.5(b)), the dimensionless scour extent increases at a decreasing rate with increasing values of the approach Froude number. This behaviour of scour is reasonable as there must be a limitation to the extent of scour that can occur around the contraction due to the geometrical limitation of the structure and the channel, as well as the limitation of the size to which the vortices can develop.

At MP 6, it can be seen that although the dimensionless scour extent is increasing at a decreasing rate with increasing values of approach Froude number, the rate at which the scour extent increases is higher than for those of the upstream measuring points. This is an unexpected result as it is known that the wake vortices shed from the downstream inner corners of the contracted section will be weaker than the upstream vortices for the same increase in approach Froude number (approach velocity). Owing to the limited number of data points available for analysis for this opening ratio (only

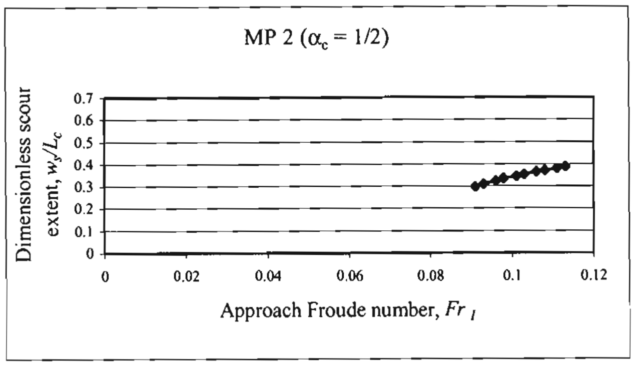

(a)

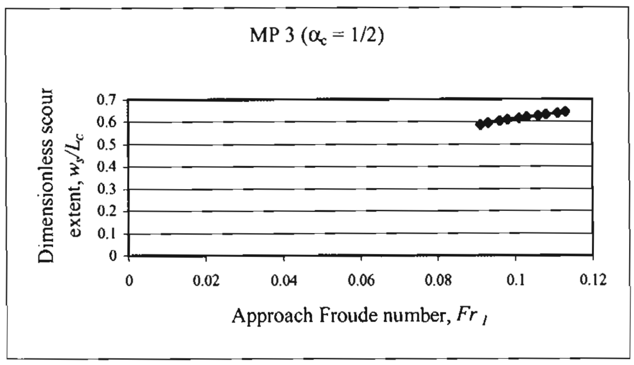

(b)

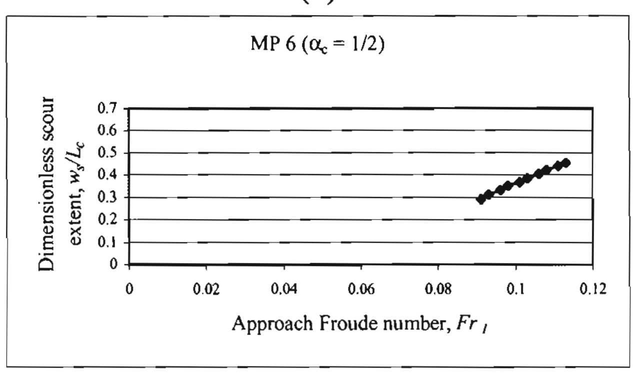

(c)

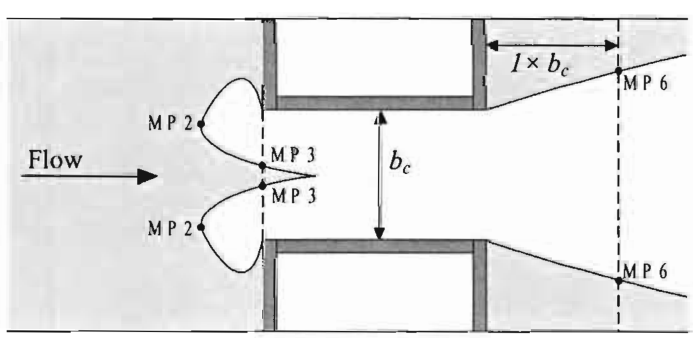

Figure 7.5: Results showing the influence of the approach Froude number on the scour extent around a long contraction for α_c = ½, Y_1 / L_c = 0.95

9 data points), it is a possibility that any outlying point that might not have been detected could have influenced the interpolation between the approach Froude number values. This could result in an irregular relationship between the dimensionless scour extent and the approach Froude number. Smaller data sets are more prone to influences of error in interpolation and at the same time make it more difficult to be able to detect outlying points.

Another possible explanation that can be offered for the scouring behaviour at MP 6 concerns the likely lateral instability in the wake downstream of the contraction. Around the upstream face of the contraction, the vortices that form and the paths that they follow are fixed by the geometry of the contraction and the channel, whereas downstream of the contraction, the paths of the vortices are not fixed. The downstream wake vortices are shed from side to side from the corners of the exit to the contraction thus resulting in an unstable environment. The higher the approach Froude number, the more shearing action that occurs downstream of the contraction, thus resulting in a higher instability in the wake. It is therefore expected that at higher approach Froude numbers, more sand would be scoured away from either side of the paths of the vortices due to the increased instability of the vortex paths. Seeing that the experiments for the larger of the two opening ratios were run at higher Froude numbers (see paragraph below), this might offer an explanation as to why this scour behaviour at MP 6 was not observed for the smaller opening ratio.

When the results showing the influence of the approach Froude number on the dimensionless scour extent are considered for the two opening ratios (Figure 7.2 and Figure 7.5), it can be seen that the range of approach Froude numbers over which the data spans is different. For opening ratio $\alpha_c = ¼$, the data can be seen to range over approach Froude numbers of 0.04-0.065 whereas for $\alpha_c = ½$ the approach Froude numbers can be seen to range between 0.09-0.13. The differing ranges of approach Froude number are attributable to the limitations experienced in the determination of the conditions of the experiments used in the investigation. In the experimental process, the flow rates and approach depths chosen for each contracted section were limited by the lowest possible depth within the contracted reach below which constriction scour would exist, and the height of the long contraction section which was 300 mm (see Section 4.2.2). Conditions were also chosen so that sufficient scouring would occur in the region downstream of the contracted section such that reasonable deductions could be made on the scouring process in this region. An effective comparison between the two opening ratios can thus not be readily made in regard to the influence of the approach Froude number on the extent of scour. It is expected, however, that for the same increase in Froude number for the two opening ratios, the resulting increase in the extent of scour should be greater for the smaller opening ratio than for the larger. This could be explained by the fact that for an increase in the approach Froude number (approach velocity) the acceleration of the flow into the opening of the contraction would be more severe through a smaller opening in comparison to a larger opening thus resulting in the stronger convergence of the streamlines. The stronger the convergence of the streamlines, the steeper the velocity gradients and the stronger the resulting vortices.

As for the smaller opening ratio, in general the influence of the approach Froude number on the scour extent around long contractions compares favourably to the findings in the literature that considered local scour depths around abutments under conditions of clear-water scour (Laursen, 1963; Zaghloul, 1983; Melville, 1992 and Lim, 1997).

7.5 Influence of the approach depth on the scour extent

In the following section, the results of the influence of the approach depth on the extent of scour around a long contraction for the two opening ratios, α_c = ½ and ¼, are considered separately. A brief description of the calculation procedure leading up to the results is given, which is then followed by a detailed discussion.

It should be noted that the data points for the experiment associated with live-bed conditions were included into the data sets. Also, the plotted lines of dimensionless scour extent versus the dimensionless approach depth were not extended beyond the range of the available data, as it was unsure of the exact behaviour of the plots beyond the scope of the available data sets.

7.5.1 Results for approach depth for opening ratio α_c = ¼

In order to determine the influence of the approach depth on the lateral extent of scour around a long contraction for an opening ratio α_c = ¼ (see Section 5.7.2 for calculation method), an approach Froude number of 0.054 was chosen to be kept constant. This value of approach Froude number was chosen as it was observed to extend over a fairly large range of dimensionless approach depth values. The values of dimensionless approach depth and the corresponding dimensionless scour extent values were then read off from the curve representing $Fr_1 = 0.054$ from the plots of w_s/L_c versus Y_1/L_c (with interpolated curves of Fr_1) for MP 2, MP 3 and MP 6, and the results presented in a plot of w_s/L_c versus Y_1/L_c. The results are shown in Figure 7.6.

7.5.2 Discussion on results obtained for opening ratio $\alpha_c = 1/4$

When considering Figure 7.6, it can be seen that the dimensionless scour extent increases with increasing values of the dimensionless approach depth. For MP 2 (Figure 7.6(a)), the dimensionless scour extent values appear to be increasing approximately linearly with the approach depth. This result differs from those of MP 3 (Figure 7.6(b)) and MP 6 (Figure 7.6(c)) that show the scour extent to increase at a decreasing rate. The results also show that it is a possibility that the plotted lines of the dimensionless scour extent versus the dimensionless approach depth could pass through the origin. This is an expected result as scour could not possibly occur at a zero depth of flow.

For the upstream measuring points, MP 2 and MP 3, the resulting relationship between the lateral extent of the scour and the approach depth can be explained by the interference of the "roller" or "bow wave" on the principal and corner vortices. The roller is known to reduce the strength of the vortices with which it comes into contact, thus as the roller forms near to the surface of the flow, it would logically follow that it would have more of an influence on the existing vortex structures for shallower flows and less of an influence for deeper flows.

When considering the rate of increase of the scour extent with the approach depth, it is to be expected that the scour extent should increase at a decreasing rate. This is a reasonable assumption as there must be a limiting depth beyond which the roller will no longer have a significant influence on the vortices responsible for the scour. This trend is indicated by MP 3, although the dimensionless scour extent appears to be increasing almost linearly with the dimensionless approach depth for MP 2. A possible explanation for the behaviours shown for MP 2 and MP 3 could be offered by the consideration of the degree of influence that the roller has on the principal and corner vortices.

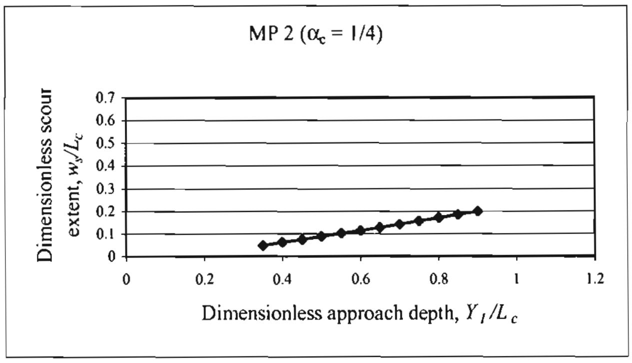

(a)

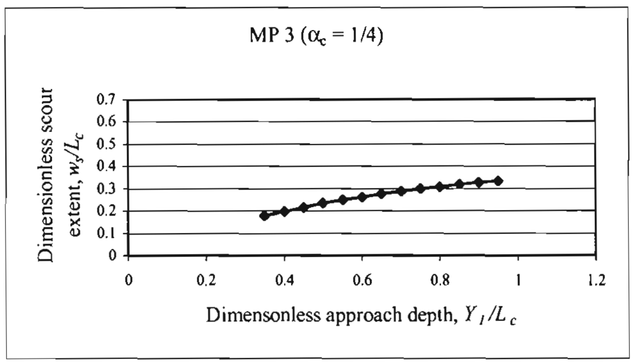

(b)

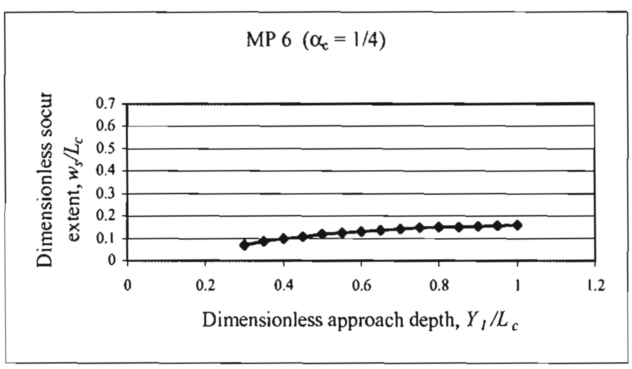

(c)

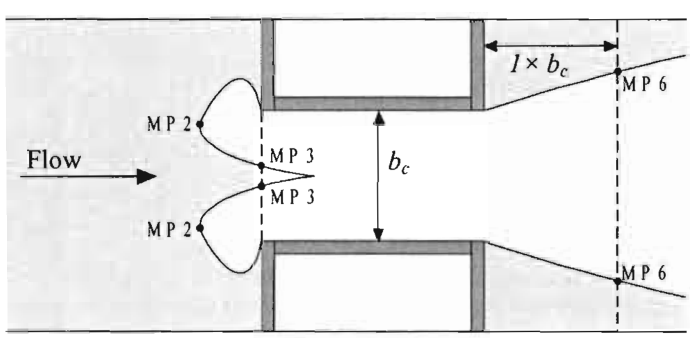

Figure 7.6: Results showing the influence of the approach depth on the scour extent around a long contraction for α_c = ¼, Fr_1 = 0.054

For $\alpha_c = ¼$, it has been shown in Chapter 6 that at MP 2 the lateral extent of scour is influenced by both the principal vortex and the corner vortex, whereas at MP 3 the corner vortex can be seen as the predominant scouring agent. Seeing that the principal vortex forms along the same boundary between the dead water region and the fast-flowing water in the main channel as the roller, this vortex will be more exposed to the roller than the corner vortex, which forms at the inner corners of the entrance to the contraction and is shed downstream towards the centre of the flume. It is also known that the roller is counter-rotating to the principal vortex and thus is likely to have more of an influence on the vorticity of the principal vortex than the corner vortex that rotates at right angles to the roller. Thus at MP 2 it can be expected that an increase in depth will have more of a marked impact on the extent of scour as the influence of the roller on the principal vortex decreases than at MP 3, where the decrease in the influence of the roller will be less felt.

For the upstream measuring points, although the dimensionless scour extent is increasing approximately linearly with the dimensionless approach depth at MP 2, it is expected that there is a limiting depth beyond which the scour extent will become independent of the approach depth. Melville (1992), who conducted research on scour depths around abutments, recognised this limit as when the ratio of the approach depth (Y_l) to the length of the abutment perpendicular to the flow (L_a) is greater than or equal to 1, after which the scour depth was rendered independent of the approach depth. In the case of this investigation, although the plotted values do not go beyond $Y_l / L_c = 1$, it is expected that the limiting approach depth to length ratio for a long contraction should be greater than that provided by Melville. The reason for this is that in the case of scour depths around abutments, the principal vortex becomes concealed within the scour hole thus rendering it less vulnerable to the influence of the roller. In this investigation of the lateral extent of scour, however, the principal vortex and corner vortex were exposed above the bed and thus were more vulnerable to being affected by the counter-rotating roller.

When the relationship between the approach depth and the scour extent is considered for the downstream measuring point, MP 6, it can be seen that the dimensionless scour extent increases with increasing values of the approach depth but at a lesser rate than was seen for the upstream measuring points. This can be explained by considering the lateral movement of the trailing wake vortices responsible for scouring in the downstream region. In the case of this investigation, because the vortices were prevented from eroding downwards into the bed, the lateral movement of the vortex will be dependent on the depth of the flow. The deeper the flow, the more freedom the vortices have to oscillate from side to side as they are carried by the flow downstream. It is therefore expected that larger scoured regions should develop for deeper flow rather that for shallow flows where the lateral movement of the vortices is more restricted. From Figure 7.6 it can be seen that the plot is increasing at a decreasing rate and appears to be reaching an asymptotic value at which the scour extent will become independent of the approach depth. This is a reasonable result because for the same geometry of the channel and the same approach velocity, the vortices that form must have a limiting size. There must also be a limiting depth beyond which the lateral movement of the vortex will no longer be influenced by the depth.

For the upstream measuring points, the result that the scour extent increases with increasing approach depth compares favourably with the findings of Laursen (1963), Zaghloul (1983) and Lim (1997). Melville (1992) determined that the scour depth scaled with the approach depth when the abutment was either classified as "intermediate" for which $1 < L_a / Y_1 < 25$, or as "long" for which $L_a / Y_1 > 25$. In the case of this investigation, when the ratios of the length of the upstream face of the long contraction perpendicular to the approach flow (L_c) to the approach depth (Y_1) were calculated, the majority of the experiments fell under the "intermediate" category as defined by Melville. It can thus be said that the results compare favourably to the findings of Melville. It was however noted in this investigation that the limiting depth beyond which the scour extent will become independent of the approach depth should occur at a value greater than that predicted by Melville ($Y_1 / L_c = 1$), due to the increased exposure of the corner and principal vortex to the roller.

Although no literature was found for local scouring downstream of a long contraction, it is believed that the measurements for MP 6 showing the scour extent increasing with increasing approach depth would also apply to situations that consider local scour depths around structures.

7.5.3 Results for approach depth for opening ratio $\alpha_c = ½$

In order to determine the relationship between the approach depth and lateral extent of scour around a long contraction for an opening ratio α_c = ½ (see Section 5.7.2 for calculation method), an approach Froude number of 0.103 was chosen to be held constant. This value of approach Froude number was observed to extend over a fairly large range of dimensionless approach flow values and thus provided a good representation of the measured data. The values of dimensionless approach depth and the corresponding dimensionless scour extent values were then read off from the curve representing $Fr_1 = 0.103$ from the plots of w_s/L_C versus Y_1/L_C (with interpolated curves of Fr_1) for MP 2, 3 and 6, and the results presented in a plot of w_s/L_C versus Y_1/L_C. The results are shown in Figure 7.7.

7.5.4 Discussion on results obtained for opening ratio $\alpha_c = ½$

The dimensionless scour extent for the upstream measuring points, MP 2 (Figure 7.7(a)) and MP 3 (Figure 7.7(b)), can be seen to increase initially with increasing dimensionless approach depth values, after which it appears to stabilise at $Y_1/L_C \approx 0.85$ and then to decrease slowly from $Y_1/L_C \approx 1.00$. The plotted lines for MP 2 and MP 3 also appear as though they could pass through the origin of the graph if their curves were continued towards the origin. This is an expected result seeing that at a zero approach depth there could not possibly be any scouring.

In comparison to the results obtained for opening ratio α_c = ¼ it can be seen that for opening ratio α_c = ½, the scour extent appears to be generally independent of the approach depth from $Y_1/L_C \approx 0.85$. This can be explained by considering the role of the two vortices, namely the corner and principal vortex, on the scouring process for this opening ratio.

It was observed that for α_c = ½ the corner vortex appeared to be the dominant vortex responsible for scouring around the upstream region of the contraction, in comparison to the principal vortex that was seen as being quite weak and thus not to contribute significantly to the scouring process. This is evident from the Figure 7.7(a) and (b) where it can be seen that the resulting relationship between the dimensionless scour extent and the dimensionless approach depth are similar for both MP 2 and MP 3.

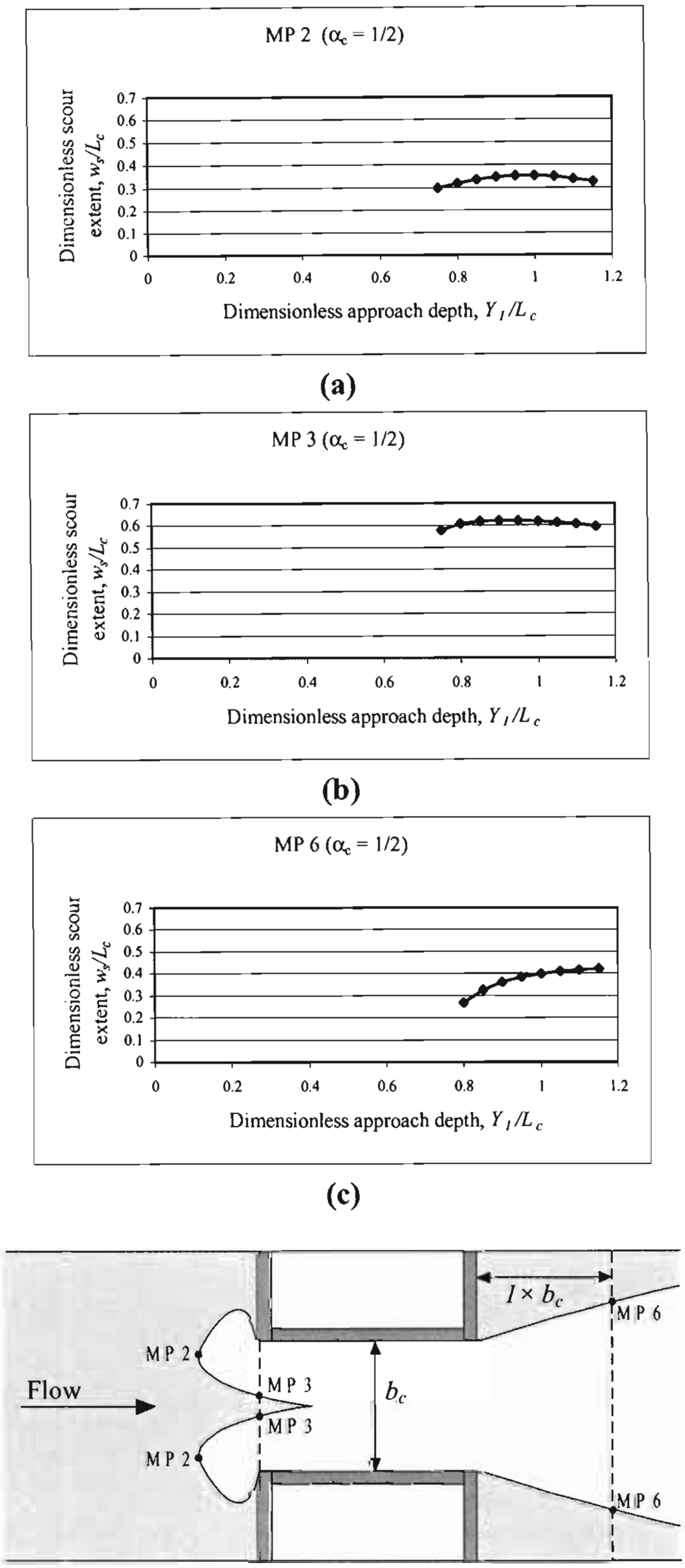

Figure 7.7: Results showing the influence of the approach depth on the scour extent around a long contraction for $\alpha_c = ½$, $Fr_1 = 0.103$

Seeing that it has been established in Section 7.5.2 that the roller has less of an influence on the corner vortex than the principal vortex, it would thus be expected that at MP 2 the influence of the approach depth on the scour extent should be less for $\alpha_c = ½$ than for $\alpha_c = ¼$. This is the observed result. It is also believed that for the same approach velocity, the strength of the roller for $\alpha_c = ½$ will be less than that for $\alpha_c = ¼$. This is because the acceleration of the flow through the larger opening would be less than that for the smaller opening. This would imply that for a larger opening ratio, the increase in pressure along the boundary between the dead water region upstream of the contraction and the fast-flowing water in the main channel would be less than that for the smaller opening ratio, thus resulting in a weaker vortex. The roller would thus in general have less of an influence on the scour extent for the larger opening ratio. It in fact appears from Figure 7.7(a) and (b) that for $Y_1 / L_c \geq 0.85$ the corner vortex is not influenced by the roller in any manner.

Note that although it is expected that the roller will be less influential on the scouring process for the larger opening ratio, it cannot be certain that the extent of the scour will become independent of the approach depth at a limiting approach depth (Y_1) to length (L_c) ratio less than that as found by Melville (1992), which is $Y_1 / L_a \geq 1$. The reason for this is that in the case of local scour depths, the principal vortex, which was seen as being the dominant vortex, became concealed within the scour hole and was thus less exposed to the roller than the vortices in this investigation that exist above the bed. It is a possibility, however, that in this case of lateral scour around a long contraction for $\alpha_c = ½$, the roller will be too weak in comparison to the corner vortex to have an influence on the scouring process. In order to have a better understanding of these findings, it is recommended that a larger data set be determined, as due to time constraints, the data set used in this investigation was limited to only 9 points.

For MP 2 and MP 3, it is unexpected that after the scour extent becomes independent of the approach depth, it will begin to decrease with further increases in the approach depth. It is a possibility that this slow decrease of the scour extent with increasing approach depth could have been caused due to a slight error introduced by the interpolation process employed in the analysis. Seeing that the data set for this opening ratio was limited, the interpolating algorithm would become quite sensitive to any possible outlying data that might not have been detected.

For the downstream measuring point, MP 6 (Figure 7.7(c)), the dimensionless scour extent appeared to increase at a decreasing rate with increasing approach depth. As explained for opening ratio α_c = ¼, this phenomenon occurs due to the lateral movement of the downstream wake vortices that can be seen to increase with the flow depth. It can also be seen in Figure 7.7(c) that the scour extent values increase at a decreasing rate with increasing approach depth to what appears to be an asymptotic value. As explained for the smaller opening ratio, there must be a limit to the size of the vortex for the same approach velocity and geometry of the channel, as well as a limiting depth beyond which the vortex will no longer be influenced by the bed. It should be noted however that for MP 6, the plotted line does not appear to extrapolate to the origin of the graph. This is an unexpected result as scour is not expected to occur at a zero depth of flow. The possible reason for this irregularity could be due to a slight error introduced by the interpolation procedure employed in the analysis due to the limited data set.

The general trend between the extent of scour and the approach depth for MP 2 and MP 3 above does not compare well with the findings of Laursen (1963), Zaghloul (1983) and Lim (1997), who found that under clear-water scour conditions, the scour depth around an abutment increased with increasing values of approach depth. The results found in this investigation do, however, compare favourably with the findings of Melville (1992) for "short" abutments (L_a / $Y_1 \leq 1$), which were defined as being independent of the approach depth. It was however found in this investigation that when L_c / Y_1 was calculated for each experiment, the majority of the experiments fell under Melville's definition of "intermediate" abutments ($1 < L_a / Y_1 < 25$), which were defined as scaling with both the Y_1 and L_a. These variations in the findings between this investigation and the literature could be attributed to the fact that it has been found that the scouring processes around a long contraction differ to that around abutments where the scoured region is allowed to deepen. In the case of scour depth measurements, it was found that the principal vortex was the dominant scouring agent, whereas as in the case of lateral scour around a long contraction for opening ratio α_c = ½, the dominant scouring agent appeared to be the corner vortex. Although the differing vortex systems could provide a possible explanation for the variation between the findings of this investigation and the literature, it was however felt that more data should be collected to confirm this.

7.6 Influence of the opening ratio on the lateral extent of scour

The influence of the opening ratio on the lateral extent of scour around a long contraction could not be determined in the same manner as shown for the approach Froude number and the approach depth, as only two opening ratios were considered in the investigation, namely, α_c = ¼ and α_c = ½. Therefore, in order to determine the influence of the opening ratio on the scour extent around a long contraction, two-dimensional plots of the ratio of the equilibrium scour extent to the approach depth (y-axis) versus the approach Froude number (x-axis) for MP 2, 3 and 6 were produced. The data points were plotted for both opening ratios on the same set of axes and a best-fit line was drawn through them. The resulting plots are presented in Figure 7.8.

It should be noted that although the approach depth of the experiments varied, the results served to demonstrate the difference in the scour extent for the two opening ratios at a given depth.

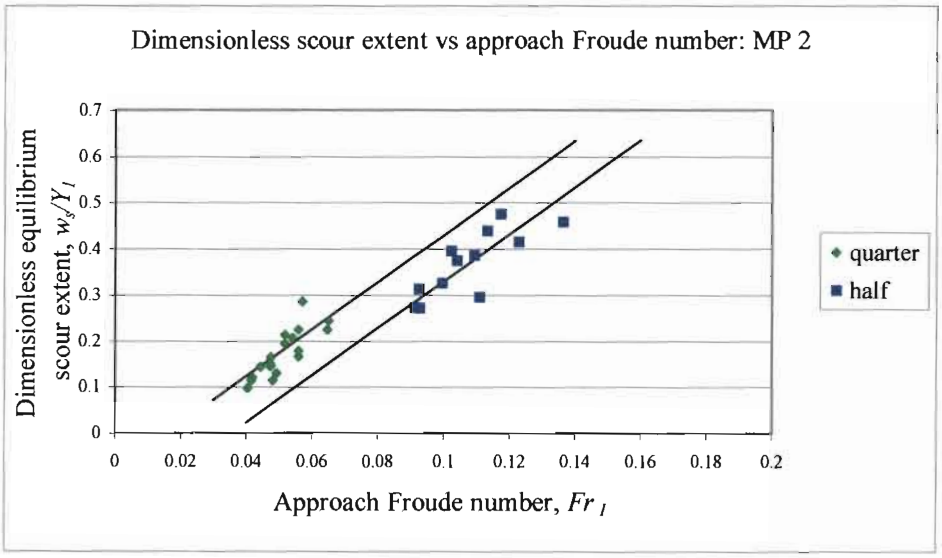

(a)

Figure 7.8: Figure showing the influence of the opening ratio on the scour extent at different positions around a long contraction

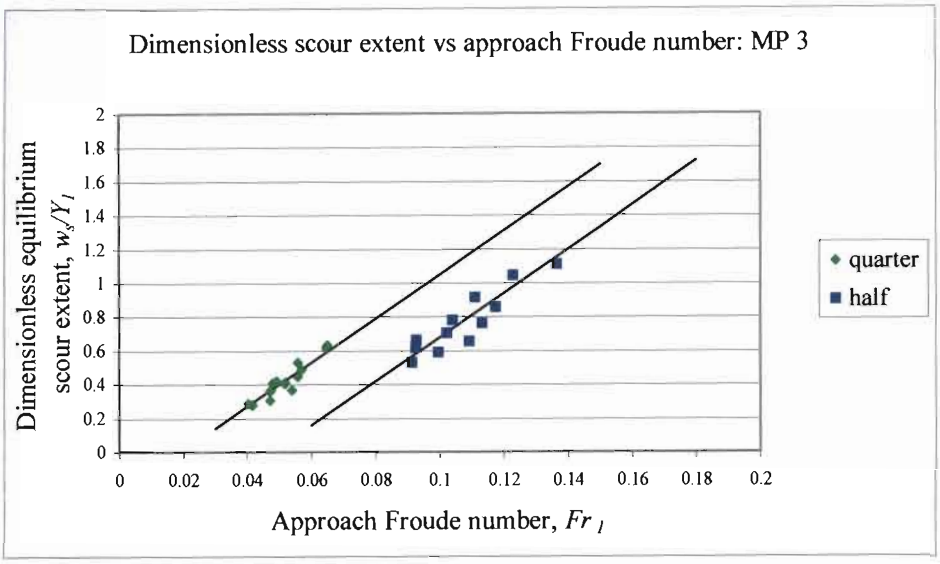

(b)

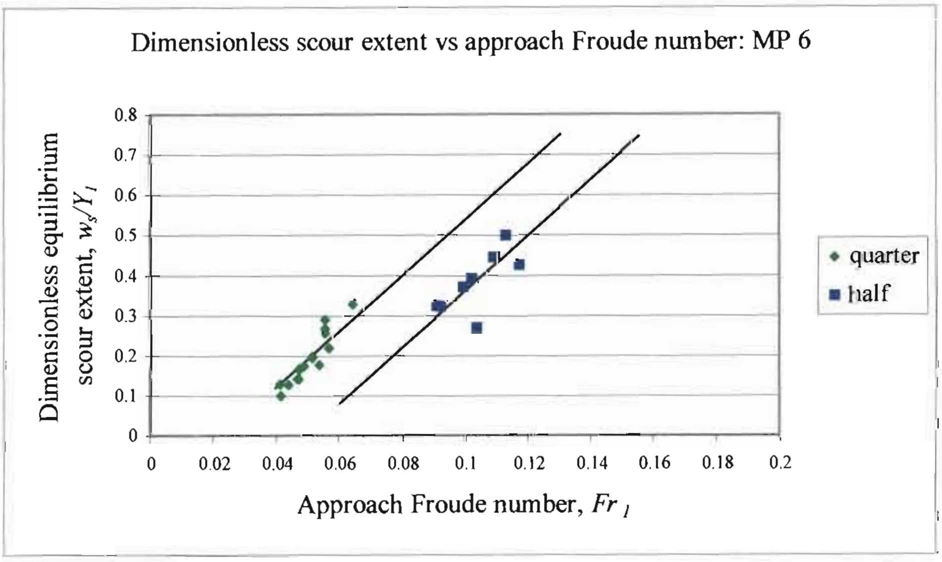

(c)

Figure 7.8: Figure showing the influence of the opening ratio on the scour extent at different positions around a long contraction (continued)

For all of the measuring points, it can be seen from Figure 7.8(a),(b),(c) that for the same approach conditions, in other words, the same approach depth and Froude number, the scour extent is larger for the smaller of the two opening ratios ($\alpha_c = ¼$). It can therefore be deduced that the scour extent is also dependent on the length of the upstream face of the long contraction perpendicular to the flow (L_C). A possible reason for this is that for the same approach conditions, a larger flow section is blocked by the contraction with the smaller opening ratio, thus resulting in a greater acceleration of flow through the opening and into the contracted reach. When considering the upstream region of the long contraction (MP 2 and MP 3), a greater acceleration of the flow around the corners of the entrance to the contraction would result in the formation of vortices of higher vorticity that would in turn cause larger scoured regions. Considering the region downstream of the contraction (MP 6), higher velocity flows within the contracted reach implies a greater shearing action between the dead water regions behind the downstream faces of the contraction and the fast-flowing water in the main channel. The wake vortices that are shed from the corners of the exit to the contraction would therefore be of a higher vorticity, thus resulting in larger scour extents.

It is interesting to note that for the same approach conditions, the difference in the resulting scour extents for the two opening ratios for MP 2 and MP 6 are very similar. For MP 3, however, for the same approach conditions as for MP 2 and MP 6, the difference between the resulting scour extents for the two opening ratios is greater. The possible reason for this is that at MP 3 the corner vortex appeared to be predominantly responsible for the scouring. The corner vortex forms as a result of the convergence of the streamlines at the corners of the entrance to the contraction thus resulting in a steep velocity gradient and subsequent low pressure. At MP 2, it appears as though both the corner vortex and the principal vortex play an important role. The principal vortex forms as a result of a pressure increase and resulting downflow between the dead water region upstream of the contraction and the fast-flowing water in the main channel. When the flow accelerates around the corners of the entrance to the contraction and into the contracted reach, the increase in the velocity gradient will be greater at these corners due to the strong convergence of the streamlines, compared with that along the boundary along which the principal vortex is formed. It therefore follows that the increase in scour extent with acceleration will be greater at MP 3 than at MP 2. The wake vortices shed from the corners of the exit to the contraction that are responsible for scouring at MP 6 have been shown to be weaker that the vortices that form at the entrance corners for the same approach conditions. It is thus also expected that the difference in scouring between the two opening ratios will be more severe at MP 3 than at MP 6.

From the above discussion it can be seen that the local scour extent around a long contraction is dependent on the opening ratio and thus can be said to be dependent on the length of the faces of the long contraction perpendicular to the approach flow.

This is in agreement with the findings in the literature that considered local scour depths around abutments for clear-water scour conditions (Laursen, 1963; Zaghloul, 1983; Melville, 1992 and Lim, 1997).

7.7 Comparison of experimentally measured scour values with findings in the literature

In the preceding discussion, the influence of the parameters on the initial local scour (scour extent) around a long contraction under clear-water conditions were compared with the findings in literature that considered local scour depths around abutments. Comparisons were made to this literature as it was initially believed that local scouring around a long contraction could be considered as a variant of local scouring around an abutment. It was also believed that the measured local scour extent values could be related to the local scour depth by the angle of repose of sediment in water.

Although it was seen that the influence of the various parameters on the local scour extent around a long contraction showed similar trends to the findings of previous research on scour depths around abutments, it could be seen that the vortex systems responsible for scouring around a long contraction appeared to differ somewhat to that around abutments. It was thus of interest as to whether the scour extent around a long contraction could in fact be favourably compared to the scour depths around an abutment under the same conditions of flow, by transforming the scour extents into depths using the angle of repose of sediment in water. In the case of this investigation, an angle of repose of approximately 30° was used, as this corresponds to rounded sediment particles that satisfy the condition $d_{50} \leq 1$ mm (Van Rijn, 1993).

The literature used in the comparison was that which considered clear-water conditions and these were found to be Laursen (1963), Zaghloul (1983), Melville (1992) and Lim (1997). Zaghloul and Melville, however, only considered the prediction of local scour depths around abutments at the threshold conditions of clear-water scour and thus could not be used. It was therefore decided to use the scour depth prediction formulae derived by Laursen (Equation 2.24) and Lim (Equation 2.30) to act as a comparison to the scour values obtained in this investigation. Both Laursen and Lim used an analytical semi-empirical approach in the prediction of local scour depths around abutments. Figure 7.9 shows the differences between the measured

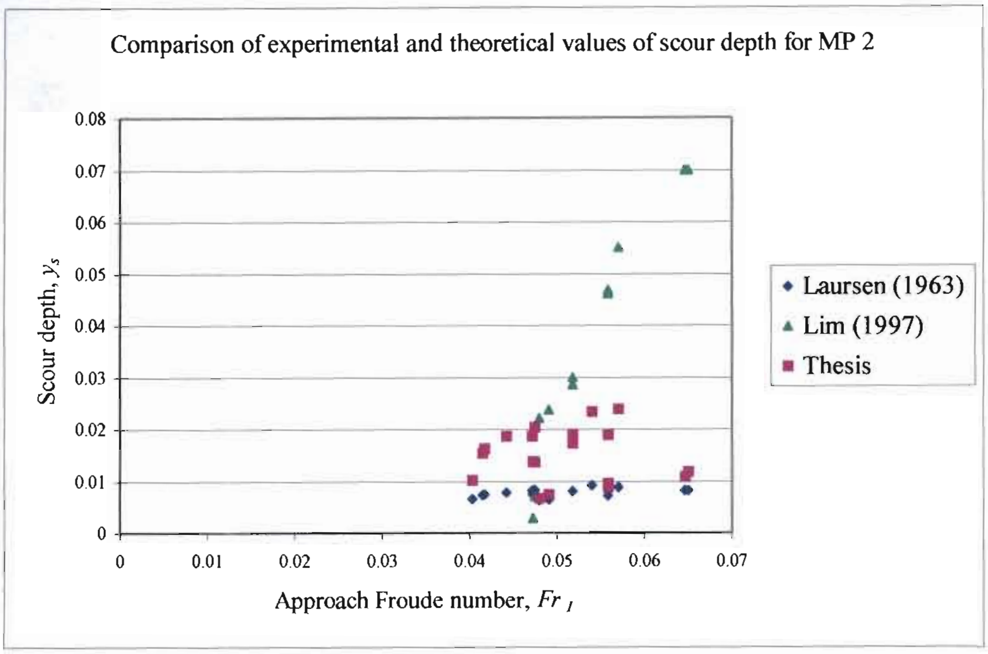

(a)

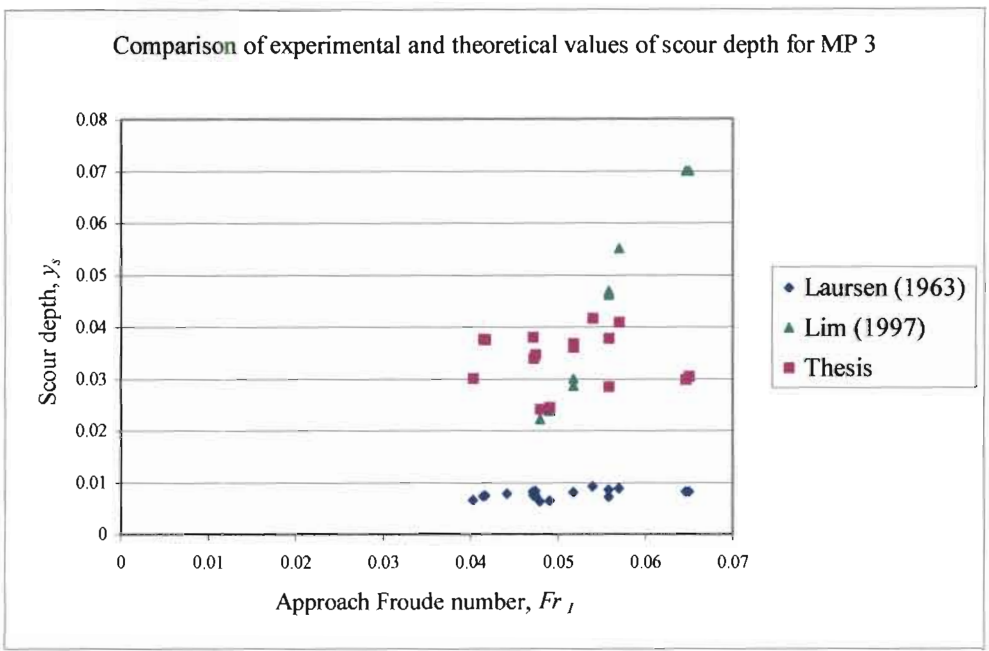

(b)

Figure 7.9: Graphs showing the comparison between the scour depths inferred from the experiments (that measured scour extent) to those derived by Laursen (1963) and Lim (1997) for (a) MP 2 and (b) MP 3

local scour extent values that were translated into local scour depths using the chosen angle of repose of sediment in water, and the values of local scour depths as calculated by Laursen and Lim. The scour extents at MP 2 and MP 3 were both transformed into their corresponding depth values and compared with the literature.

As it can be seen in Figure 7.9, the values of the local scour depths derived from the experimentally measured scour extent values around a long contraction generally fall somewhere between the scour depths predicted by Laursen (1963) and Lim (1997). It should be noted, however, that the predicted scour depth values differed quite substantially. This emphasises the fact that there is still no comprehensive or unifying theory that would enable an engineer to predict the local scour depths around abutments with confidence. The available equations often give contradictory estimates due to the complexity of the three-dimensional vortex systems that cause the scour.

Although the scour depths derived from the scour extent and the angle of repose are of the same magnitude as those predicted by the published equations, the initial scour extent around a long contraction is subject to a slightly different combination of vortices than for scour depths around abutments. Caution should thus be taken if the scour extent is to be used as a predictive tool for the corresponding scour depth. The most obvious use of scour extent data is thus rather as a guide for the installation of armouring, for example riprap, over the area that is expected to be influenced by local scouring.

Chapter 8

Error and limitations

8.1 Introduction

Experimental work performed in a laboratory is subject to error. This chapter aims at estimating the error figures associated with this investigation.

8.2 Error percentages associated with laboratory measurements

8.2.1 Flow measurements

The flow rate (*l*/s) over the V-notch weir is calculated by the following equation:

$$Q = 1370 h_v^{5/2} \tag{8.1}$$

where h_v = overflow height upstream of the V-notch weir (m)

In order to determine the value of h_v, a Vernier Depth Gauge, which could be read to the nearest 0.1 mm, was employed to measure both the surface elevation of the water upstream of the weir as well the elevation of the vertex of the weir. Although the water surface upstream of the weir was fairly flat and thus could be determined with a fair amount of accuracy using the Vernier Depth Gauge, some difficulty was experienced in measuring the elevation of the vertex of the weir. The estimated error in the measurement of h_v was approximated to be 1 mm.

The values of h_v measured in the experimental process ranged between 90-150 mm, therefore the error percentage range was calculated to be 0.7-1.1%. To determine the error associated with the calculation of the flow, this error range was multiplied by 5/2 thus giving a maximum error percentage of 3% for the flow.

8.2.2 Approach depth measurements

In order to determine the depth upstream of the long contraction, Y_1, both the elevation of the sand bed along the bottom of the flume and the water surface elevation at certain points had to be measured. The Vernier Depth Gauge was used to measure both elevations.

Fluctuations in the water level during the running of the experiments caused some difficulty when using the Vernier Depth Gauge to measure the water surface elevation at the chosen points upstream of the contraction. The error in reading the water surface was estimated to be 1 mm. Seeing that the water surface elevation measurements were found to range between 139.1 mm and 290.0 mm, the error percentage was calculated to range between 0.3 – 0.7%.

The bed surface elevation was measured without difficulty and the error in this case was estimated to be 0.5 mm. Seeing that the bed elevation measurements ranged between 55.3 mm-55.9 mm, the percentage error was calculated as 0.9%.

Thus the maximum error involved in calculating the approach depth is the cumulative maximum error involved in measuring the water surface and bed elevations and was found to be 2%.

8.2.3 Dimensionless approach depth

In the dimensional analysis approach used in this investigation, the approach depth was rendered dimensionless by the scaling factor $\lambda = L_c$. The error associated with the measurement of the length of the upstream face of the contracted section perpendicular to the flow, L_c, was estimated to be 0.2 mm. Seeing that the range of L_c varied between 153.5 mm and 230.1 mm, the percentage error was calculated to range between 0.09-0.13%. The maximum error involved in calculating the dimensionless approach depth is the cumulative maximum error for the approach depth and the scaling factor and was found to be 3%.

8.2.4 Approach Froude number

The approach Froude number was calculated using the following equation:

$$Fr_1 = \frac{U}{\sqrt{gY_1}} \tag{8.2}$$

where U = average velocity in the approach channel = $\dfrac{Q}{B_1 Y_1}$

The width of the approach channel, B_1, was measured to be 609.5 mm. The error associated with the measurement of the width was estimated as 2.0 mm, thus giving a percentage error of 0.3%. The percentage error for the average velocity in the approach channel could thus be determined by the addition of the percentage error calculated for the flow, width of the channel and the approach depth and was found to be 3.2-4.7%.

Gravitational acceleration, g, can vary between 9.78 m/s^2 and 9.82 m/s^2. For the purpose of this thesis, however, a gravitational acceleration of 9.81 m/s^2 was used. It is assumed that this value has an associated error of 0.3%.

In order to determine the error percentage involved in the calculation of the approach Froude number, the error percentages determined for the approach velocity, approach depth and gravitational acceleration had to be cumulated, however the percentage error for the gravitational acceleration and the approach depth would have to be multiplied by ½ .

The maximum percentage error thus associated with the approach Froude number was found to be 6%.

8.2.5 Scour extent calculations

The scour extent at the various scour measuring points around the long contraction were measured using the laser-pointer rig.

For the measuring points around the upstream face of the long contraction, in other words, MP 1, 2, 3 and 4, the scour extent measurements that were used in the analysis were only those measured under conditions of zero flow once the experiment had been stopped. When the refraction of the light beam from the laser-pointer rig was tested under still conditions through a depth of water approximately equalling that of the maximum depth used in the experiments, namely 230 mm, no refraction of the light beam was observed and thus the error due to refraction was assumed to be negligible. The diameter of the light beam on the bottom of the flume was approximately 1 mm, thus an error of 0.5 mm could be expected when taking scour extent measurements. When calculating the error percentage for each of the measuring points, the maximum and minimum scour extent values were considered that were measured at each of these points.

In the analysis of this investigation only MP 2 and MP 3 were considered in the calculations, thus for MP 2 the maximum error percentage was found to be 5% and for MP 3 it was found to be 2%.

For the measuring points downstream of the long contraction, namely MP 5, 6 and 7, the scour measurements taken hourly throughout the duration of the experiment were used in the analysis to predict the equilibrium scour extent if the scour extent had not stabilised within the duration of the experiment.

To test the refraction error involved in the measurement of the scour extent caused by the flowing water, the measurement of the scour extent taken at the end of the experiment for each of the downstream measuring points was compared with the same measurement point but in conditions of zero flow. Particular attention was given to those experiments that were observed to have stabilised within the duration of the experiment. Seeing that MP 6 was the only downstream point considered in the analysis and results of this investigation, the error percentage was only calculated for this point. It was observed that for the flowing water condition the measurement differed from the still measurement by at most 1.1 mm and least 0.2 mm. Taking a conservative approach, the refraction error was taken as 1.1 mm, thus giving a percentage error range of 1.7-6.0%. The error associated with the diameter of the light beam on the bottom of the flume gave an error percentage of 0.8-2.9%. Therefore the total cumulative error in the scour extent measurement associated with MP 6 was found to be a maximum of 5%.

8.2.6 Dimensionless scour extent

The scour extent was rendered dimensionless by the scaling factor $\lambda = L_{c.}$ It has been determined in Section 8.2.3 that the error percentage range associated with the scaling factor is 0.09-0.13%. The maximum percentage error for the dimensionless scour extent was therefore calculated to be 5% for MP 2, 2% for MP 3 and 5% for MP 6. Owing to the small percentage error associated with the scaling factor, the error percentages calculated for the dimensionless scour extent can be seen to be the same as those for the scour extent.

8.2.7 Total error associated with the determination of the influence of the approach Froude number on the lateral extent of scour

The total error associated with the determination of the relationships between the approach Froude number and the lateral extent of scour around the long contraction was calculated by the addition of the errors associated with the scour extent and the approach Froude number. The error associated with the scaling factor was not considered as it appeared on both axes of the graphs showing the resulting relationships, and thus cancelled each other out.

Following the above mentioned method of calculation, the total error was thus found to be 10% for MP 2, 7% for MP 3 and 9% for MP 6.

8.2.8 Total error associated with the determination of the influence of the approach depth on the lateral extent of scour

The total error associated with the determination of the relationship between the scour extent and the approach depth was calculated by the addition of the error percentages associated with the scour extent and the approach depth. The error associated with the scaling factor was not considered as the scaling factor appeared on both axes of the graphs showing the resulting relationships. The total percentage error for the relevant measuring points was thus found to be 6% for MP 2, 3% for MP 3, and 5% for MP 6.

8.2.9 Total error for the determination of the influence of the opening ratio on the lateral extent of scour

The total error associated with the determination of the influence of the opening ratio of the long contraction on the scour extent was calculated by the addition of the error percentages associated with the scour extent, approach depth and approach Froude number. The total error percentages for the relevant measuring positions were thus found to be 12% for MP 2, 9% for MP 3, and 11% for MP 6.

8.3 Other possible sources of error

Other sources of error that might have caused a disturbance in the scouring process around the long contraction could have been due to the following:

i) Any contaminants, such as large particles, that were carried down the flume and through the test section.
ii) A sudden surge in the pressure of the pumps.
iii) A sudden lowering of the tailgate.
iv) Particles that might have become interlocked and thus were scoured away earlier than had they been single particles.

Seeing that the lateral extent of the scour only progressed by very small amounts every hour, in other words by fractions of a millimetre, especially as the scour extent was stabilising, any small disturbance would have affected the progression of the scour extent quite significantly. Cases such as these were observed in the data, thus rendering these points unable to be used in the analysis.

8.4 Limitation associated with laboratory experiments compared to field situations

As with most research based on laboratory studies, this investigation was based on findings under idealised conditions. A rectangular flume with glass immoveable sides and a horizontal bed consisting of a uniform sediment layer was used throughout the experimental procedure.

Natural rivers, however, have irregular cross-sections with movable sides. The river bed is usually non-horizontal with non-uniform sediment and stratified conditions. Other complications such as floating debris and vegetation also occur in natural rivers. Rivers also change their geometry over time through a process of general scouring.

Laboratory tests are based on models where the scale has been greatly reduced. The extrapolation to full-scale conditions could bring in error.

Chapter 9

Conclusions

9.1 Introduction

The aim of this thesis was to investigate initial local scouring around a rectangular "long" contraction under clear-water scour conditions. Two contraction sections were considered with opening ratios of $\alpha_c = ½$ and ¼. Dimensional Analysis was used to identify the parameters that have an influence on the initial local scouring around the structures. The approach Froude number, Fr_1, the dimensionless approach depth, Y_1/L_C, and the opening ratio were selected. If the influence of these parameters could be determined, this would aid in the prediction of the extent of initial scouring around a long contraction. Thus, measures could be taken to protect the bed and hence the structure.

This chapter sets out the main findings and conclusions of this investigation.

9.2 Coherent structures responsible for the development of the initial local scouring around a rectangular long contraction

The identification of the dominant vortices responsible for the scouring of the bed as well as their interactions with each other was found to be of great importance in the consideration of the influence of the parameters on the scour extent around the long contraction. In the region around the upstream face of the long contraction, three vortices were recognised as having an influence on the development of the scour, namely, the corner vortex, the principal vortex and the "bow-wave" or "roller".

When considering the contraction section for the larger opening ratio, $\alpha_c = ½$, the dominant scouring agent was observed to be the corner vortex that formed at the upstream edges of the contracted section. For the smaller opening ratio, $\alpha_c = ¼$, both the principal and the corner vortex were observed to be influential on the scouring process, although the resulting scoured regions appeared to be more characteristic of scouring caused by the corner vortices than that of the principal vortex. This differs from the findings in the literature, which considers local scour depths around abutments, where it was found that the principal vortex was the dominant scouring agent. In the case of scour depths, however, the principal vortex became concealed within the scour hole and was thus protected from the approach flow. In the case of this investigation, the vortices were exposed to the approach flow, which could provide an explanation for the decrease in the influential role of the principal vortex on the bed.

The influence that the roller has on the scouring along the bed is dependent on its degree of interaction with the corner and principal vortex. Seeing that the roller forms along the surface, this degree of interaction is also dependent on the depth of the flow.

For the region downstream of the long contraction the wake vortex trail initiated from the corners at the exit was seen as being responsible for the scouring. In comparison to the upstream vortices, the downstream wake vortices were seen to be weaker for the same approach conditions.

9.3 Scour conditions

For this investigation it was decided to perform the experiments under conditions of clear-water scour around the upstream face, through the contracted reach, and downstream of the long contraction. The boundary between clear-water and live-bed conditions was not found to be clearly defined in the literature, and thus for the purpose of this investigation, the boundary was set at an intensity of motion of $I = 1\times10^{-3}$ s^{-1} ($u_* / v_{ss} = 0.195$). The latter intensity of motion represents the limiting movement of the sediment in the approach channel to the scoured region, below which clear-water conditions and above which live-bed conditions can be deemed to exist. When the definition was tested in this investigation, it appeared to be reasonable.

It was recognised in the experimental process that under clear-water conditions, the time taken for the scour extent to reach equilibrium, and the resulting value of scour extent, was dependent on the size and the strength of the dominant vortices responsible for the scouring. It was observed that a large percentage of the equilibrium scour extent occurred initially due to the strong vorticity associated with the low pressure centres of the vortices. As this vorticity decreases towards the outside of the vortex, so too does the influence of the vortex on the bed until the bed is no longer affected by the vortex. As the size and strength of the vortices depend on the approach velocity, the equilibrium scour extent around a long contraction can also be seen to be dependent on the approach velocity. This is similar to the findings in the literature on scour depths around abutments, although the conditions at which equilibrium was reached were found to differ. In addition, it was observed that the scour extent around a long contraction under clear-water conditions reached a stable value. This differs from the findings for scour depths around abutments where it is contested as to whether equilibrium clear-water conditions can in fact be reached.

9.4 Dimensional Analysis

When considering the influence of the various parameters on the initial local scouring (scour extent) around the long contraction, only the relationships between the parameters and the scour extent were considered at measuring points (MP) 2, 3 and 6 (Figure 9.1). Scouring at the other measuring points was found to be influenced by error inducing factors, and the measurements were disregarded.

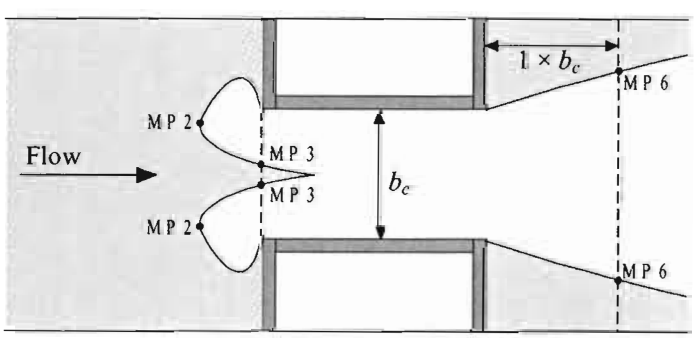

Figure 9.1: Diagram displaying the relevant measuring points (MP) in the flume

9.4.1 Approach Froude number

In general, for both opening ratios, the scour extent was observed to increase at a decreasing rate with increasing values of the approach Froude number at the relevant measuring points (Figure 9.2). Under clear-water scour conditions, the lateral extent of the scour was found to be dependent on the approach velocity. The approach Froude number is a function of the approach velocity, thus it is logical that the scour extent should scale with the approach Froude number. The increase in the scour extent at a decreasing rate with approach Froude number could be attributed to the geometrical limitations of the structure and the channel, and the limitation of the size to which the vortices can develop.

The resulting plots of dimensionless scour extent versus approach Froude number were not found to pass through the origin of the graph if the plots were extended towards the origin. This was expected as there must be a limiting approach Froude number (approach velocity) beyond which the vortices will be strong enough to begin to entrain the sediment.

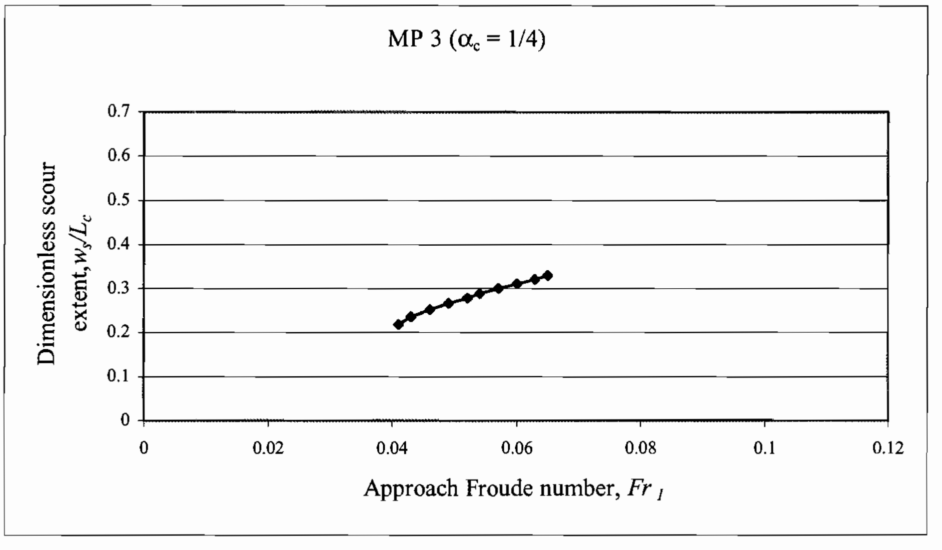

Figure 9.2: Figure showing a typical example of the relationship between the dimensionless scour extent and the approach Froude number

It was established that unlike for the other measuring points, for opening ratio $\alpha_c = ¼$, the scour extent appeared to increase approximately linearly with the approach Froude number at MP 2. This was seen to occur as a result of the interaction between the principal and corner vortices at this point. In comparison to the larger opening ratio ($\alpha_c = ½$) and the other measuring points, the principal vortex was found to be influential on the scouring process at MP 2 for $\alpha_c = ¼$.

It was observed for $\alpha_c = ¼$ that at MP 6 the increase in the dimensionless scour extent with approach Froude number was less steep than for the upstream measuring points

(MP 2 and MP 3). This was expected as for the same approach velocity the wake vortices shed from the corners of the exit to the contraction will be weaker than the vortices that form around the upstream face of the contraction. For $\alpha = ½$, however, it was found that the increase in the dimensionless scour extent with approach Froude number was steeper at MP 6 than for the upstream measuring points. This irregularity could be attributable to the limited data set available for the analysis (9 points). With a limited data set, the interpolating algorithm used in the analysis would become quite sensitive to any undetected outlying data points. An alternative explanation for this behaviour however can be offered by consideration of the lateral instability of the wake downstream of the exit to the contraction. The instability of the wake is higher for higher approach Froude numbers. Seeing that the range of approach Froude numbers was higher for $\alpha_c = ½$ in comparison to $\alpha_c = ¼$, this could explain the difference in the resulting scour behaviours observed at MP 6 for the two opening ratios.

The fact that the lateral extent of the scour scales with the approach Froude number (approach velocity) is in agreement with the literature that considers scour depths around abutments under clear-water conditions (Laursen, 1963; Zaghloul, 1983; Melville, 1992 and Lim, 1997).

9.4.2 Approach Depth

For the contraction section of the smaller opening ratio, $\alpha_c = ¼$, the dimensionless scour extent was seen to increase in general with increasing values of the dimensionless approach depth (Figure 9.3). The plots of the dimensionless scour extent versus the dimensionless approach depth also appeared as though they would pass through the origin of the graph. This was expected as scouring cannot occur at a zero depth of flow.

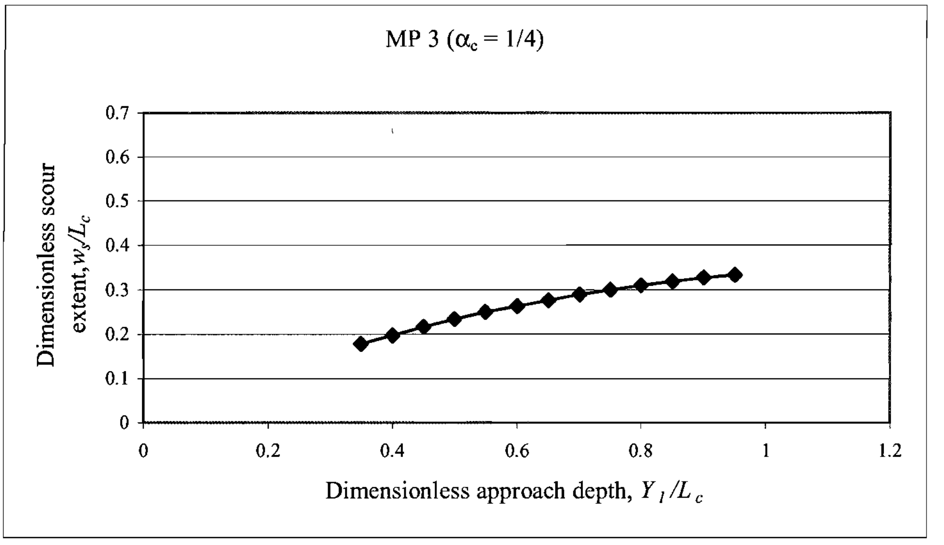

Figure 9.3: Figure showing a typical example of the relationship between the dimensionless scour extent and the dimensionless approach depth for α_c = ¼

For the upstream measuring points, MP 2 and MP 3, the resulting relationship between the dimensionless scour extent and the dimensionless approach depth was seen to be as a result of the influence of the roller on the corner and principal vortex. The roller is known to reduce the vorticity of the vortices with which it comes into contact. Seeing that the roller forms near to the surface of the flow, it will have less of an influence on the vorticity of the vortices at deeper flows thus resulting in larger scoured regions. The influence of the roller on the scoured region was found to be most felt at MP 2 where the dimensionless scour extent was seen to increase approximately linearly with increasing dimensionless approach depth as opposed to MP 3 where the dimensionless scour extent was seen to increase at a decreasing rate with the dimensionless approach depth. Owing to the location of the roller and that it is counter-rotating to the principal vortex, it was believed that the principal vortex would be most influenced by the roller. This offered an explanation for the difference in the scouring behaviour at MP 2 where both the principal and the corner vortices are responsible for the scour, and at MP 3 where the corner vortices are the dominant scouring agents.

For the smaller opening ratio, α_c = ¼, the increase in the scour extent with increasing approach depth for MP 2 and MP 3 compared well with the findings of Laursen (1963), Zaghloul (1983) and Lim (1997) who considered local scour depths around abutments under clear-water scour conditions. The results were also found to compare favourably with the findings associated with Melville's (1992) definition of an "intermediate" abutment which is defined as $1 < L_a / Y_l < 25$. By consideration of the results, it was believed however that the limiting dimensionless depth beyond which the scour extent would become independent of the approach depth would be greater than the limit that was found by Melville (1992), in other words, when $L_a / Y_l = 1.0$. The reason for this is that for scour depths around abutments the principal vortex became concealed within the scour hole and was thus less exposed to the roller in comparison to the vortices in this investigation that were exposed above the bed.

At the downstream measuring point, MP 6, the increase in the dimensionless scour extent with the dimensionless approach depth was attributed to the lateral movement of the trailing wake vortices responsible for the scouring. The deeper the flow, the more freedom the vortices have to oscillate from side to side as they are carried by the flow downstream thus resulting in larger scoured regions. The dimensionless scour extent was observed to increase at a decreasing rate with the dimensionless approach depth as there must be a limiting size to which the vortices can develop, and a limiting depth after which the lateral movement of the vortex will no longer be affected by the approach depth. Although no information was found for the scouring downstream of a contraction, it is believed that the findings in this investigation would also apply to the case of scour depths around structures.

For the contracted section of the larger opening ratio, $\alpha_c = ½$, the dimensionless scour extent for the upstream measuring points (MP 2 and 3) appeared to be generally independent of the dimensionless approach depth from $Y_l / L_c \approx 0.85$ after which it began to decrease from $Y_l / L_c \approx 1.00$ onwards (Figure 9.4).

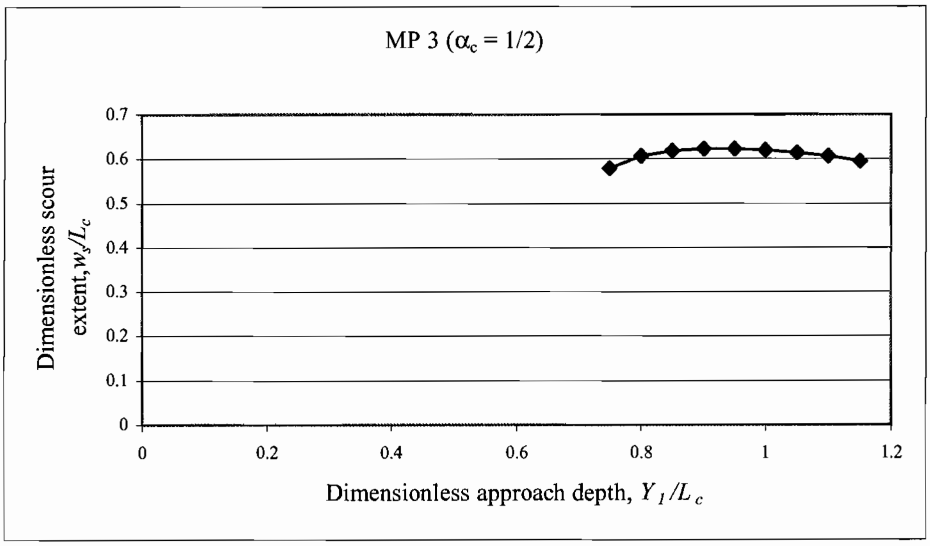

Figure 9.4: Figure showing a typical example of the relationship between the dimensionless scour extent and the dimensionless approach depth for $\alpha_c = ½$

For the larger opening ratio, the dominant scouring agent for the upstream region of the contraction was seen to be the corner vortex. Seeing that the roller has less of an influence on the corner vortex than on the principal vortex, it was expected that the influence of the roller on the scour extent would be less for the larger opening ratio. Also for the larger opening ratio, it is expected that the roller be weaker and therefore have less of an influence on the corner vortex in comparison to the smaller opening ratio. It in fact appears from the independence of the dimensionless scour extent with the dimensionless approach depth that the roller has minimal if no influence on the corner vortex, even though the corner vortex would also have decreased in strength for the larger opening ratio. The decrease in the dimensionless scour extent with increasing dimensionless approach depth from $Y_1 / L_C \approx 1.00$ was seen as an irregular result. This anomaly might have occurred as a result of a slight error introduced by the interpolation process, as due to the limited data set available for the analysis, the interpolating algorithm was quite sensitive to any outlying datum that might not have been detected.

For the downstream measuring point, MP 6, the dimensionless scour extent increased with increasing values of the dimensionless approach depth. The explanation for this is the same as that presented for the smaller opening ratio above. An irregularity was however observed for this measuring point, as the plot of the dimensionless scour extent versus the dimensionless approach depth did not appear as though it would extrapolate through the origin of the graph. This anomaly could have occurred as a result of the limited data set used for this opening ratio.

The resulting relationships between the dimensionless scour extent and the dimensionless approach depth were only found to compare favourably to the findings of Melville (1992) for "short" abutments (L_a / Y_l ≤ 1.0), for which the scour depths were found to be independent of the approach depth. In the case of this investigation, however, when Y_l / L_c was calculated for each experiment, the majority of the experiments were seen to fall under the "intermediate" category as defined by Melville. Although it is expected that the roller will have less of an influence on the scour extent for the larger opening ratio, it is not entirely certain that the scour extent would become completely independent of the approach depth. It is thus recommended that in order to be completely confident of the results obtained for the larger opening ratio, a larger data set should be used. It was evident in the results that the limited data set might have caused a slight error in the interpolation process required in the analysis.

9.4.3 Opening Ratio

When considering the influence of the opening ratio on the lateral extent of scour around a long contraction at the selected measuring points, it was found that the for the same approach conditions, in other words, the approach Froude number and depth, the scour extent values for the smaller opening ratio, α_c = ¼, were larger than those for the larger opening ratio, α_c = ½ (Figure 9.5).

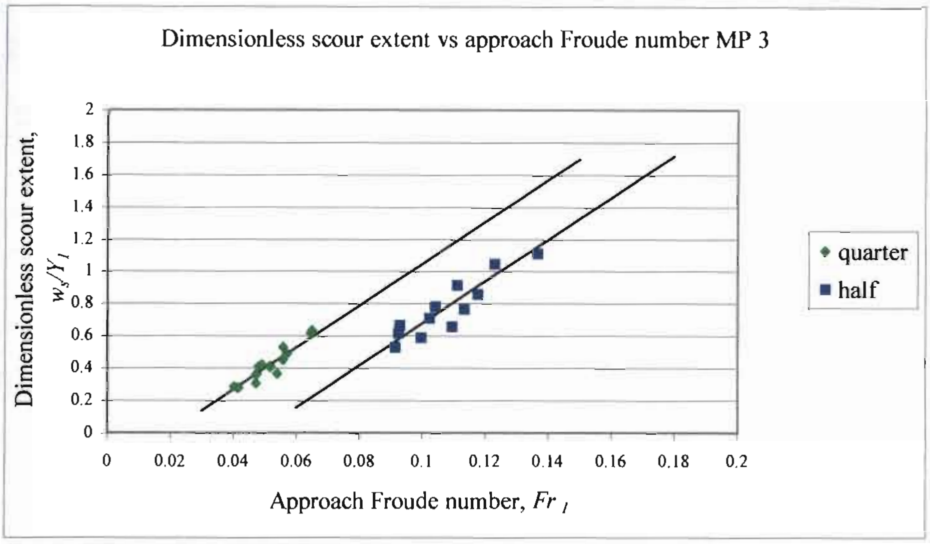

Figure 9.5: Figure showing a typical example of the difference in the scour extent for opening ratios $\alpha_c = ½$ and $\alpha_c = ¼$ for the same approach conditions

For the measuring points in the upstream region, the reason for this behaviour was attributed to the fact that for the same approach conditions, a larger section of the flow would be blocked by the contraction with the smaller opening ratio, thus creating a greater acceleration of flow through the opening of the contraction and thus the consequent formation of stronger vortices. In the case of MP 6, the resulting relationships can be explained by the fact that in the downstream region the shearing action between the dead water regions downstream of the faces of the long contraction and the fast-flowing water in the main channel would be more severe for a smaller opening ratio. This is because for the same approach conditions, the flow of the water will be faster through a smaller contraction than for a larger (continuity), thus resulting in the formation of stronger vortices.

For the same approach conditions, the difference in the resulting scour extents for the two opening ratios for MP 2 and 6 were found to be very similar, however at MP 3 the difference in the resulting scour extent was found to be much larger. At MP 3 the corner vortex was seen as being the dominant scouring agent, whereas at MP 2 both the principal and corner vortices were seen as having an influence on the scouring process. When the flow accelerates through the opening of the contracted section, it is believed that the increase in the velocity gradient around the corners of the entrance to the contraction will be steeper than that along the boundary along which the principal vortex forms. This results in the formation of a stronger corner vortex and therefore more severe scouring at MP 3.

Seeing that the dimensionless scour extent was found to be dependent on the opening ratio, it can thus also be concluded that the scour extent is also dependent on the length of the faces of the contraction perpendicular to the approach flow, L_c. This compares well to findings in the literature that show the scour depth around an abutment to increase with increasing length of the abutment perpendicular to the flow, L_a (Laursen, 1963; Zaghloul, 1983; Melville, 1992 and Lim, 1997).

9.5 Relating the extent of scour to the scour depth

The equilibrium scour extents at MP 2 and MP 3 were converted into the corresponding depths using the angle of repose of sediment in water, which is approximately 30°. These values were compared to theoretical scour depths derived by Laursen (1963) and Lim (1997) who conducted research on scour depths around abutments under clear-water conditions. The experimental depths derived from the scour extent and angle of repose were found to generally fall somewhere between the depths predicted by Laursen and Lim. It can thus be said the conversion of the initial scour values around a long contraction to the depth value using the angle of repose of sediment in water provides a fair approximation of the corresponding scour depths.

9.6 Prediction of initial local scouring around a long contraction

As the data sets used in the analysis were limited, especially for α_c = ½, the relationships found between the parameters and the initial local scour around a long contraction in this investigation should be considered as a guide for further research rather than solely for design purposes. With a limited amount of data, any outlying data point that might not have been detected could influence the results, especially when using interpolation techniques in the analysis. Also with a limited data set, the range of information available is also reduced.

If larger data sets were used, the plotted relationships between the various parameters (approach Froude number, approach depth and opening ratio) and the initial local scouring (scour extent) around a long contraction could provide a predictive method of determining the extent of the initial local scouring around such a structure. This would mean that if the geometry of the contraction, the approach depth and approach Froude number were known, the likely extent of initial scouring could be read off the plots. This would give an indication of the extent of the area around the structure that would be required to be protected. An effective method of protection against scour would be to fill the vulnerable area with riprap. Protection of the bed would prevent the undermining of the foundation of the structure and thus its possible failure.

It should be noted however that the results obtained from experimental procedures should not be used blindly, and should be considered as a guide for the hydraulic engineer rather than a definite solution due to the obvious differences between ideal laboratory conditions and the reality of natural rivers.

Chapter 10

Recommendations for future research

This section is aimed at providing possible recommendations for future research in this field. The recommendations are based on observations made during the experimental process and during the analysis of the results.

i) In the experimental procedure, the experiments should be run continuously until equilibrium conditions are reached both upstream and downstream of the contraction. This would eliminate the need for a predictive method to determine the equilibrium scour extent, as well as the possible error associated with using such a method. This would also prevent disturbances resulting from restarting the test at the beginning of each day.

ii) A limited data set can result in possible erroneous relationships between the parameters under investigation and the lateral extent of the scour around the long contraction. This is due to the use of interpolation procedures in the preparation of the results that become very sensitive to outlying data points in a small data set. Also a small data set renders it difficult to be able to detect possible outliers. It is thus important to conduct a sufficient amount of experiments so as to limit the influence of error on the outcome of the results.

iii) In this investigation only two opening ratios were considered. A plot of the dimensionless scour extent versus the opening ratio could therefore not be produced, as only two points would be insufficient to define a line with any confidence. A direct relationship between the scour extent and the opening ratio could thus not be determined. It is therefore recommended that at least three and preferably four opening ratios should be considered in the experimental procedure.

iv) In this investigation the influence of the sediment was excluded from the analysis. Under clear-water conditions, however, it is known that for local scour depths around abutments, the scour depth is influenced by the sediment size.

Further research could be undertaken to examine the possible influence of the sediment size on the scour extent around a long contraction.

v) A blunt long contraction angled 90° to the approach flow was the only section considered in this investigation. Further research could thus be performed for contractions of various shapes and alignments to the approach flow to determine the possible influence that these variations would have on the measured scour extents.

vi) In this investigation only one length of the long contraction parallel to the approach flow was considered. This length equalled the width of the approach channel. It was found that for the majority of the experiments, the sediment within the contracted reach was removed as a result of the local effects around the upstream face of the contracted section and that this sediment influenced scouring in the region downstream of the contraction. It could thus be considered for further research to vary the length of the contracted reach parallel to the approach flow in order to determine the influence that this would have on the scoured regions around the contraction.

vii) This thesis only considered clear-water conditions. It is believed that the prevailing mode of sediment transport upstream of the scoured area will determine the influence of the various parameters on the scour, especially in terms of the approach velocity and the sediment size. Further research could thus be undertaken to determine the behaviour of the scour extent under live-bed conditions. This would require the continuous supply of sediment to the scoured areas and hence ideally a transport flume would have to be used.

References

Ackers, P. & W. R. White (1973). "Sediment Transport: New Approach and Analysis." *J. Hydr. Div. ASCE,* Vol. 99, HY11, pp 2041 – 2060.

Ahmad, M. (1953). "Experiments on Design and Behaviour of Spur Dikes." *Proc., Int. Hydr. Convention*, ASCE, New York, pp 21-26.

Armitage, Neil. (2002). *A unit steam power model for the prediction of local scour.* PhD(Eng) thesis, University of Stellenbosch, South Africa.

Bagnold, R. A. (1966). "An approach to the Sediment Transport Problem from General Physics." *U.S. Geol. Survey Professional Paper 422-I,* 37 pages.

Ballio, F. & Orsi, E. (undated) www.diiar.polimi.it/franz/francesco/articoli/seoul.PDF

Barr, D. I. H. (1975). "Two additional methods of direct solution of the Colebrook-White function." *Proc. Instn Civ. Engrs*, Part 2, Vol 59, pp 827 – 835.

Beckerath, A. (1992). *Wastewater measurement and control.* Endree Hauser Holding AG.

Breusers, H. N. C. & Raudkivi (1991). *Scouring. IAHR Hydraulic Structures Design Manual 2.* A. A. Balkema.

Chadwick, Andrew & John Morfett (1998*). Hydraulics in Civil and Environmental Engineering, 3rd Edition.* E & FN SPON.

Cheng, N. -S. (1997). "Simplified Settling Velocity Formula for Sediment Particle." *J. Hydr. Engrg. ASCE*, Vol. 123, No. 2, pp 149 – 152

Cheng, N. –S. & Y. –M. Chiew (1998). "Pickup Probability for Sediment Entrainment." *J. Hydr. Div. ASCE*, Vol. 124, No. 2, pp 232 – 235.

Cheng, N. –S. & Y. –M. Chiew (1999). "Analysis of Initiation of Sediment Suspension from Bed Load." *J. Hydr. Div. ASCE*, Vol. 125, No. 8, pp 855 - 861.

Chien, Ning & Zhaohui Wan (1999). *Mechanics of Sediment Transport*. ASCE Press.

Colebrook, C. F. & C. M. White (1937). "Experiments with fluid friction in roughened pipes." *Proc. Roy. Soc. London*, Vol. A161, pp 367 – 381.

Cunha, L. V. (1973). Discussion on "Erosion of sand beds Around Spur Dikes" by Mohammad Akram Gill. *J. Hydr. Div. ASCE*, Vol. 98, No. HY9, pp 1637 – 1639.

Doddiah, D., M. Alberson & R. Thomas (1953). "Scour from jets". *Proc. Minnesota Internaional Hydraulic Convention*, Minneapolis, pp 161 – 169.

Einstein, H. A. (1942). "Flow on a moveable bed." *Proc. 2nd Hydraulic Conference*, State University of Iowa, Iowa City, Iowa, p 332.

Einstein, H. A. (1950). *The bed load function for sediment transportation in open channel flows*. Tech. Bull. 1026, U.S. Department of Agriculture, Washington, D.C.

Engelund, F. & J. Fredsoe (1976). "A sediment transport model for straight alluvial channels." *Nordic Hydro*, 7, pp 293 – 306.

Engelund, F. & E. Hanson (1972). *A Monograph on Sediment Transport in Alluvial Streams*. Teknisk Forlag, Copenhagen.

Ettema, R. (1980). *Scour at bridge piers*. School of Engineering Report No. 216, University of Auckland, New Zealand.

Fortier, S., & F. C. Scobey (1926). "Permissible Canal Velocities." *Trans. ASCE,* Vol. 89, pp 940 - 984.

Franzetti, S., S. Malavasi & C. Piccinin (1994). "Sull'erosione alla base della pile di ponte in acque chiare." *Atti del XXIV Convegno di Idraulica e Construzioni Idrauliche*, Napoli, Vol. II, pp 13 – 24.

Froehlich, D.C. (1989). "Local Scour at Bridge Abutments." *Proc. ASCE Ant. Hydr. Conf.* ASCE, New York, pp 13-18.

Garde, R. J., K. Subramanya & K. D. Nambudripad (1961). "Study of Scour Around Spur Dikes." *J. Hydr. Div. ASCE*, Vol. 87, No. HY6, pp 23-37.

Gill, Mohammad Akram (1972). "Erosion of sand beds around spur dikes". *J. Hydr. Div. ASCE*, Vol. 98, No. HY9, pp 1587-1602.

Gill, Mohammad Akram (1981). "Bed Erosion in Rectangular Long Contraction". *J. Hydr. Div. ASCE*, Vol. 107, No. HY3, pp 273-284.

Graf, W. H. (1998). *Fluvial Hydraulics: Flow and Transport Processes in Channels of Simple Geometry*. John Wiley & Sons.

Grass, A. J. (1970). "Initial instability of fine bed sand." *J. Hydr. Div. ASCE*, Vol. 96, No. HY3, pp 619 – 632.

Hamill, Les (1999). *Bridge Hydraulics*. E & FN SPON, Routledge, 367 pages.

HEC-18 (2001) *Evaluating Scour at Bridges, Fourth Edition. U.S. Department of Transportation, Federal Highway Administration Publication*, No. FHWA NHI 01-001, Hydraulic Engineering Circular No. 18, 378 pages.

Hoffmans G. J. C. M. & H. J. Verheij (1997). *Scour Manual*. A. A. Balkema.

Hjulström, F. (1935). "Studies of the Morphological Activity of Rivers as Illustrated by the River Fyris." *Bulletin of the Geological Institute of Uppsala*, Vol. 25, Chap. 3.

Kandasamy, J. K. (1989). *Local scour at skewed abutment*. Rep. No. 375, School of Engineering, University of Auckland, New Zealand.

Komura, S. (1966). "Equilibrium depth of scour in long constrictions." *J. Hydr. Div. ASCE*, Vol. 86, No. HY5, pp 17-37.

Kramer, H. (1935). "Sand mixture and sand movement in fluvial model." *Trans. ASCE*, Vol. 100, pp 798 – 873.

Kwan, T. F. (1984). *A study of abutment scour.* Report No. 328, School of Engineering, University of Auckland, New Zealand.

Laursen, E. M. (1962). "Scour at bridge crossings." *Trans. ASCE*, Vol. 127, No. 1, pp 166-180.

Laursen, E. M. (1963). "Analysis of relief bridge scour." *J. Hydr. Div. ASCE*, Vol. 89, No. 3, pp 93 – 118.

Levy, E. E. (1956). *River Mechanics*. National Energy Press, Moscow (in Russian).

Lim, Siow-Yong (1997). "Equilibrium Clear-Water Scour Around an Abutment." *J. Hydr. Div. ASCE*, Vol. 123, No. 3, pp 237-243.

Lim, Siow-Yong & Nian-Sheng Cheng (1998(a)). "Prediction of Live-bed Scour at Bridge Abutments." *J. Hydr. Div. ASCE*, Vol. 124, No. 6, pp 635-638.

Lim, Siow-Yong & Nian-Sheng Cheng (1998(b)). "Scouring in Long Contractions." *J. Irrig. and Draining Eng. ASCE*, Vol. 124, No. 5, pp 258-261.

Liu, Hsin-Kuan (1957). "Mechanics of Sediment-Ripple Formation." *J. Hydr. Div. ASCE*, Vol. 83, No. HY2, 23 pages.

Liu, H.-K., F. M. Chang & M. M. Skinner (1961). *Effect of bridge construction on scour and backwater.* CER 60 HKL 22, Colorado State Univ., Civ. Engrg. Section, Ft. Collins, Colorado.

Melville, B. W. (1992). "Local Scour at Bridge Abutments." *J. Hydr. Div. ASCE*, Vol. 118, No. 4, pp 615-631.

Melville, B. W. & R. T. F. Kwan (1994). " Local scour and flow measurements at bridge abutments." *J. Hydr. Research IAHR*, Vol. 32, No. 5, pp 661- 673.

Melville, B. W. (1997). "Pier and Abutment Scour: Integrated Approach." *J. Hydr. Div. ASCE*, Vol. 123, No. 2, pp 125-136.

Melville, B. W. & Y. –M. Chiew (1999). "Time Scale for Local Scour at Bridge Piers." *J. Hydr. Div. ASCE*, Vol. 125, No. 1, pp 59-65.

Parker, G., P. C. Klingeman & D. G. McLean (1982). "Bedload and size distribution in paved gravel-bed streams." *J. Hydr. Div. ASCE*, Vol. 108, pp 544-571.

Raudkivi, A. J. (1986). "Functional trends of scour at bridge piers." *J. Hydr. Engrg. ASCE,* Vol. 112, No. 1, pp 1 – 13.

Raudkivi, A. J. (1998). *Loose Boundary Hydraulics*. A. A. Balkema.

Raudkivi, A. J. & R. Ettema (1977). " Effect of Sediment Gradation on Clear-water Scour." *J. Hydr. Div. ASCE*, No. HY10, pp 1209 – 1213.

Raudkivi, A. J. & R. Ettema (1983). "Clear-water Scour at Cylindrical Piers" *J. Hydr. Div. ASCE*, Vol. 109, No. 3, pp 339-350.

Richardson, E. V., M. A. Steven & D. B. Simons (1975). "The Design of Spurs for River Training." *Proc. 16th Congress, IAHR*, Sao Paulo, Vol. 2, pp 382 – 388.

Rooseboom, A. (1975). *Sediment Transport in Rivers and Reservoirs*. D. Eng dissertation, University of Pretoria, South Africa (in Afrikaans).

Rooseboom, A. (1992). *Sediment Transport in Rivers and Reservoirs – A Southern African Perspective*. Report No. 297/1/92 of the Water Research Commission of South Africa.

Rouse, H. (1940). "Criteria for similarity in the transporatation of sediment." *Proc. 1st Hydraulic Conference*, Bull. 20, State University of Iowa, Iowa City, Iowa.

Shamov, G. E. (1952). "Formulas for Determining Near-Bed Velocity and Bed Load Discharge." *Proc. Soviet National Hydrology Institute*, Vol. 36 (in Russian).

Shen, Hsieh Wen (1962). "Development of bed roughness in alluvial channels." *J. Hydr. Div. ASCE*, Vol. 88, No. HY3, pp 45 – 58.

Shields, A. (1936). *"Anwendung der Aenlichkeitmechanik und der Turbulenzforschung auf die Geschiebebewegung." Mitteilungen der Preussischen Versuchsanstalt für Wasserbau und Schiffbau*, Heft 26 (in German). (English translatin by W. P. Ott and J. C. van Uchelen, *Hydrodynamics Laboratory Publication No. 167*, Hydrodynamics Lab. California Inst. Of Tech., Pasedena).

Shvidchenko, A. B. & G. Pender (2000). "Initial motion of streambeds composed of course uniform sediments." Proc. Instn. Civ. Engrs Water and Mar. Engrng, 142, Dec., pp 217-227.

Statistica Version 5.0, StatSoft, Inc., http://www.statsoft.com

Straub, L. G. (1934). "Effect of channel contraction works upon regimen of movable bed streams." *Trans. Am. Geophysical Union*, Part II, pp 454 – 463.

Van Rijn, L. C. (1993). *Principles of sediment transport in rivers, estuaries and coastal seas*. Aqua Publications, The Netherlands.

Vanoni, V. A. (1975) – editor. *Sedimentation Engineering*. ASCE Press.

Yang, C. T. (1972). "Unit Stream Power and Sediment Transport." *J. Hydr. Div. ASCE*, Vol. 98, HY10, pp 1805 – 1826.

Yang, C. T. (1973). "Incipient Motion and Sediment Transport." *J. Hydr. Div. ASCE,* Vol. 99, HY10, pp 1679 - 1703.

Yang, C. T. (1996). *Sediment Transport: Theory and Practice*. McGraw-Hill.

Zaghloul, N. A. (1983). " Local Scour Around Spur-Dikes." *Journal of Hydrology*, Vol. 60, pp 123-140.

Zanke, U. (1978). *Zusammenhänge zwiscen strömung und Sedimenttransportes, Teil1: Berechnung des Sedimenttransportes, -allgemeiner Fall-, Teil 2: Berechnung des Sedimenttransportes hinter befestigten Sohlenstrecken, -Sonderfall sweidimensionaler Kolk-*. Mitteilungen des Franzius-Instituts der TU Hannover, Heft 47, 48.

Appendix A

Engineering drawings of experimental apparatus

Sand-spreader
Simone Lyons
Department of Civil Engineering
University of Cape Town

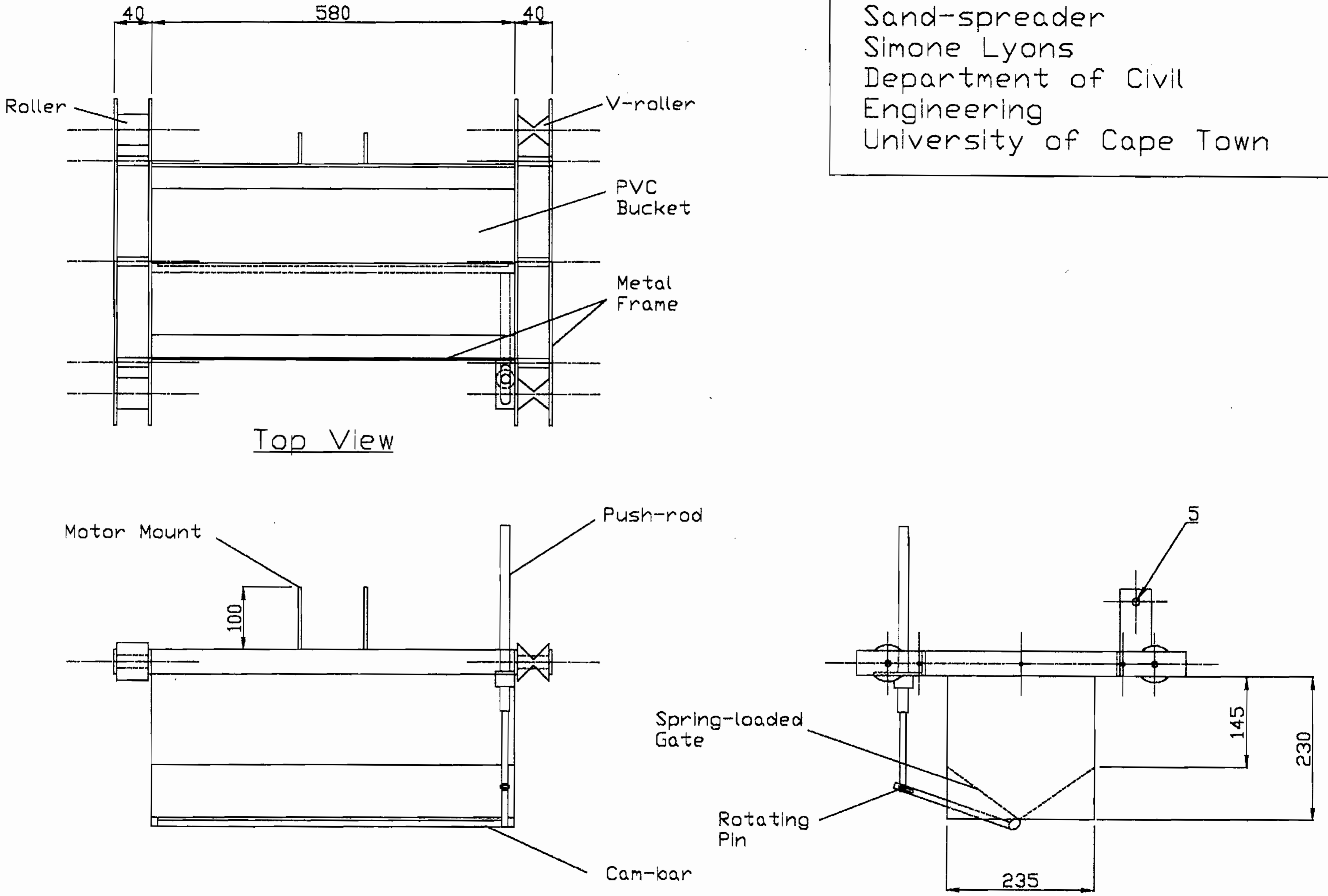

Top View

Front View

Side View

Laser-pointer
Simone Lyons
Department of Civil Engineering
University of Cape Town